2016-01-01

Fiberglass Goes Green: Developing Phosphate Glass For Use In Biodegradable Composites

Christina Lee Arendt
University of Texas at El Paso, mclanec@vt.edu

FIBERGLASS GOES GREEN: DEVELOPING PHOSPHATE GLASS FOR USE IN BIODEGRADABLE COMPOSITES

CHRISTINA LEE ARENDT

Doctoral Program in Materials Science and Engineering

APPROVED:

Stephen Stafford, Ph.D., Chair

David Roberson, Ph.D.

Felicia Manciu, Ph.D.

Peter Golding, Ph.D.

Charles Ambler, Ph.D.
Dean of the Graduate School

To Dustin, for always being there.

To Mom and Dad, for your unwavering support.

In memory of Maxine Shelly Turner.

"A sister is forever a friend and forever remembered"

FIBERGLASS GOES GREEN: DEVELOPING PHOSPHATE GLASS FOR USE IN BIODEGRADABLE COMPOSITES

by

CHRISTINA LEE ARENDT, B.S., M.S.

DISSERTATION

Presented to the Faculty of the Graduate School of

The University of Texas at El Paso

in Partial Fulfillment

of the Requirements

for the Degree of

DOCTOR OF PHILOSOPHY

Materials Science and Engineering

THE UNIVERSITY OF TEXAS AT EL PASO

May 2016

Acknowledgements

This work would not exist without the help of many people along the way. I must first thank Dr. Roy Arrowood for being my advisor for many a semester, and Dr. Stephen Stafford for stepping in to help at the very end. I am particularly grateful to Dr. Shane Walker for allowing the use of the ICP-OES and to Isaac Campos for his assistance in preparing the specimens and running the machinery. I would also like to thank the Materials Science team at Pacific Northwest National Laboratory, particularly Mike Schweiger, for their support. Their expertise in glass dissolution and testing has been invaluable.

Finally, I have had many "cheerleaders" along the way. I could never name all of them, but a few include my parents, Nick and Jann McLane; my husband, Dustin; my big, Jessica Palazzolo; my "twin," Katie Klumpp; my best friend during my time in El Paso, Jonathan Contreras; and last, but not least, my "potatoes" - you know who you are. I appreciate all your love and support.

Abstract

Composite materials, such as the glass fiber reinforced polyester thermosets known as "fiberglass," are used in many applications. However, recycling processes for these materials are inefficient and not widely available. Specially engineered degradable polymers offer an opportunity to redesign these composites. Additionally, the composite could be tailored to be multi-use, such that upon degradation, the resulting products could be used as part of a zeoponic substrate (artificial soil) for growing plants. Such a material would be beneficial for long-duration space missions, terraforming, or in other agricultural applications.

The research presented in this dissertation focuses on developing phosphate glass for use as the fiber reinforcement for such a composite. Due to the under-utilization of phosphate systems, there is a lack of thermodynamic data on these systems. The modified associate species method of phase diagram calculation was used in an attempt to gain more information about the desired system, as it is a good predictor of the phase relations in oxide melts, slags, and glasses and requires less data than other methods. Further research into the thermodynamic properties of phosphates is still needed to develop accurate phase diagrams and melting temperatures for this system.

Seventeen glass formulations were developed and melted. Six of these formulations were chosen for dissolution testing. Of these six, Glass 17 was chosen for intensive

testing and characterization. This glass was tested in water, hydrochloric acid solutions, and citric acid solutions. The weight loss was measured and ICP-OES was performed on the leachate solution. Scanning electron microscopy (SEM) and X-ray diffraction were performed on the tested specimens. Shrinking-core models were fit to the dissolution data. Fibers were drawn from the glass and characterized using SEM. The data shows that this glass is not dissolving congruently, as is expected of phosphate glasses. Instead, selective leaching is occurring, leading to the development of a non-protective surface layer during dissolution.

Contents

List of Figures

List of Tables

Chapter 1

Statement of the Problem

Current composite materials, such as the glass fiber reinforced polyester thermosets known as "fiberglass," are used in many structural applications. Once these materials have reached the end of their lifespan, they are typically discarded, since recycling processes are not widely available. Because neither the polymer matrix nor the glass fibers are biodegradable, this contributes to the issue of waste management. A car body that is built using the current materials will still be relatively intact many years from now, when the vehicle is no longer functional. However, specially engineered degradable polymers offer an opportunity to redesign these composites. Additionally, the composite could be tailored to be multi-use, such that upon degradation, the resulting products could be used as part of a zeoponic substrate (artificial soil) for growing plants. Such a material would be beneficial for long-duration space missions, terraforming, or in other agricultural applications.

In creating a hydro-biodegradable composite, there are three main focuses: the fibers, matrix, and coatings used in the composite. In order for the composite to work as intended, the fibers and the matrix must both be hydro-biodegradable, while the composite must have a waterproof coating so it does not degrade before the intended time. The main focus of this research will be on developing the fibers,

since there are many different types of coatings and hydro-biodegradable polymers that can be used as the matrix, including polylactic acid, polyvinyl alcohol, and polyethylene glycol. These polymers, and copolymers thereof, can easily be tailored to a designated degradation time. [66] To create hydro-biodegradable fibers, however, is a more challenging prospect.

Phosphate-based glasses are a good choice for this application. Calcium phosphate crystals have been used in biodegradable dental implants [28], but phosphate systems are historically under-utilized, leading to a dearth of information surrounding these systems. Thus the first step of the proposed work will be to calculate the phase diagrams for these systems in an effort to obtain the compositions and melting temperatures of glass compositions related to the interests of this research. Identifying eutectic points is of particular interest, as those compositions allow using lower furnace temperatures during melting and fiber production. The modified associate species method of phase diagram calculation is a good fit for this. Firstly, the associate species method accurately predicts the phase relations in oxide melts, slags, and glasses, by treating complex oxide solutions as an ideal solution of end-member species and intermediate associate species. [21] Secondly, the modified associate species method allows for estimation of thermodynamic values of the intermediate associate species, where they are unknown. [70] These properties of the modified associate species method make it a good fit for the calculations involved in this work.

Chapter 2

Background

In the following sections the fundamental concepts necessary to understand this investigation are presented. Section 2.1 discusses the modified associate species method of phase diagram prediction. Section 2.2 explains the science of zeoponics. Section 2.3 discusses phosphate glasses. Section 2.4 discusses some of the standards for testing the chemical durability of glasses and the advantages and disadvantages of each test.

2.1 The Modified Associate Species Method

Modeling the chemical thermodynamics of oxide systems is difficult due to the strong interactions between constituents. Simple solution models cannot take into account the complex thermochemical reactions that occur upon mixing [34] and standard nonideal solution models only provide acceptable results when no discontinuities in the mixing interactions occur [18]. The modified associate species model, however, avoids these difficulties by considering associated solution components that account for the known nonideal interactions. These associate species are treated as complex liquids and solids with identifiable stoichiometries and Gibbs energies of formation. [21] The modified associate species method thus represents complex oxide systems

as an ideal mixture of these associate species and the end-member species.

Due to the necessity of the associate species representing the negative interaction energies in the system, so-called "fictive" species must be used in their liquid phases when the phase equilibria cannot be calculated with only species that are present in the solid phase. The composition of these fictitious species can typically be determined by the composition of the region of the phase diagram where inaccuracies are occurring. [18] The effect of these fictitious species can be seen in two papers by Besmann and Spear. Both their 1999 paper [70] and their 2002 paper [18] examine the Na_2O-Al_2O_3 system. The 1999 paper includes only one associate species, $NaAlO_2$, while the 2002 paper uses both $NaAlO_2$ and the fictitious species $Na_2Al_4O_7$:1/3. The primary difference between the two phase diagrams, seen in Figures 2.1a and 2.1b, is a shift of the eutectic point from approximately 57% Al_2O_3 to around 66% Al_2O_3. Other differences are more subtle, but as can be seen in Figures 2.1c and 2.1d, these differences are due to the importance of the $Na_2Al_4O_7$:1/3 species, which has high activity over the entire compositional range. It should also be noted that the area of strongest effect on the phase diagram is the region surrounding a Na_2O:Al_2O_3 ratio of 1:2, the same ratio as is present in the fictitious species $Na_2Al_4O_7$:1/3.

Once the known solid and liquid species have been identified and fictitious species have been selected, the calculation process can begin. Gibbs energies of formation for each species must be fit to known data or estimated, if necessary. Liquid and solid solutions of the components must be modeled and the free energy minimized to determine the equilibrium composition of the system. Calculations can be done

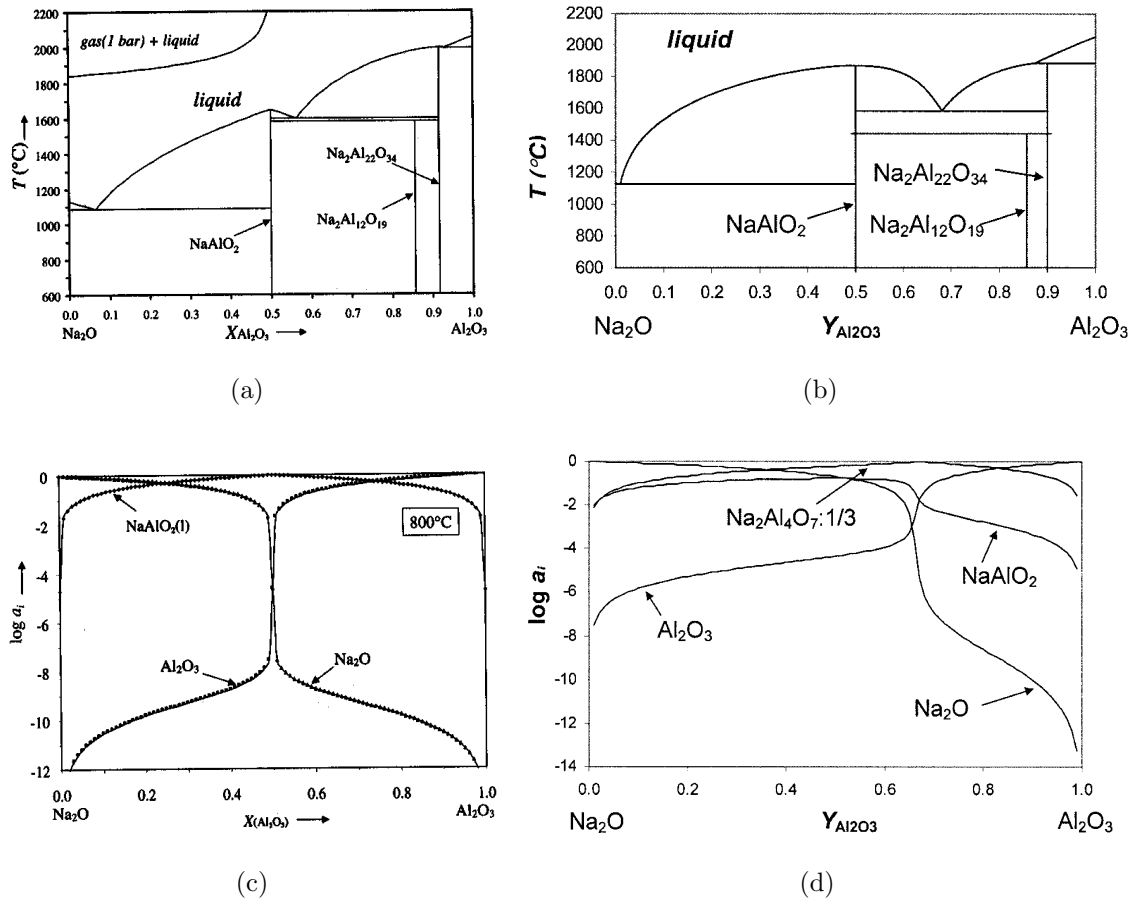

Figure 2.1: Phase diagrams (a) & (b) and activities at 800° C (c) & (d) of the Na_2O-Al_2O_3 system illustrating the importance of fictitious associate species. (a) & (c) from [70]. See Appendix B for documentation of permission to republish this material. (b) & (d) from [18]. See Appendix D for documentation of permission to republish this material.

for both binary and multi-component systems.

2.2 Zeoponics

Zeoponics is the science of cultivating plants in artificial soils, which has developed from the desire for extended duration human space missions and has found additional uses on Earth in accelerating plant growth. [8] Substrates composed of zeolites (microporous aluminosilicates) and phosphate minerals are used as both soil and slow-release fertilizers. Zeoponic plant growth in space is desirable over hydroponic systems due to its relative simplicity, compared to the monitoring systems and pumps required for hydroponic farming. [73]

The phosphate mineral often used in zeoponic systems is hydroxyapatite, usually written as $Ca_{10}(PO_4)_6(OH)_2$. Using hydroxyapatite (HA) is advantageous because it can easily be synthesized via precipitation-hydrolysis [87] or hydrothermal methods [40]. HA can also be produced with the macro- and micro-nutrients needed for plant growth substituted into the structure. This nutrient-substituted HA can provide plants with the macronutrients Ca, P, Mg, and S and the micronutrients B, Cl, Cu, Fe, Mn, Mo, Ni, and Zn. The availability of these nutrients to the plants is proportional to their substitution level in the HA. [32]

When HA is combined with NH_4- and K-exchanged clinoptilolite, which provides the remaining necessary macronutrients, a nutrient-complete zeoponic fertilizer is achieved. However, the best results for the growth of radishes, a plant sensitive

to NH_4^+ levels, occurred when dolomite was also added to the zeoponic substrate. [33] The additional Ca^{2+} from the dolomite increased the absorption of NH_4^+ by the radishes. The Ca^{2+} also removes NH_4^+ and K^+ from the clinoptilolite via ion exchange. However, the addition of dolomite to the substrate causes a reduction in the P concentration. This is potentially beneficial, though, as poor seed production in wheat has been attributed to Ca deficiency and high P concentrations. [17] Another addition that aids in the growth of radishes is nitrifying bacteria, which converts NH_4^+ to NO_3^-. A diagram of the dynamics of this system can be found in Figure 2.2.

A benefit of using zeoponics to grow plants is the nutrient availability over time. Because zeoponic substrates release nutrients slowly, they can be used for several generations of crops. In fact, in the studies done with radishes, the highest yield

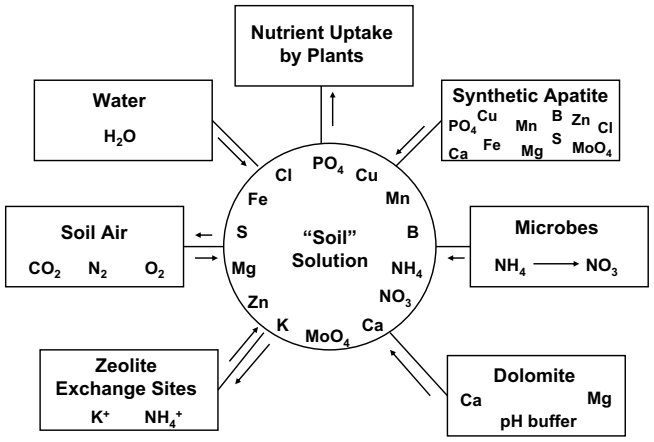

Figure 2.2: The dynamics of a nutrient-substituted hydroxyapatite-clinoptilolite-dolomite-nitrifying bacteria zeoponic system. All macro- and micro-nutrients required for plant growth are supplied. From [33]. See Appendix C for documentation of permission to republish this material.

by weight was the third crop grown in the same substrate. [33] Therefore, zeoponic substrates have the advantage that they can be used for an extended period of time without supplements. The substrates could likely also be tailored to individual crops, which would prevent the need for crop rotation.

2.3 Phosphate Glasses

Phosphate glasses have experienced a recent surge in interest as biomaterials [3, 4, 58], laser glasses [26, 52, 81], and for nuclear waste immobilization [46, 59, 69], among other applications. Calcium phosphate glasses in particular are intriguing due to their hydro-biodegradability and biocompatibility, and therefore are often used in biomedical applications. Implants using calcium phosphate glasses promote bone grow-in in orthopedic [51] and dental [28] applications. These glasses exhibit a large number of easily hydrated P-O-P bonds, and thus slowly dissolve away, allowing the new bone to grow into the space left behind. [2] It has also been shown that phosphate glasses, like hydroxyapatite, have the potential to be designed as controlled-release fertilizers. [16]

Iron phosphate glasses, on the other hand, have excellent chemical durability. This is thought to be due to the formation of the more hydration resistant Fe-O-P bonds. [2, 6] This has led to interest in utilizing iron phosphate glasses for the vitrification of nuclear waste materials. [43] Iron phosphate glasses are able to tolerate high alkali loads [37, 86] while still meeting Department of Energy durability requirements. [44, 29]

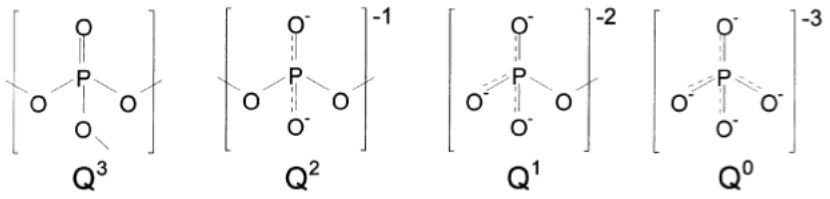

Figure 2.3: A diagram showing the structures of the four types of phosphate tetrahedra. From [22]. See Appendix C for documentation of permission to republish this material.

2.3.1 Structure

The basic building block of phosphate glasses is the phosphate tetrahedron, PO_4. These tetrahedra are linked together into chains or rings via covalent bridging oxygen. [22] The phosphate atom has a formal charge of +5, with four oxygen atoms available for charge balance. This results in three types of oxygen atoms that can be present in the tetrahedron: bridging oxygen (BO), non-bridging oxygen (NBO), and double-bonded oxygen (DBO). Both NBOs and DBOs are considered terminal oxygen (TO), as they do not connect phosphate atoms into chains (NBOs connect phosphate atoms to non-phosphate atoms, as P-O-M bonds). [36] Tetrahedra can be classified using Q^n terminology, where n is the number of bridging oxygens present in the tetrahedron. [22] A Q^3 tetrahedron will have 3 BOs and 1 DBO and no net charge. [45] A diagram illustrating all four structures can be seen in Figure 2.3.

The ratio of bridging oxygen to terminal oxygen in a phosphate glass can be determined by

$$\frac{BO}{TO} = \frac{1}{2}(3 - 4x), \tag{2.1}$$

where $x\mathrm{M_2O}(1-x)\mathrm{P_2O_5}$. [22] More specifically, the fraction of BOs in the glass is

$$BO = \frac{1}{2}\left(3 - \frac{x}{1-x}\right), \tag{2.2}$$

while the fraction of TOs is [36]

$$TO = \frac{x}{1-x} + 1. \tag{2.3}$$

Adding modifying oxides to a pure phosphate structure creates NBOs at the expense of BOs. This depolymerization of the network can be written generically as:

$$2\,\mathrm{Q^n} + \mathrm{M_2O} \longrightarrow 2\,\mathrm{Q^{n-1}}. \tag{2.4}$$

Phosphate networks can be classified by the amount of modifying oxide, which sets the O/P ratio and therefore the number of tetrahedral linkages between neighboring phosphate tetrahedra. A binary system $x\mathrm{M_2O}(1-x)\mathrm{P_2O_5}$ can be sorted into ultraphosphate ($x < 0.5$, O/P < 3) and polyphosphate ($x > 0.5$, O/P > 3) regions, with some sub-regions such as metaphosphates ($x = 0.5$, O/P $= 3$), pyrophosphates ($x = 0.67$, O/P $= 3.5$), and orthophosphates ($x = 0.75$, O/P $= 4$). Ultraphosphate glasses have a mix of $\mathrm{Q^2}$ and $\mathrm{Q^3}$ tetrahedra, with the fraction of each given by the following equations:

$$f(\mathrm{Q^2}) = \frac{x}{1-x} \tag{2.5}$$

$$f(\mathrm{Q^3}) = \frac{1-2x}{1-x}. \tag{2.6}$$

The crosslink density (q) of ultraphosphates is given as [24]

$$q = \frac{1 - 2x}{1 - x}, \tag{2.7}$$

though the number of crosslinks is small when compared to silicate glasses. [45] Ultraphosphate glasses are highly cross-linked, but due to Q^3 sites being very reactive to water, they have limited usefulness. [22]

Metaphosphate glasses ($x = 0.5$) are, in theory, entirely composed of Q^2 tetrahedra forming polymer-like chains and rings. Chain alignment in metaphosphates, which can occur during extrusion or drawing of the fibers [55], can cause anisotropic optical and mechanical properties in the glass. The phosphate chains in metaphosphate glasses are linked through bonds between terminal oxygens and modifying cations. Both DBOs and NBOs tend to coordinate the modifier cations, forming M-O-P bridges, and in fact, the bond length for the DBOs is only 0.005 nm longer than that of NBOs. [36] The modifier-TO bond is more covalent with increasing modifier field strength, and thus the properties of metaphosphate glasses are based more on M-O-P bonds than P-O-P bonds. [22]

Metaphosphate glasses could more accurately be called "long-chain polyphosphates." [22] Polyphosphates ($x > 0.5$) are Q^2 chains terminated by Q^1 tetrahedra, where $\bar{n}$ decreases as the O/P ratio (or x) increases. When the pyrophosphate composition ($x = 0.67$, O/P = 3.5) is reached, the chains have decreased in length to become phosphate dimers, or two Q^1 tetrahedra linked by a common BO. For the

range between metaphosphate and pyrophosphate compositions, the fraction of Q^1 and Q^2 tetrahedra is given by:

$$f(Q^1) = \frac{2x - 1}{1 - x} \tag{2.8}$$

$$f(Q^2) = \frac{2 - 3x}{1 - x}. \tag{2.9}$$

Because of the elimination of easily hydrated P-O-P Q^2 bonds, iron pyrophosphate glasses can be 1000 times more durable than iron metaphosphate glasses. Continuing to increase the O/P ratio to orthophosphate levels ($x = 0.75$, O/P = 4) leads to a structure made up of isolated Q^0 tetrahedra. Theoretically, the fraction of Q^0 and Q^1 tetrahedra in the range between pyrophosphate and orthophosphate is

$$f(Q^0) = \frac{3x - 2}{1 - x} \tag{2.10}$$

$$f(Q^1) = \frac{3 - 4x}{1 - x}, \tag{2.11}$$

but the glass formation range is typically limited to $x < 0.55$-0.6. [22] Evidence of the shift in Q^n sites with composition can be seen in nuclear magnetic resonance (NMR) spectra, as seen in Figure 2.4.

The binary distributions given in Equations 2.5, 2.6, and 2.8 - 2.11 experience deviations due to disproportionation reactions in the glasses. [45, 63] Most commonly,

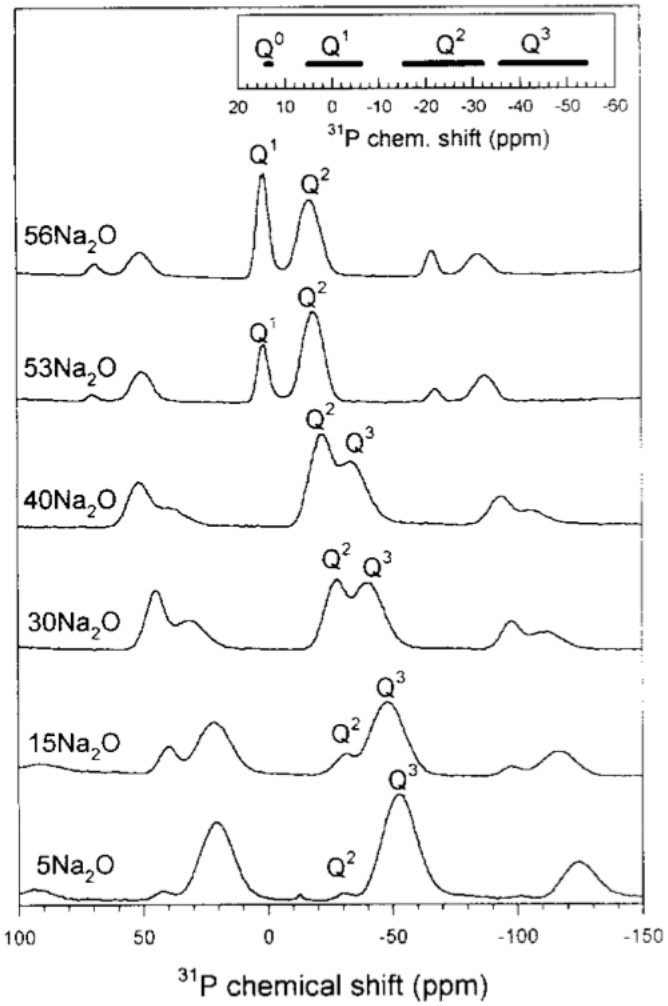

Figure 2.4: ^{31}P MAS NMR spectra showing a shift in the Q^n sites in Na_2O-P_2O_5 glasses with increasing Na_2O content. From [45]. See Appendix C for documentation of permission to republish this material.

disproportionation of the Q^1 site occurs as:

$$2\,Q^1 \longleftrightarrow Q^0 + Q^2. \tag{2.12}$$

There is little evidence of disproportionation occurring in Q^2 tetrahedra because of the relatively low stability of Q^3 tetrahedra; however, this reaction may occur in ultraphosphate glasses and possibly some calcium phosphate glasses. [45]

Phosphate glasses have a wide distribution of chain lengths in the network. [64] The theoretical average chain length ($\bar{n}$) can be calculated as

$$\bar{n} = \frac{2}{\sum_{i=1}^{n}[M_i]Z_i/[P] - 1}, \tag{2.13}$$

where $[M_i]$ is the cation concentration, Z_i is the cation valence,and $[P]$ is the phosphorus anion concentration. [53] Of course, in practice, the actual average chain length is lower than the number calculated. This is due to the presence of water in the structure of the glass. [24] Pure P_2O_5 is hygroscopic, as are P_2O_5-rich regions in the glass. [45] Metaphosphates theoretically have an average chain length of infinity [60], though in reality $\bar{n}$ is closer to 40-100 [22] because of water depolymerizing the glass network. [45] The H:P ratio in phosphate glasses has been found to be approximately 1:20. When this number is used in $\bar{n}$ calculations for metaphosphate glasses, the resulting numbers are much closer to the actual average chain length of the glass. [24]

2.3.1.1 Elemental Effects on Structure of Phosphate Glasses

In a phosphate glass, P acts as a network former, while Ca [27], Na [25], K [48], Mg [50], and Mn [61] act as network modifiers. Fe is a more interesting prospect due to the valence changes during the process of glass making. [88] Fe^{2+} is a network modifier, but Fe^{3+} acts more like a network former than a network modifier. [2, 3, 57] The ratio of Fe^{2+} to the total iron content is approximately 0.2. [41, 53, 60] The iron content of the glass therefore affects the network connectivity as

$$NC = \frac{3 * (2 * [P_2O_5 - Fe_2O_3] + 2 * 4 * [2 * Fe_2O_3]) - 2 * (RO + R_2O)}{2 * P_2O_5 + 2 * Fe_2O_3}, \quad (2.14)$$

where RO is the mole fraction of alkali metals and R_2O is the mole fraction of alkali earth metals. [3] P_2O_5 and Fe_2O_3 are the mole fractions of those components, as well.

> The above equation is based on the assumption that the charge on the phosphorous atom (P^{5+}) is locally charge balanced by the iron atom (Fe^{3+}). The $[P_2O_5 - Fe_2O_3]$ was representative of the P_2O_5 not charge balanced by the Fe_2O_3 (i.e. the PO_4 tetrahedra still has one double bonded oxygen), and the $[2 * Fe_2O_3]$ represents the PO_4 with no double-bonded oxygen, hence $* 4$. The above equation also only applies when the Fe_2O_3 content is below that of the P_2O_5. [3]

Increasing the amount of iron in a phosphate glass will decrease the average chain length, $\bar{n}$, as higher iron oxide content will lead to more NBOs in the phosphate

tetrahedra and more iron metaphosphate groups in the glass. [57] Iron phosphate glasses with high molar ratios of Fe/P and O/P can be prone to crystallization. An increase in the O/P ratio suggests a higher number of Fe-O-P bonds relative to P-O-P bonds. Glasses with longer P-O-P chains are more difficult to crystallize. [89]

Calcium behaves similarly to iron in this regards. In $(CaO)_x(P_2O_5)_{1-x}$ glasses, when x = 0.61, most of the phosphate atoms were found to be in diphosphate and triphosphate groups, while when the calcium level was decreased to x = 0.55, the glass contained more chains and less terminal or small group phosphate atoms. [64] Adding calcium leads to the breakage of P=O bonds and depolymerizes the glass, even when the base glass is already strongly depolymerized. It has also been noted that the Ca/P molar ratio of the glasses has an effect on the bioactivity, bioreactivity, and devitrification of the products studied. [49, 51] The glass network is strengthened by adding CaO, due to the ionic cross-links that are formed between NBOs. [63]

Calcium, iron, and magnesium are some of the elements that create cross-linking in phosphate glasses. Sodium does not, due to its valence of 1. "... the cross-linking of the glass structure by di- and tri-valent metals has a more significant (over-riding) effect on properties than the state of the phosphate chain backbone." [60]

2.3.2 Dissolution

Studies show that the dissolution behavior of phosphate glasses can be tailored to the application, and in fact, the dissolution rates can vary by orders of magnitude. [24, 28, 42] As a general rule, the more alkali the glass contains, the lower the

durability will be. [24] The addition of divalent oxides, on the other hand, increases durability, with Ba and Pb additions having the greatest effect. [20] This is because divalent cations serve as ionic cross-links between the non-bridging oxygens in the glass, similar to a metal chelate structure. It has been suggested that the durability of phosphate glasses is maximized when each terminal phosphate has only one proton associated with it. [24]

The dissolution rate of phosphate glasses increases with increasing temperature. The dissolution rate is also sensitive to the solution pH, with the rate increasing approximately a hundredfold when the solution pH goes from pH 5 to pH 1. When this happens, the solution proton concentration increases by a factor of 10,000, so the dissolution rate is roughly proportional to the proton concentration to the 1/2 power. This is because there is a direct correlation between the moles of H^+ consumed and the amount of glass dissolved; the ratio between moles of P released by the glass to moles of H^+ consumed is roughly 20. In most systems, dissolution is inhibited when the solution becomes saturated in the least soluble species that can leach from it, but this is not found to be true in phosphate glasses. The surface area to volume ratio is unimportant for phosphate glass dissolution. [24]

Phosphate glasses are considered to be Type V glasses [24], according to Hench and Clark's classification system [35], meaning that they experience congruent dissolution [30]. This means that elements and ions are not selectively leached away from the surface of the glass, but rather that the glass experiences complete network dissolution. In Type V conditions, heterogeneous attack of the surface can occur.

[30, 35, 53] This can leave surface features, such as etch pits, on the glass, since the corrosion is limited by surface reaction.

In phosphate glasses, hydrolysis of short chain polymeric phosphates is not controlling the dissolution, as this behavior is too slow. Instead, the glass experiences simple hydration of entire phosphate chains. These chains are dissolved intact from the surface of the glass and never repolymerize. [53] This is supported by measurements showing that the average chain length of dissolved chains in solution is approximately the same as the average chain length of the bulk glass. This also explains some of the solubility effects seen in the dissolution of phosphate glasses. The pH dependance for the dissolution of phosphate glasses does not match that of the least soluble calcium orthophosphate (apatite), seen in Figure 2.5, because the anions dissolving from the glass are not orthophosphates. This also explains why hydroxyapatite crystals have been seen precipitating on the surface of the glass during dissolution. This crystalline layer does not inhibit the decomposition of the glass, even when the solution is saturated in apatite; in fact, dissolution continues until the glass is entirely converted to apatite crystals. This is because the apatite crystals are formed via the slow hydrolysis of phosphate polymers. This step is so slow it occurs after the dissolution of the glass has already occurred. [24]

Phosphate glasses have been shown as having two reaction stages. [24, 53] In the first stage, dissolution proceeds as a function of $t^{1/2}$, while the second stage is linear with respect to time. However, there is some debate about the cause of this behavior. Bunker et al. (1984) explains that this phenomenon is due to the

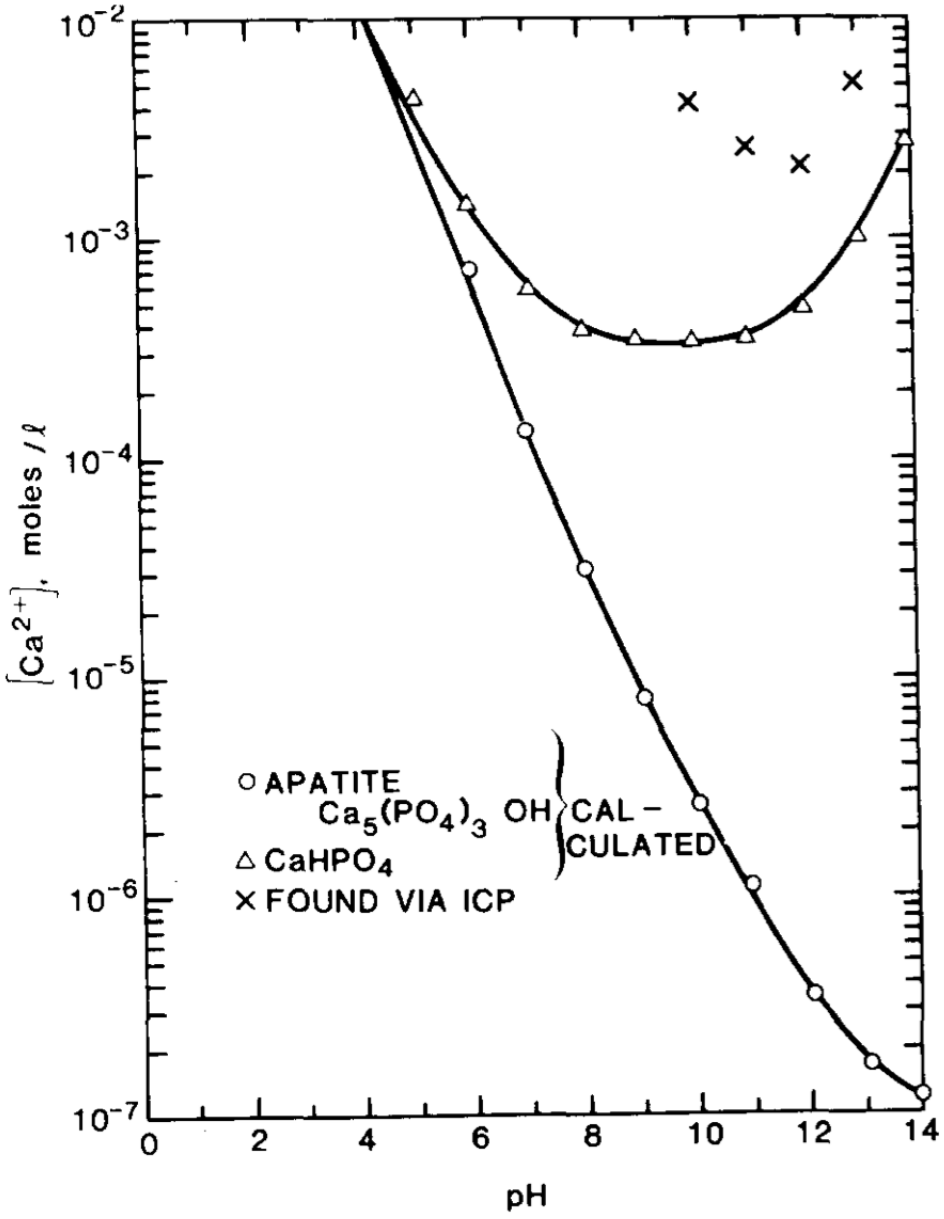

Figure 2.5: A diagram showing the calculated solubility of two calcium phosphate compounds versus the measured solubility of calcium phosphate glass. The solubility of the glass does not match that of crystalline calcium phosphates. From [24]. See Appendix C for documentation of permission to republish this material.

mechanics of dissolution in phosphate glasses. The observed $t^{1/2}$ stage is believed to be controlled by the rate at which water diffuses into the glass, as this controls the rate at which the hydration of entire phosphate chains can occur. This rate occurs only until the surface chains are completely surrounded by water, at which point the second, linear with respect to time, stage begins.

Delahaye et al. (1998), on the other hand, argues that the linear with respect to time behavior in the second stage is not inherent to phosphate glasses, but is rather a function of the leaching solution composition. In a system where the leaching solution was replenished throughout the experiment, they found the initial $t^{1/2}$ dissolution rate, which was similar to that reported by Bunker et al., held steady throughout the experiment. Their conclusion was that increasing ionic strength in the leaching solution led to a decrease in the dissolution rate of the glass.

Ma (2014) uses two shrinking-core models to describe the dissolution kinetics of phosphate glasses. The glass is assumed to be perfect spherical particles and reactions with the solution are assumed to first occur at the outer surfaces of the particles. As the solution diffuses into the particle, the remaining, unreacted glass is treated as though it shrinks in a uniform manner. Therefore, for the first stage of reaction, a 3-D diffusion model is used,

$$1 - (1 - \alpha)^{1/3} = k_{DM} t^{1/2}, \tag{2.15}$$

where k_{DM} is the temperature dependent reaction rate parameter and α is the mass fraction of a particle that has reacted at time t. In the second stage of reaction, a contracting volume model is used, where

$$1 - (1 - \alpha)^{1/3} = k_{CVM}t. \tag{2.16}$$

Ma showed that this two-model approach fit iron-sodium-phosphate glasses over a range of O/P and Fe/P ratios and hypothesized that smaller values of k_{DM} means there is slower diffusion of the solution into the glass, while smaller values of k_{CVM} occurred in glasses with a higher Fe/P ratio due to the slower hydration rates of Fe-O-P bonds as compared to Na-O-P bonds. If it is assumed that the reaction rate constants have an Arrhenius dependance on absolute temperature, the activation energy (Q) can be determined by:

$$k_{DM} = k_0 \exp(-Q/RT), \tag{2.17}$$

where R is the gas constant and k_0 is the frequency factor.

2.4 Glass Testing Standards

There are many national and international standards available for testing the chemical durability of glasses, though many are written specifically for glass waste forms. These include standards from the United States Environmental Protection Agency (EPA), the American Society for Testing and Materials (ASTM), and the

American Nuclear Society (ANS). These tests are usually fairly distinct from one another and are therefore difficult to compare, though some themes are prevalent, such as semi-dynamic tank leaching tests. An overview of several tests, with discussion of the advantages and disadvantages of each, follows. As there is quite a large number of standards for glass testing available, not every standard can be discussed here. The author has chosen to review only select EPA Methods and ASTM Standards, along with ANS 16.1, leaving out such tests as ISO 719, from the International Organization for Standardization [38], and MCC-1, from ANS [72], among others.

2.4.1 EPA Methods

There are at least six EPA Methods which can be used to characterize glass waste forms. The most widely used test is Method 1311, the Toxicity Characteristic Leaching Procedure (TCLP). This method is meant to mimic "worst case" conditions for waste disposal - co-disposal in a municipal solid waste landfill. It is therefore considered by some to be misused and/or overused, and thus a battery of other methods (Method 1313, Method 1314, Method 1315, and Method 1316) have been developed as a replacement for this method. These methods are meant to be used in a more case-specific manner, though each covers a wide range of conditions. Finally, Method 1320, the Multiple Extraction Procedure (MEP), can also be used on glass waste forms.

2.4.1.1 Method 1311 Toxicity Characteristic Leaching Procedure

The Toxicity Characteristic Leaching Procedure is a test "designed to determine the mobility of both organic and inorganic analytes present in liquid, solid, and multiphasic wastes" [75]. The following summary and discussion is of the method as applied to glass waste forms.

To prepare for the test, the glass must be size-reduced (crushed and sieved to 9.5 mm). Next, the extraction fluid must be determined. A sample of the glass must be further size-reduced to a 1 mm diameter. This 5 g sample is added to 96.5 mL of reagent water and stirred for 5 minutes; the pH is then measured. If the pH is less than 5.0, extraction fluid 1 (glacial acetic acid and sodium hydroxide in reagent water, diluted to pH 4.93 $\pm$ 0.05) is used. If the pH is greater than 5.0, 3.5 mL hydrochloric acid is added to the sample. The sample is heated to 50 °C and held at temperature for 10 minutes. The solution is allowed to cool to room temperature and the pH is measured again. If the pH is now less than 5.0, extraction fluid 1 is used. If the pH is greater than 5.0, extraction fluid 2 (glacial acetic acid in reagent water, diluted to pH 2.88 $\pm$ 0.05) is used.

A 100 g (or larger) specimen of the glass is added to an extractor bottle, along with an amount of the correct extraction fluid such that the weight of the extraction fluid is 20 times the weight of the specimen. The bottle is sealed and rotated end-over-end at 30 $\pm$ 2 rpm for 18 $\pm$ 2 hours at an ambient temperature of 23 $\pm$ 2 °C. At the end of the test period, the pH is measured and aliquots are taken for chemical analysis.

The results of the TCLP test are the concentrations of nuclides of interest.

TCLP is advantageous in that is has a very short duration, just 18 hours, and is a very simple to test to run. While the method does require the use of a tumbler that can meet the specified rpm requirement, the pre-test work is simple and requires only 5 g of glass. However, the full test does require at least 100 g of glass. TCLP is performed using a weakly acidic solution at room temperature; combined with the short duration of the test, it should be an acceptable method to use on non-durable glasses. However, the results from TCLP testing are really only comparable with other TCLP results and the method does require chemical analysis to be performed.

2.4.1.2 Method 1313 Liquid-Solid Partitioning as a Function of Extract pH Using a Parallel Batch Extraction Procedure

EPA Method 1313 [76] is a test designed to determine the liquid-solid partitioning curve for a glass over a pH range from 2 to 13. The liquid-solid partitioning is a measure of the solubility and release of nuclides. During the test, nine extractions of the material are performed in parallel, each at a different pH.

To prepare for the test, the glass must be size-reduced (crushed and sieved, typically to 0.3 mm/sieve size 50) and a pre-test titration should be performed. To perform the titration, five 10 g samples of the material are added to containers along with reagent water and nitric acid (or potassium hydroxide). The volume of acid or base added is determined by the relative alkalinity of the material, though one extraction will have no acid added, so as to determine the "natural" pH of the material.

The total amount of liquid for each extraction should be 100 mL, for a liquid-to-solid ratio of 10 mL/g. The containers are sealed and tumbled end-over-end at 28 ± 2 rpm at 20 ± 2 °C for 24 hours, after which the pH of each is measured and used to plot a titration curve (the pH as a function of the amount of acid added).

After the titration curve for a material has been determined, the parallel extraction can begin. First, the nine target pHs must be determined. Those should be pH 2, 4, 5.5, 7, 8, 9, 12, 13, and the natural pH. However, if the natural pH falls within ±0.5 of any of the target pHs, the natural pH takes precedence and an extraction at pH 10.5 should be added as the ninth target. As before, the samples of the material are added to a container with water and acid or base, sealed, and tumbled end-over-end at room temperature for 24 hours (or more for larger particle sizes). For these extractions, however, the mass of the sample is determined by the particle size (20 g for a particle size of 0.3 mm) and the volume of acid or base should be determined from the titration curve; the liquid-to-solid ratio remains 10 mL/g, however. At the end of the test period, the pH is measured and aliquots are taken for chemical analysis. The concentrations of nuclides can be plotted against the measured pH of each extraction to determine the liquid-solid partitioning curve. An example of curves for different types of species can be seen in Figure 2.6.

Method 1313 is advantageous in that it has a very short duration, just 24 hours, and provides information over a wide pH range. Due to the short duration and room-temperature test conditions, Method 1313 should be an acceptable test for non-durable glasses. Method 1313 can also be run simultaneously with Method 1316;

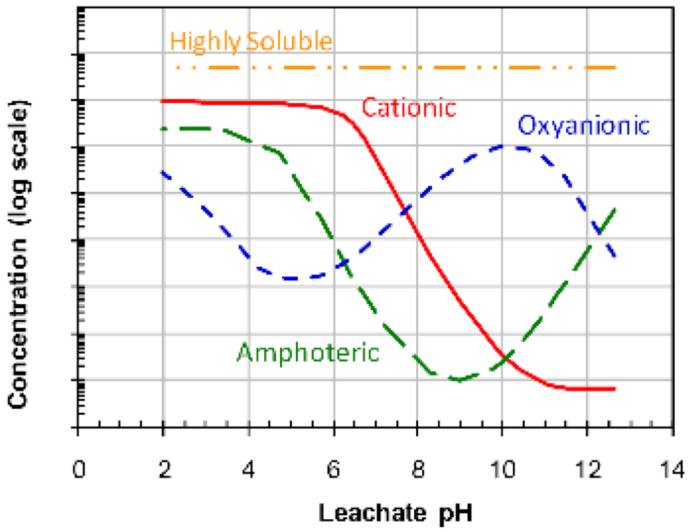

Figure 2.6: A diagram of the liquid-solid partitioning curves for different types of species, as determined by EPA Method 1313. From [76]

if this occurs, there is sample overlap between the two tests. However, Method 1313 does require a pre-test titration and a tumbler that can meet the rpm requirement specified in the method. Additionally, the 20 g minimum sample size per extraction, plus the 50 g needed for the pre-test extraction, means a minimum of 230 g of glass must be used to run the test as written. However, duplicate tests can be run using just an additional 180 g of glass. Method 1313 also requires chemical analysis to be performed to determine the liquid-solid partitioning curve.

2.4.1.3 Method 1314 Liquid-Solid Partitioning as a Function of Liquid-Solid Ratio for Constituents in Solid Materials Using an Up-Flow Percolation Column Procedure

EPA Method 1314 [77] is a test designed to determine the liquid-solid partitioning curve of a glass as a function of liquid-to-solid ratio under percolation conditions. During the test, reagent water is introduced to a column of packed granular material in an up-flow condition. Nine aliquots of varying volume are taken during testing to vary the liquid-to-solid ratio (L/S).

To prepare for the test, the glass must be size-reduced (crushed and sieved). The maximum particle size should be less than 1/20 of the column diameter. For the recommended column size of 5 cm, this means a particle size of 2.5 mm/sieve size 8. The powdered glass is then packed into a cylindrical column 30 cm in length. First, a 1 cm thick layer of quartz sand is packed into the column and tamped down, followed by a minimum of 300 g of glass material, and finally another 1 cm thick layer of quartz sand. A diagram of the testing apparatus can be seen in Figure 2.7. A pump is then attached to the bottom of the column with a flow rate of 0.75 $\pm$ 0.25 L/S per day (225 $\pm$ 75 mL per day for a 300 g sample). Reagent water is pumped into the column until the material is completely wetted and the liquid is level with the top of the column; the pump is then turned off and the column is allowed to equilibrate for 21 $\pm$ 3 hours.

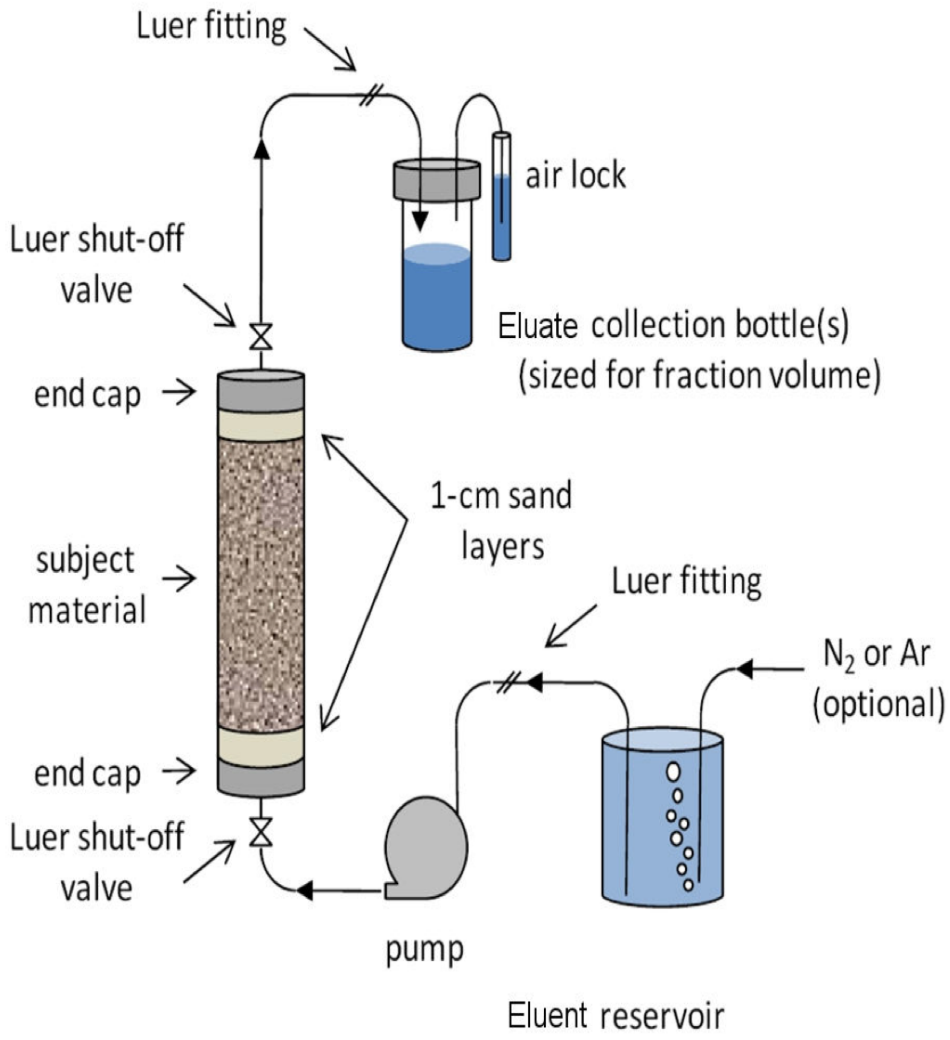

Figure 2.7: A diagram of the apparatus for EPA Method 1314. From [77]

Table 2.1: A schedule of L/S ratios, volumes, and approximate test duration for EPA Method 1314. The volume listed is for a sample mass of 300 g; the test duration is based on an eluate production rate of 0.75 L/S per day (225 mL per day).

Interval L/S		0.2	0.3	0.5	0.5	0.5	2.5	0.5	4.5	0.5
Cumulative L/S		0.2	0.5	1.0	1.5	2.0	4.5	5.0	9.5	10.0
Volume (mL)		60	90	150	150	150	750	150	1350	150
Approximate Interval	(hours)	6.4	9.6	16	16	16	80	16	144	16
Duration	(days)	0.3	0.4	0.7	0.7	0.7	3.3	0.7	6.0	0.7
Approximate Cumulative	(hours)	6.4	16	32	48	64	144	160	304	320
Duration	(days)	0.3	0.7	1.3	2	2.7	6	6.7	12.7	13.3

Once preparations are completed, the test is begun by restarting the pump. During testing, the eluate production rate should be monitored to ensure it falls in the acceptable 0.75 ± 0.25 L/S per day range. The pump flow rate and the eluate production rate may not be identical. Eluate is collected in bottles sized appropriately for each volume fraction; at the end of each collection period, a new collection bottle is attached to the apparatus. A schedule of L/S ratios, volumes, and approximate test duration can be seen in Table 2.1. At the end of each volume interval, the pH is measured and aliquots are taken for chemical analysis. The concentrations of nuclides can be plotted against the cumulative L/S ratio of each volume interval to determine the liquid-solid partitioning curve. A cumulative release curve can be obtained similarly, by plotting the cumulative concentration of a nuclide against the cumulative L/S ratio.

Method 1314 is a complicated test that requires a large amount of equipment, expertise, and experience to run properly. While the test is done at room temperature with reagent water, the longer duration of the test (approximately 13 days or more) may make it unsuitable for use with non-durable glasses. Method 1314 also requires a large amount of glass - 300 g for each run. Finally, Method 1314 requires chemical analysis to determine the liquid-solid partitioning curve. Method 1314 would be a good choice of test only if percolation conditions are of interest.

Method 1314, when compared to ASTM C1662 (SPFT), is a more strictly defined test. However, Method 1314 can be completed in a single test, while SPFT requires that a suite of tests be run for a single glass. This means Method 1314 can be completed for a single glass is the space of about two weeks, while SPFT can take months for one glass. Method 1314 does require a large amount of glass (300 g), but while the specimens for SPFT runs could be quite small, the requirement that many tests be run means that the total amount of glass required could be much larger than that of Method 1314. Finally, particle size, flow rates, and intervals for Method 1314 are fixed by the standard, which means that no guess-and-check is required to run Method 1314, which is untrue for inexperienced users of SPFT.

2.4.1.4 Method 1315 Mass Transfer Rates of Constituents in Monolithic or Compacted Granular Materials Using a Semi-Dynamic Tank Leaching Procedure

EPA Method 1315 [78] is a semi-dynamic tank leaching test that provides release rates for nuclides under diffusion-controlled release conditions. Method 1315 is very

Table 2.2: A comparison of the testing conditions for EPA Method 1315, ASTM C1308, and ANS 16.1.

	EPA Method 1315	ASTM C1308	ANS 16.1
Number of Time Increments	9	13	7 (10)
Duration of Each Interval (hours)	2, 23, 23, 120, 168 336, 336, 168, 336	2, 5, 17, 24, 24, 24, 24, 24, 24, 24, 24, 24	2, 5, 17, 24, 24, 24 24 (336, 672, 1032)
Total Elapsed Time at Each Interval (hours)	2, 25, 48, 168, 336, 672, 1008, 1176, 1512	2, 7, 24, 48, 72, 96, 120, 144, 168, 192, 216, 240, 264	2, 7, 24, 48, 72, 96, 120 (456, 1128, 2160)
Total Duration (days)	63	11	5 (90)
Liquid-to-Solid Ratio	9 mL/cm^2	Variable, 10 cm^3/cm^2 recommended	10 cm^3/cm^2
Specimen Shapes	Bricks, tiles, cubes, wafers, cylinders, packed powder	Cylinders	Parallelepipeds, cylinders, spheres
Minimum Dimension	5 cm	2.5 cm	1 cm
Temperature	18 - 22 °C	19 - 21 °C + other	17.5 - 27.5 °C

similar to ASTM C1308 and ANS 16.1, but can also be performed on powdered samples, in addition to the solid specimens used in all three tests. A comparison of the conditions used for the three tests can be found in Table 2.2.

To prepare for the test, the specimens must be prepared and placed in sample holders. Monolithic specimens may be either molded or cut from a larger specimen. These specimens can be in the form of bricks, tiles, cubes, wafers, or cylinders. The faces can be exposed in a variety of ways to produce 1-, 2-, and 3-D mass transfer scenarios, but the sample holder must not obscure more than 2% of the

exposed surface area. Compacted granular specimens must be open-faced cylinders; the holders must have an outer diameter matched as closely as possible to the inner diameter of the testing tank so that the majority of the eluent is above the sample. The granular material must be compacted into the sample holder using a variation of the modified Proctor compaction procedure. All specimens, whether monolithic or compacted granular, must have minimum dimensions of 5 cm in the direction of mass transfer.

To begin the test, leaching vessels are filled with reagent water so that the liquid-to-specimen-surface area ratio is 9 ± 1 mL/cm^2. The leaching vessel should be chosen so that headspace in the vessel is minimized and the specimen is completely submerged in the eluent (or so that the majority of the eluent is above the sample in 1-D scenarios). The specimen is placed in the vessel and an airtight lid is added. At the end of each leaching interval, the specimen is removed from the vessel, weighed, and placed in a clean vessel with fresh eluent. The pH of the eluate is measured and aliquots are taken for chemical analysis.

Once nuclide concentration for each interval has been determined, an interval concentration graph can be produced by plotting the interval concentration against the cumulative leaching time. Similarly, the cumulative release may also be plotted against cumulative leaching time. Finally, the interval flux can be calculated and plotted against the mean leaching time for each interval. To calculate the interval

flux, F_i, at the end of the ith interval,

$$F_i = \frac{M_i}{t_i - t_{i-1}}, \tag{2.18}$$

where t is the time at the end of the interval and M_i is the mass released during the interval in mg/m^2, calculated as follows:

$$M_i = \frac{C_i V}{A}, \tag{2.19}$$

where C_i is the nuclide concentration for the interval, V is the eluent volume, and A is the surface area of the specimen.

Method 1315 is a simple semi-dynamic tank leaching test requiring only a small amount of equipment to run. Once the samples are prepared, little work has to be done during the test other than filling new leaching vessels and transferring the specimens. While Method 1315 is a fairly lengthy test (63 days in total), the shorter intervals within the test, when combined with the room temperature testing conditions, mean that the test could be suitable for non-durable glasses. If glass monoliths are used for the test, there is less work involved in preparing the specimen, but a larger amount of glass must be used. For example, a cylindrical specimen measuring the minimum 5 cm in diameter and 5 cm heigh would require 98.2 cm^3 of glass, or approximately 255 g of glass, assuming a fairly standard glass density of 2.6 g/cm^3. A compacted granular specimen would require more work to prepare, but could use less glass than a monolith if a short specimen holder is used. Method 1315 does

require chemical analysis to be performed.

Method 1315, as compared to ASTM C1308 and ANS 16.1, requires a larger specimen but has more flexibility in the shape of the specimens used. Method 1315 is a longer test than both ASTM C1308 and the unextended version of ANS 16.1, but it has a better distribution of the interval durations. Neither ASTM C1308 nor the unextended version of ANS 16.1 has an interval length above 24 hours, while the interval lengths for Method 1315 range from 2 hours to 14 days. The extended version of ANS 16.1 does have longer intervals, but the interval durations skip directly from 24 hours to 14 days and only increase from there, which leads to a very uneven interval distribution when compared with Method 1315.

2.4.1.5 Method 1316 Liquid-Solid Partitioning as a Function of Liquid-to-Solid Ratio in Solid Materials Using a Parallel Batch Procedure

EPA Method 1316 [79] is a test designed to determine the liquid-solid partitioning curve for a glass over a range of liquid-to-solid ratios. During the test, five extractions of the material are performed in parallel, and can be done such that each has the same amount of liquid and varying masses of glass.

Before the test can begin, the glass must be size-reduced (crushed and sieved, typically to 0.3 mm/sieve size 50). Samples of the material are then added to containers with reagent water such that the target liquid-to-solid ratio is achieved for each. An example set-up based on a target liquid volume of 200 mL can be found in Table 2.3.

Table 2.3: An example set-up based on a target liquid volume of 200 mL for EPA Method 1316.

Liquid-to-Solid Ratio (mL/g)	10.0	5.0	2.0	1.0	0.5
Sample Mass (g)	20	40	100	200	400
Liquid Volume (mL)	200	200	200	200	200

Smaller volumes of liquid can be used, if less is required for chemical analysis, but the minimum sample mass is determined by the particle size (20 g for a particle size of 0.3 mm). As in Method 1313, the containers are sealed and tumbled end-over-end at room temperature for 24 hours (or more for a larger particle size). At the end of the test period, the pH is measured and aliquots are taken for chemical analysis. The concentrations of nuclides can be plotted against the liquid-to-solid ratio of each extraction to determine the liquid-solid partitioning curve.

Method 1316 is advantageous in that it has a very short duration, just 24 hours, and provides information over a wide range of liquid-to-solid ratios. Due to the short duration and room-temperature test conditions, Method 1316 should be an acceptable test for non-durable glasses. Method 1316 can also be run simultaneously with Method 1313; if this occurs, there is sample overlap between the two tests. However, Method 1316 does require a tumbler that can meet the rpm requirement specified in the method. Method 1316 also requires chemical analysis to be performed to determine the liquid-solid partitioning curve. Additionally, depending on the liquid volume requirements of the chemical analysis technique used, very large amounts of

glass my be required to run the test. For example, in order to obtain 200 mL of liquid from each specimen, a total of 760 g of glass is required for all five specimens. At the very least, the minimum sample size is 20 g for each specimen, a total of 100 g, which returns only 10 mL of liquid for the specimen with the lowest liquid-to-solid ratio.

2.4.1.6 Method 1320 Multiple Extraction Procedure

The Multiple Extraction Procedure [80] is a test designed to mimic the effects of acid rain on waste in a poorly designed landfill. In this test, the Extraction Procedure (EP) test (EPA Method 1310b) [74] is used as a portion of the procedure. As with TCLP, this method can be applied to solid, liquid, or multiphasic materials; however, the following summary and discussion is of the method as applied to glass waste forms.

To begin the test, 100 g of the glass must be size-reduced (crushed and sieved to 9.5 mm) and the EP test is run. The 100 g sample of the glass is added to a rotary extractor with 1600 g of water at 20-40 °C. Once agitation has begun, the pH of the solution is measured. If the pH is greater than 5.0, acetic acid is added to the solution until the pH decreases to 5.0 $\pm$ 0.2. This monitoring and adjustment of the solution pH should occur at 15-, 30-, and 60-minute intervals, increasing the interval duration whenever the pH is adjusted less than 0.5 pH units. The adjustment period should be continued for at least 6 hours; however, no more than 400 mL of acid should be added in total to the solution. The sample should be agitated in the solution for 24 hours. At the end of this period, if the pH is above 5.2 and the maximum amount

of acid has not been added, the pH should be adjusted to 5.0 ± 0.2 and the test should continue for another 4 hours, adjusting the pH at 60-minute intervals. At the end of the test, a volume of water (V) should be added to the solution such that

$$V = 400 - A, \tag{2.20}$$

where A is the volume of acid added during the test, in mL. The glass is filtered out of the solution and aliquots are taken for chemical analysis.

Next, synthetic acid rain is prepared by diluting a 60/40 sulfuric acid/nitric acid solution to pH 3.0 ± 0.2. The glass remaining after the EP test is weighed, and added to the extractor with the synthetic acid rain equal to 20 times the weight of the solid. The solution is agitated for 24 hours, then the glass is filtered out of the solution and aliquots are taken for chemical analysis. This is repeated another eight times, or more if the concentration of nuclides in solution are found to be increasing between the seventh or eighth extraction and the final extraction. The results of the MEP test is the concentration of nuclides of interest for each extraction.

The Multiple Extraction Procedure is an extremely situationally specific test, making it inappropriate for general-purpose testing of glasses. The EP portion of the test could be extremely work-intensive if an automatic pH adjuster is not used. There is also the need to filter the solution and take aliquots after every 24 hours of testing adding to the labor required to run MEP. While MEP requires a fairly large specimen size, 100 g, and requires the use of a rotary extractor and chemical analysis. Due

to the pH requirements of the test and the 10-day duration, this test may not be suitable for non-durable glasses. However, since aliquots are taken every 24 hours, it may be acceptable.

2.4.2 ASTM Standards

There are four ASTM standards which are widely used on glass waste forms. Two of the more popular options include ASTM C1285, the Product Consistency Test (PCT), and ASTM C1663, the Vapor Hydration Test (VHT). Additionally, ASTM C1308 can be used to test glass monoliths and ASTM C1662, the Single-Pass Flow-Through Test (SPFT) can be used to measure glass dissolution rates.

2.4.2.1 ASTM C1285 The Product Consistency Test

The Product Consistency Test [11] is a static leaching test that measures the chemical durability of glass waste forms. Test Method A has a very strict set of requirements, while Test Method B allows for flexibility in the duration, temperature, particle size, liquid-to-solid ratio, and leachant used in the test.

To prepare for Test Method A, the glass must be size-reduced (crushed and sieved to 0.149 to 0.074 mm/ASTM -100 to +200 mesh) and cleaned of adhering fines. A 1 g (or more) sample is placed into a 304L stainless steel vessel; ASTM Type 1 water is added such that the liquid-to-solid ratio is 10 $\pm$ 0.5 mL/g. The sealed vessel is placed into an oven or water bath at 90 $\pm$ 2 °C. After 7 days ($\pm$ 2% or 3.4 hours), the vessel is cooled to room temperature. The pH is measured and aliquots are taken

for chemical analysis. Test Method B is performed in the same manner, with each variation of duration, temperature, particle size, liquid-to-solid ratio, or leachant used tested in triplicate.

PCT is the most flexible test of the discussed glass testing standards. This means the test can be altered in such a way to be suitable for both durable and non-durable glasses. PCT is simple to run and requires no special equipment, although it does require chemical analysis. PCT requires neither a long time (Test Method A has a duration or 7 days) nor large amounts of glass (1 g minimum). One issue with PCT is that Test Method B results are not comparable across tests with different variations on PCT-A methods.

2.4.2.2 ASTM C1308

ASTM C1308 [12] is a semi-dynamic tank leaching test that provides release rates for nuclides under diffusion-controlled release conditions. The test is very similar to EPA Method 1315 and ANS 16.1, but can be performed at room temperature or at elevated temperatures to accelerate release. A comparison of the conditions used for the three tests can be found in Table 2.2.

To prepare for the test, the glass must be formed into cylindrical specimens with a diameter-to-height ratio between 1:1 and 1:2; the minimum dimension of the specimen is 2.5 cm. An appropriate leachant volume must be selected based on the specimen surface area and estimated leach rate. Additionally, the volume must be high enough to eliminate solution feedback effects, but low enough so nuclide concentra-

Table 2.4: Interval durations and total elapsed time for ASTM C1308.

Interval Duration	(hours)	2	5	17	24	24	24	24	24	24	24	24	24	24
	(days)	0.08	0.2	0.7	1	1	1	1	1	1	1	1	1	1
Total Elapsed Time	(hours)	2	7	24	48	72	96	120	144	168	192	216	240	264
	(days)	0.08	0.3	1	2	3	4	5	6	7	8	9	10	11

tions can be calculated. A volume-to-specimen-surface-area ratio of 10 cm^3/cm^2 or lower is suggested (to reduce wastewater handling for large specimen sizes). The leachant may be reagent water or another solution, such as synthetic or actual groundwater. Materials should be tested at a minimum of three temperatures, one of which must be 20 °C.

To begin the test, the specimen should be suspended in the leachant from the cover of the leaching container. The leachant should be replaced at 2 hours, 5 hours, 17 hours, and 24 hours, then daily to a total test duration of 11 days. A chart showing the interval durations and total elapsed time can be seen in Table 2.4. To replace the leachant, the cover with specimen attached should be removed from the previous container and placed onto a new container with the determined volume of fresh leachant. The leachant may be pre-heated to the testing temperature if practical. Aliquots should be taken from the leachant for each interval for chemical analysis. The incremental and cumulative fraction released of nuclides of interest can be plotted against the cumulative time; additionally, the effective diffusion coefficient can be calculated using a computer program available from ASTM.

ASTM C1308 is a simple semi-dynamic tank leaching test requiring only a small amount of equipment to run. Once the samples are prepared, little work has to be done during the test other than filling new leaching vessels and transferring the specimens. C1308 is not a very long test - only 11 days - but must be run at multiple temperatures, one of which is room temperature. The room temperature test is likely suitable for non-durable glasses, but the elevated temperature tests, depending on which temperatures are used, may not be. The glass monoliths used for the test, cylindrical specimens measuring the minimum 2.5 cm in diameter and 2.5 cm heigh, would require 12.7 cm^3 of glass, or approximately 33 g of glass, assuming a fairly standard glass density of 2.6 g/cm^3. ASTM C1308 does require chemical analysis to be performed.

ASTM C1308, as compared to EPA Method 1315 and ANS 16.1, has more stringent specimen requirements. C1308 can only be performed with cylindrical specimens with a particular aspect ratio. C1308 allows for a smaller minimum dimension than Method 1315, but requires a larger minimum dimension than ANS 16.1. Both C1308 and the unextended version of ANS 16.1 have a maximum interval duration of 24 hours, and in fact, the first five days of these tests are identical. C1308 can be viewed as a version of ANS 16.1 where the daily sampling is extended from 5 days to 11 days.

2.4.2.3 ASTM C1662 Single-Pass Flow-Through

The Single-Pass Flow-Through Test [13] is a dissolution test designed to measure the forward dissolution rate of silicate glasses, or to determine the effect a specific

species' concentration has on the dissolution rate. By pumping reagent water, chemical solutions, or groundwater through a reaction cell containing either crushed glass or a monolithic specimen at several flow rates, kinetic model parameters for glass corrosion can be calculated.

Specimens for SPFT can be either monolithic, for low surface areas, or crushed glass, to have high surface areas. The particle size for crushed glass specimens must be large enough that there is no more than a 15 mass percent decrease in the surface area during testing. All the glass used in the suite of SPFT tests using crushed glass specimens must come from the same source. Monolithic specimens can be prepared in any shape where the geometric surface area can be measured directly. All the monoliths used for the suite of SPFT tests should be prepared from the same batch of glass, and the surface finishes should be consistent. A final polish of 600 grit is recommended, so that comparisons across different glasses can be made.

Before testing can begin, the system must be cleaned by flushing at least three system volumes of the test solution through all tubing and containers used in the apparatus. The flow rate to achieve the desired F/S° ratio should be determined, and the pump should be set to the desired flow rate. Test solution should be passed through the system to determine the actual flow rate through the system.

Next, the glass should be placed in the reaction cell, which can either be a column-type reactor or a bottle-type reactor. Schematics of these two types of reaction cells can be seen in Figure 2.8. The first set of aliquots should be taken after at least one

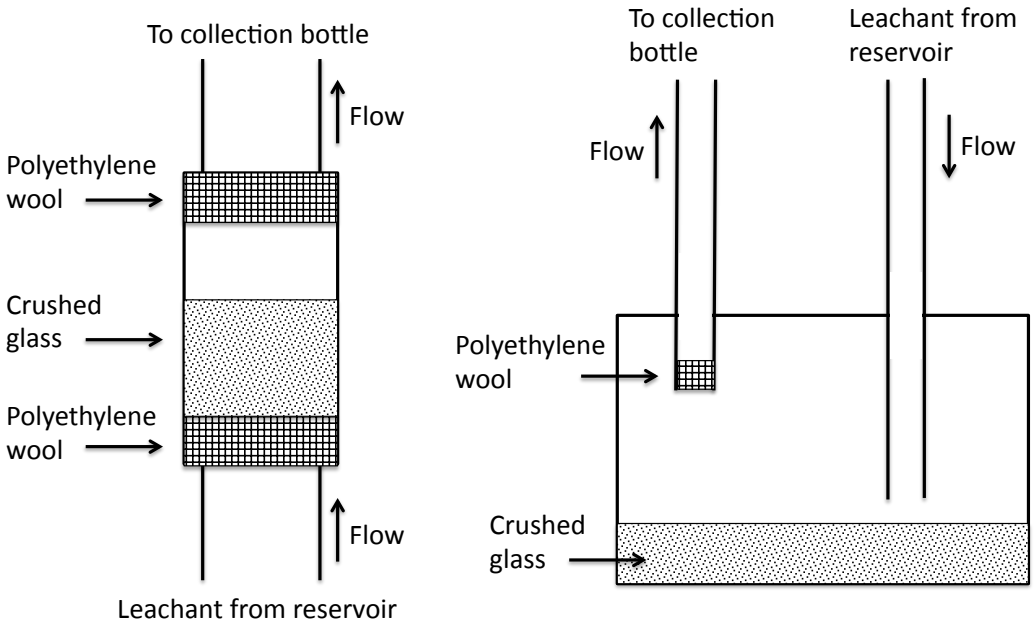

Figure 2.8: A diagram of the reaction cells used for SPFT. Either column-type reactors (left) or bottle-type reactors (right) may be used. After [13]

system volume of test solution has been pumped through the system. One aliquot is taken for elemental analysis and to determine the flow rate, while the second is taken to determine pH. If the flow rate calculated from the first aliquot deviates by more than 10% from the target flow rate, the pump speed must be adjusted. Aliquots should be taken at least every 2 days for a 14-day period.

To determine the forward dissolution rate of the glass, SPFT must be performed at several flow rates, pH values, and temperatures. There will be an upper threshold and a lower threshold value of the flow rate for each glass. At the upper threshold, further increasing the flow rate will not affect the glass dissolution rate, because the glass is already dissolving at its maximum rate for the temperature and pH. At the

lower threshold, further decreasing the flow rate will not affect the glass dissolution rate, because the glass is dissolving as though the system is static. The dissolution rate of the glass is calculated as

$$rate = \frac{[C_i(i) - C_i^\circ] \cdot \left(\frac{F}{S^\circ}\right)}{f_i}, \tag{2.21}$$

where $C_i(i)$ is the steady-state concentration of component i in the effluent solution, C_i° is the concentration of component i in the blank test, F is the solution flow rate, S° is the initial surface area of the glass specimen, and f_i is the mass fraction of component i in the glass. A plot of the measured dissolution rates versus the steady-state concentration of dissolved silica is used to extrapolate to a dissolved silica concentration of 0 to determine the forward glass dissolution rate. The intrinsic rate constant (k_0) can then be calculated as

$$\log k_0 = \log rate - \eta \cdot pH + \frac{E_a}{2.303RT}, \tag{2.22}$$

where η is the pH dependance, E_a is the activation energy, R is the gas constant, and T is absolute temperature. The values of η and E_a can be determined via data regression in a plot of log rate against pH at various temperatures.

SPFT is a complicated test that requires a large amount of equipment, expertise, and experience to run properly. Additionally, due to the need to perform tests at multiple flow rates, temperatures, and pH values, running a suite of SPFT tests on a single glass can take months of effort. SPFT is likely not a suitable test for non-

durable glasses due to its longer duration (14 days) and elevated temperatures. As the specimen size is not specified, SPFT could likely be performed with very small amounts of glass per test, but the need for a suite of tests means that in the end, large amounts of glass would need to be used. While SPFT provides the most specific dissolution rate information of any of the tests discussed herein, the amount of time and equipment required to run the test precludes choosing it unless that very specific information is required.

SPFT, as compared to EPA Method 1314, is a more flexible test, but is also more rigorous. The test can be done with almost any particle size (so long as it meets the 15% surface area requirement) or with monolithic specimens. SPFT can also be done with many different flow rates, while the flow rate for Method 1314 is a specified range. The interval durations for SPFT are flexible, so long as aliquots are taken at least every two days, while the volume intervals for Method 1314 are fixed. However, Method 1314 is a single test for a single glass, which can be completed in about 13 days, while SPFT is a suite of tests, each lasting 14 days, which can take months to complete. SPFT does not have a fixed glass specimen size, so small amounts of glass could be used for each test, but due to the need to run many tests, potentially more glass could be required than is used by Method 1314.

2.4.2.4 ASTM C1663 The Vapor Hydration Test

The Vapor Hydration Test [14] is used to study the corrosion of glass at high surface-area-to-water-volume ratios and elevated temperatures. Additionally, this test can be used to provide information on the alteration kinetics of the glass and

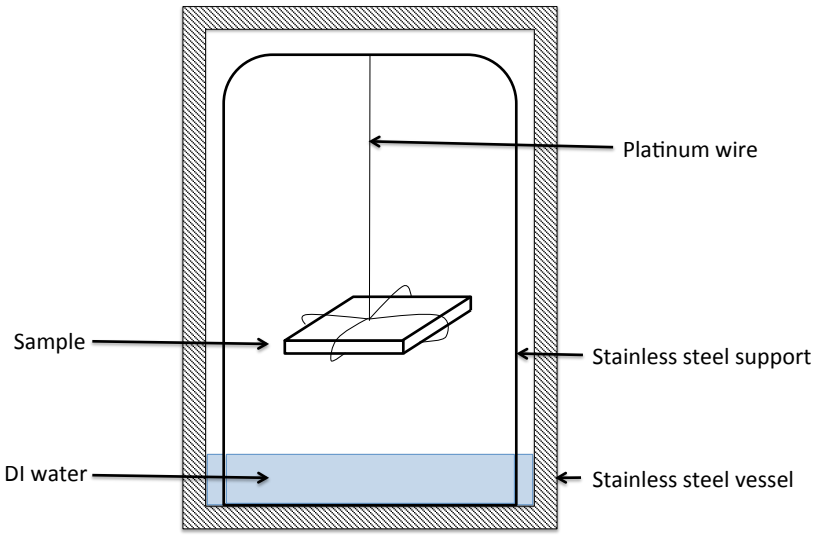

Figure 2.9: A diagram of the apparatus used for VHT. After [14]

the alteration phases that form.

Specimens for VHT are prepared from annealed bars. A specimen 10 mm by 10 mm by 1.5 mm is cut from the bar and polished to 600 grit. The specimen is suspended from platinum wire and sealed inside a stainless steel vessel with enough water to saturate the vessel with steam, which is dependent upon the size of the vessel and the temperature used during testing. For a 22 mL vessel at 200 °C, this is 0.20 mL of water. A diagram of this apparatus can be seen in Figure 2.9. After the test has concluded (typically a duration of 7 to 24 days is used), the vessel is removed from the oven and quenched in cold water. The specimen is allowed to dry, then is cut, polished, and mounted, either in epoxy or onto glass slides. The specimen is polished to a thin section, roughly 1 mm thick, with a 600 grit surface finish.

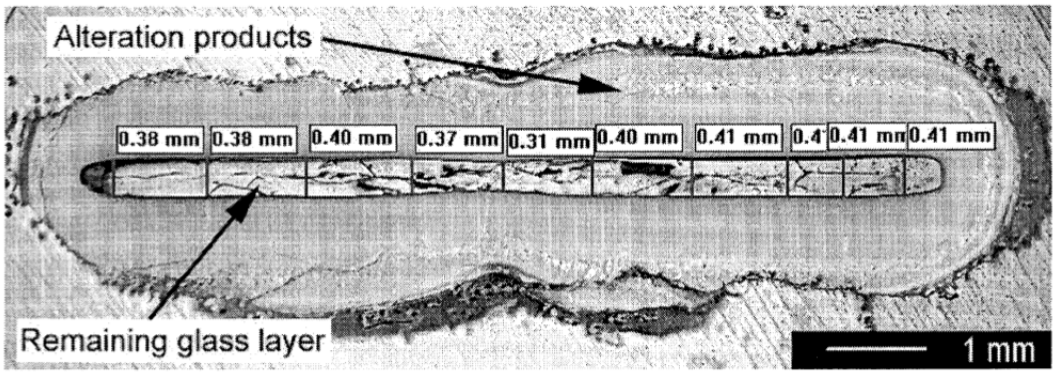

Figure 2.10: An example of the measurements made to determine alteration rate after VHT. Measurements of the remaining glass thickness are made at 10 even intervals across the width of the VHT specimen and averaged to determine d_r, the average thickness of the remaining glass layer. From [39]. See Appendix C for documentation of permission to republish this material.

Once the specimen is polished, either the remaining glass thickness or the thickness of the alteration layer is measured, as seen in Figure 2.10. The more accurate measurement is that of the remaining glass thickness, as alteration products can be fragile and thus damaged during specimen mounting and polishing. The mass of the glass converted to alteration products (per unit surface area), m_a is then calculated using the equation

$$m_a = \frac{m_i}{2w_i l_i}\left(1 - \frac{d_r}{d_i}\right), \tag{2.23}$$

where w_i, l_i, and d_i are the initial specimen width, length, and thickness, respectively; m_i is the initial specimen mass; and d_r is the average remaining glass thickness. The alteration rate, given in units of g/m^2/day, can then be determined by dividing m_a by the duration of the test. The alteration products can also be examined by XRD, SEM/EDS, or other similar methods to identify the alteration products.

The Vapor Hydration Test has the advantage of being a very easy test to run, as once the specimen containers are in the oven, one does not have to interact with them again until the end of the test duration. However, the specimens do require a good amount of preparation both before and after the test, including polishing very small specimens. Additionally, VHT requires very little material for individual specimens (many weigh less than 0.5 g), but the specimen is easiest to prepare from a larger bar of material, which somewhat negates the small specimen size. VHT can also have a duration as short as 7 days, as the standard is written, though 24 day tests are commonly used when testing glass waste forms. However, due to the elevated temperature and duration of the test, VHT is not a suitable test method for non-durable glasses. VHT is one of the few methods that does not require chemical analysis to get results; however, the measurements made to calculate the alteration rate can be quite subjective in nature, leading to results that are not as reproducible as other methods.

2.4.3 Other Methods

There are many other methods which can be used to test the durability, dissolution, and leaching of glasses and glass waste forms. One of these is ANS 16.1, a test comparable to ASTM C1308 and EPA Method 1315.

2.4.3.1 ANS 16.1

The ANS national standard for the measurement of the leachability of solidified low-level radioactive wastes by a short-term test procedure (ANS 16.1) [9] is a five

day semi-dynamic tank leaching test that provides a measure of the leach resistance performance of waste glasses. The test is very similar to EPA Method 1315 and ANS 16.1, but has an optional "extended" duration of 90 days. A comparison of the conditions used for the three tests can be found in Table 2.2.

Specimens for ANS 16.1 are monolithic cylinders, parallelepipeds, or spheres, preferably cast rather than core drilled to eliminate surface alteration. Cylindrical specimens should have a length-to-diameter ratio between 0.2 and 5 and, similarly, parallelepipeds should have a length-to-minimum-thickness ratio of 0.2 to 5. However, the preferred test specimen geometry is cylindrical. The minimum specimen dimension for all types of specimens should be 1 cm.

During the test, the specimen is suspended in a container containing a volume of room temperature (17.5 to 27.5 °C) demineralized water such that the ratio of the leachant volume, V_L, and the specimen geometric surface area, S, is given by

$$\frac{V_L}{S} = 10 \pm 0.2 \frac{\text{cm}^3}{\text{cm}^2}. \tag{2.24}$$

The specimen should be supported in a manner that does not preclude more than a small fraction of the specimen's surface, and the specimen should be completely immersed in the leachant, if it is possible without violating the surface-area-to-water-volume ratio constraint. At the end of each time interval, the specimen should be removed from the used leachant and placed into a new container with fresh leachant. This should be done as quickly as possible; in no case should the specimen be allowed

Table 2.5: Interval durations and total elapsed time for ANS 16.1. Intervals for the extended options are marked with a star.

Interval Duration	(hours)	2	5	17	24	24	24	24	336⋆	672⋆	1032⋆
	(days)	0.08	0.2	0.7	1	1	1	1	14⋆	28⋆	43⋆
Total Elapsed Time	(hours)	2	7	24	48	72	96	120	456⋆	1128⋆	2160⋆
	(days)	0.08	0.3	1	2	3	4	5	19⋆	47⋆	90⋆

to dry completely. A chart showing the interval durations and total elapsed time can be seen in Table 2.5.

Aliquots of the leachate should be taken at each interval and chemically analyzed to determine the quantity of nuclides released from the specimen during the leaching interval (for a given interval n, this is a_n). From this, the effective diffusivity and leachability index of the nuclide can be determined. To calculate the effective diffusivity for the nth interval, D_n,

$$D_n = \pi \left[\frac{a_n/A_0}{(\Delta t)_n}\right]^2 \left[\frac{V}{S}\right]^2 T, \tag{2.25}$$

where A_0 is the total quantity of the nuclide at the beginning of the first leaching interval, $(\Delta t)_n$ is the duration of the nth leaching interval, V is the volume of the specimen in cm^3, S is the specimen geometric surface area in cm^2, and T is the "mean time" of the leaching interval in seconds, as follows:

$$T = [\tfrac{1}{2}(t_n^{1/2} + t_{n-1}^{1/2})]^2. \tag{2.26}$$

If more than 20% of the nuclide has leached out, the effective diffusivity can only be calculated from a shape specific solution of the mass transport equation. Once the effective diffusivity for a given nuclide has been calculated for each interval, the leachability index, L, can be determined as follows:

$$L = \frac{1}{7}\sum_{n=1}^{7}\log(\beta/D_n), \tag{2.27}$$

where β is a defined constant, equal to 1.0 cm^2/s. If the extended test is performed, the leachability index is given the symbol $\bar{L}$ and calculated as follows:

$$\bar{L} = \frac{1}{10}\sum_{n=1}^{10}\log(\beta/D_n). \tag{2.28}$$

ANS 16.1 is a simple semi-dynamic tank leaching test requiring only a small amount of equipment to run. Once the samples are prepared, little work has to be done during the test other than filling new leaching vessels and transferring the specimens. ANS 16.1 is a fairly short test, just 5 days, but has the flexibility of the extended option, allowing for a test duration of 90 days. The unextended test at room temperature is definitely a suitable test for non-durable glasses, but the extended duration test may not be. The minimum dimension requirement of just 1 cm allows for a very small amount of glass to be a used. A cylindrical specimen measuring the minimum 1 cm in diameter and 1 cm heigh would require just 0.79 cm^3 of glass, or approximately 2.1 g of glass, assuming a fairly standard glass density of 2.6 g/cm^3. ANS 16.1 does require chemical analysis to be performed.

ANS 16.1, as compared to EPA Method 1315 and ASTM C1308, requires the smallest specimen. ANS 16.1 has more flexibility in the shape of the specimen than C1308 but less than Method 1315. ANS 16.1 can either be the shortest or the longest of the three tests, depending on whether the extended option is selected. The unextended version of ANS 16.1 can be viewed as a version of C1308 where the daily sampling is shortened to 5 days from 11 days. The extended version of ANS 16.1, in addition to being the longest of the three tests, also has the lengthiest interval durations, with the longest interval lasting 43 days.

Chapter 3

The Modified Associate Species Method

The Associate Species Method was developed to predict the phase relations in oxide melts [7, 71, 90], slags [10, 83, 85], and glasses [5, 19, 54]. Typically, the calculations are performed primarily using the programs ChemSage [31] and FactSage [15], however, licenses for these programs were not available to the author. Therefore, a program for solving associate species method problems was created using Mathematica [82] and verified by comparison with the work of Besmann and Spear. [18, 70]

3.1 Mechanics of the Associate Species Method

The thermodynamic data in the work of Besmann and Spear is given as the 298 K heat of formation ($\Delta H^{\circ}_{f,298}$ (J/mol)), the 298 K entropy (S°_{298} (J/mol·K)), the specific heat (C_p), and any necessary transition temperatures and their associated heats of formation (ΔH°_{trans}). The data for the Na_2O-Al_2O_3 system can be found in Table 3.1.

Table 3.1: Thermodynamic data for the Na_2O-Al_2O_3 system. After [18]

Species	$\Delta H^\circ_{f,298}$	S°_{298}	T	$C_p = a + bT + cT^2 + d/T^2$ (J/(mol·K))			
	(J/mol)	(J/(mol·K))	(K)	a	b (x10^3)	c (x10^6)	d (x10^{-5})
			Liquid Associate Species				
Na_2O	-370,284	108.989	1023	55.480	70.210	-30.540	-4.140
	ΔH°_{trans} (1023 K) = 1,757		1243	82.563	12.350	0	0
	ΔH°_{trans} (1243 K) = 11,924		1405	82.563	12.350	0	0
			3500	104.600	0	0	0
Al_2O_3	-1,564,604	98.679	2327	117.490	10.380	0	-37.110
			3000	192.464	0	0	0
$NaAlO_2$	-1,000,000	107.000	1000	86.485	40.295	-15.270	-20.625
			1923	100.027	11.365	0	-18.555
			3000	148.532	0	0	0
$Na_2Al_4O_7$:1/3	-1,234,000	95.000	1000	96.820	30.323	-10.180	-26.120
			1923	105.848	11.037	0	-24.740
			3000	163.176	0	0	0
			Crystalline Solids				
Na_2O	-417,982	75.040	1023	55.480	70.210	-30.540	-4.140
	ΔH°_{trans} (1023 K) = 1,757		1243	82.563	12.350	0	0
	ΔH°_{trans} (1243 K) = 11,924		1405	82.563	12.350	0	0
			3500	104.600	0	0	0
Al_2O_3	-1,675,692	50.940	2327	117.490	10.380	0	-37.110
			3000	192.464	0	0	0
			3500	104.600	0	0	0
$NaAlO_2$	-1,111,000	64.500	1000	86.485	40.295	-15.270	-20.625
			1923	100.027	11.365	0	-18.555
			3000	148.532	0	0	0
$NaAl_9O_{14}$	-7,873,000	262.000	1000	556.445	81.800	-15.270	-169.065
			2273	569.985	52.900	0	-166.995
			3000	918.390	0	0	0
$Na_2Al_{12}O_{19}$	-10,685,000	369.750	1000	760.420	132.490	-30.540	-226.800
			2000	787.503	74.630	0	-222.660
			3000	1259.445	0	0	0

Calculations begin by computing the value of ΔH_T° and S_T° for the liquid species at a given temperature. This is done using the following equations

$$\Delta H_T^\circ = \Delta H_{298}^\circ + \int_{298}^{T} C_p dT \tag{3.1}$$

$$S_T^\circ = S_{298}^\circ + \int_{298}^{T} \frac{C_p dT}{T}. \tag{3.2}$$

ΔG_T° for each species can then be calculated using the equation

$$\Delta G_T^\circ = \Delta H_T^\circ - T S_T^\circ. \tag{3.3}$$

For each of the liquid phases of associate species, the equilibrium constant (K_{eq}) for the reaction at the given temperature is then calculated. As the equilibrium constant is dependent only upon temperature, and not composition, K_{eq} can be used across the entire range of composition for the given temperature. K_{eq} is calculated using ΔG° of the reaction. As an example, for the associate species $NaAlO_2$, the equations would be as follows

$$\Delta G_R^\circ = 2\Delta G_{\mathrm{NaAlO_2}(l)}^\circ - \Delta G_{\mathrm{Na_2O}(l)}^\circ - \Delta G_{\mathrm{Al_2O_3}(l)}^\circ \tag{3.4}$$

$$K_{\mathrm{NaAlO_2}(l)} = \exp\left\{-\frac{\Delta G_R^\circ}{RT}\right\}. \tag{3.5}$$

Once calculated, the equilibrium constant can be used to determine the relative amounts of each species at every composition of the end-member species at the given temperature. The mole fractions of each species (Y) are then found by minimizing the

free energy of the system and enforcing the laws of mass action and mass balance. [68] For the Na_2O-Al_2O_3 system, the equations for mass action and mass balance are as such

$$K_{\mathrm{NaAlO_2}(l)} = \frac{Y^2_{\mathrm{NaAlO_2}(l)}}{Y_{\mathrm{Na_2O}(l)} Y_{\mathrm{Al_2O_3}(l)}} \tag{3.6}$$

$$K_{\mathrm{Na_2Al_4O_7}(l)} = \frac{Y_{\mathrm{Na_2Al_4O_7}(l)}}{Y_{\mathrm{Na_2O}(l)} Y^2_{\mathrm{Al_2O_3}(l)}} \tag{3.7}$$

$$X^*_{\mathrm{Al_2O_3}} = Y_{\mathrm{Al_2O_3}(l)} + \frac{1}{2} Y_{\mathrm{NaAlO_2}(l)} + \frac{2}{3} Y_{\mathrm{Na_2Al_4O_7}(l)} \tag{3.8}$$

$$1 - X^*_{\mathrm{Al_2O_3}} = Y_{\mathrm{Na_2O}(l)} + \frac{1}{2} Y_{\mathrm{NaAlO_2}(l)} + \frac{1}{3} Y_{\mathrm{Na_2Al_4O_7}(l)}, \tag{3.9}$$

where $X^*_{\mathrm{Al_2O_3}}$ is the mole fraction of Al_2O_3 in the end-member mixture. When this system of equations is solved for the Na_2O-Al_2O_3 system at 800 °C, the results are as shown in Figure 3.1. These results can be compared to Figure 2.1d. The activity curves have the same shape in both the computed results and in Besmann and Spear's work, though it should be noted that the actual values differ, particularly at and below the parts per million range. This can be attributed to different emphases in the way that the Mathematica program and ChemSage perform the calculations.

The free energy of the liquid solution is found using the equation

$$\begin{aligned} \Delta G^\circ_{T(l)} &= Y_{Na_2O(l)} \Delta G^\circ_{Na_2O(l)} + Y_{NaAlO_2(l)} \Delta G^\circ_{NaAlO_2(l)} \\ &\quad + Y_{Na_2Al_4O_7(l)} \Delta G^\circ_{Na_2Al_4O_7(l)} + Y_{Al_2O_3(l)} \Delta G^\circ_{Al_2O_3(l)} + G_{exs}, \end{aligned} \tag{3.10}$$

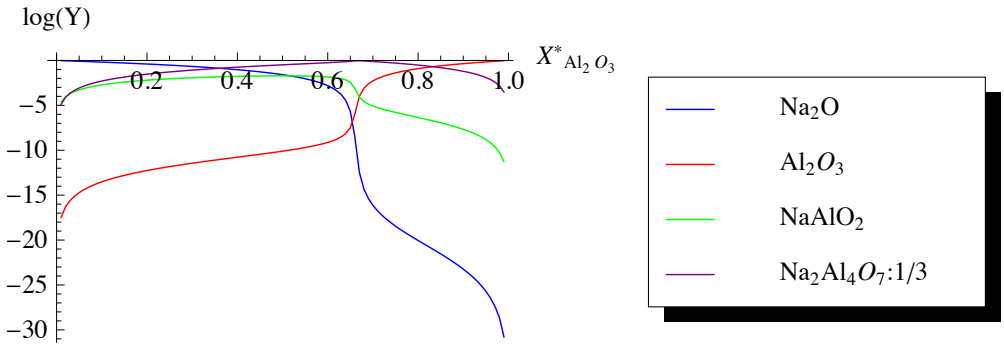

Figure 3.1: Computed mole fractions of the liquid species in the Na_2O-Al_2O_3 system at 800 °C.

where G_{exs} is the excess free energy term, which accounts for liquid-liquid immiscibility. [18] The equation for G_{exs} should be of the form

$$G_{exs} = X^*(1 - X^*)[(A_0 + A_1T) + B_0(1 - 2X^*)], \tag{3.11}$$

where the terms A_0, A_1, and B_0 are determined by trial and error. The computed free energy of the liquid solution in the Na_2O-Al_2O_3 system at 800 °C can be seen in Figure 3.2.

Now the crystalline solids must be considered. The free energy for each solid species can be calculated using Equations 3.1, 3.2, and 3.3. The free energy curves of the solid species are treated as though they have an extremely narrow stability range, so narrow that each solid phase is essentially a single point. Then the free energy of the solid solution is found using regular solution theory. [62] The computed free energy of the solid species and solid solution in the Na_2O-Al_2O_3 system at 800

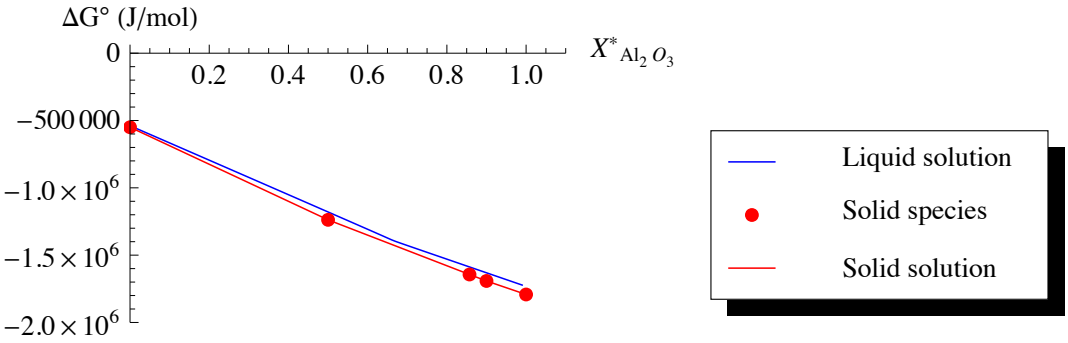

Figure 3.2: Computed free energy of the liquid solution, solid species, and solid solution in the Na_2O-Al_2O_3 system at 800 °C.

°C can be seen in Figure 3.2.

The phases of the system at the given temperature can then be found by minimizing the free energy of the system. A final phase diagram can be calculated by repeating these steps at every temperature in the range of interest. The final computed phase diagram of the Na_2O-Al_2O_3 system can be seen in Figure 3.3. There results can be compared to those of Besmann and Spear, found in Figure 2.1b. Differences in the liquid and two-phase regions are due to the formula for G_{exs} for the system not being supplied.

3.2 Results and Discussion

The CaO-K_2O-Na_2O-P_2O_5 system was chosen for phase diagram calculations, as these are the major constituents of the glass system of interest. To begin, potential

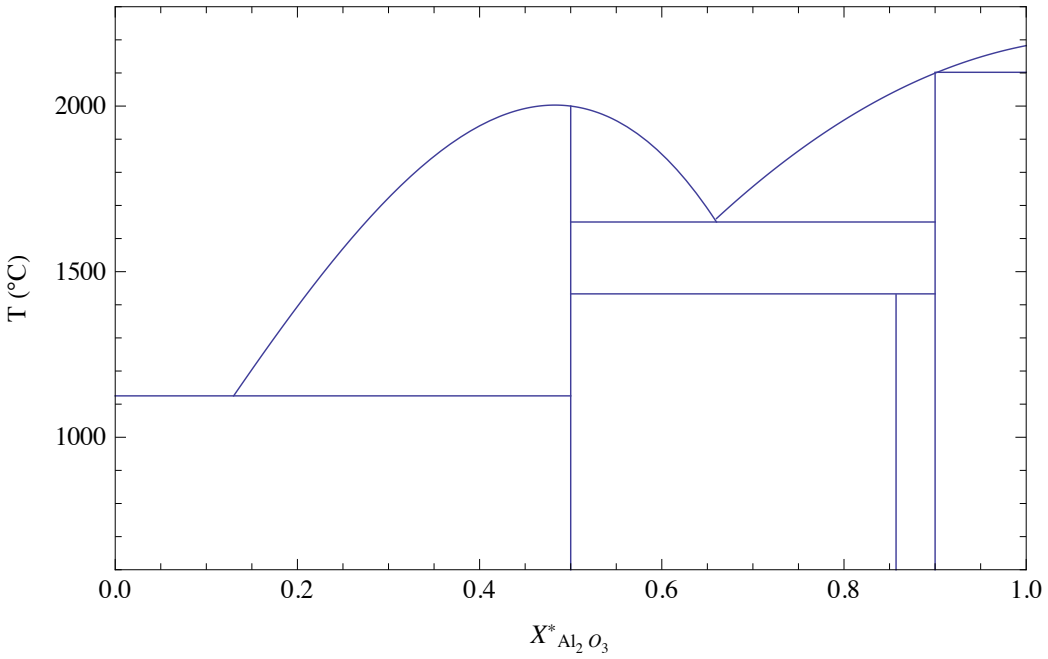

Figure 3.3: Computed phase diagram of the Na_2O-Al_2O_3 system.

species of interest had to be identified and thermodynamic data for those species must be located. These species are identified in Table 3.2. For almost all of the species identified, thermodynamic data was either missing or faulty. A large number of species in the CaO-P_2O_5 system had Gibbs free energy equations as a function of temperature published in Serena et al. (2006), however the publication had multiple errors. In one case, the same equation was given for different phases. Additionally, multiple typos meant that upon calculation, some of the results for Gibbs free energy were completely irrational. The formulas from this work were therefore deemed unacceptable for phases other than CaO and P_2O_5, values for which are widely available and therefore thoroughly vetted. The work of Sandstrom and Bostrom (2008) gave formulas for the Gibbs free energy as a function of temperature for species in

the CaO-K_2O-P_2O_5 system, but only for the solid phase. Formulas for Gibbs free energy as a function of temperature for species in the CaO-Na_2O-P_2O_5 system were published in La Iglesia (2009), however these values were found via regression calculations. Thirty-one crystalline compounds for which thermodynamic data already exists were used to calculate the contribution to the Gibbs free energy of 19 constituent units, including P_2O_5, Na_2O, K_2O, CaO, and H_2O, as both OH units and waters of hydration. The constituent units were then combined as:

$$\Delta G^\circ = \sum n_i g_i, \tag{3.12}$$

where n_i is the number of moles of the ith constituent unit per formula unit and g_i is the Gibbs free energy of the constituent unit. While this approach works well at a single temperature (for 82 values of ΔG°_{298}, 74 had an error of less than 1% and only 1 was more than 2%), only four species, three of which were calcium phosphates, were studied at high temperature, which in this publication was from 400 to 700 °C. It was therefore decided that the Gibbs free energy data in this publication was not thoroughly vetted across a wide enough range of systems and temperatures to use the Gibbs free energy data provided with this work. However, the method used in Equation 3.12 was used as a part of the phase diagram calculation efforts.

As the acceptable thermodynamic data for the CaO-K_2O-Na_2O-P_2O_5 system was extremely limited, the accuracy of using the method in Equation 3.12 was tested by comparing calculated phase diagrams against the published phase diagrams for this system. Phase diagrams for the sub-systems CaO-Na_2O-P_2O_5 (as $NaPO_3$ to

Table 3.2: Table of potential species of interest in the CaO-K_2O-Na_2O-P_2O_5 system, sorted by availability of thermodynamic data.

Acceptable Thermodynamic Data	Unacceptable Thermodynamic Data[1]	Data for Solid Phase Only[2]	Unacceptable Data For Solid Phase Only[3]	No Thermodynamic Data[4]
CaO[1]	$Ca(PO_3)_2$	$CaKPO_4$	$Ca_{10}O(PO_4)_6$	$CaK(PO_3)_3$
K_2O[5]	CaP_4O_{11}	$CaK_2P_2O_7$	$CaNaPO_4$	$CaNa(PO_3)_3$
Na_2O[5]	$Ca_2P_2O_7$	$CaK_4(PO_4)_2$	Na_3PO_4	$CaNa_4(PO_3)_6$
P_2O_5[1]	$Ca_2P_6O_{17}$	$Ca_{10}K(PO_4)_7$	$Na_4P_2O_7$	KPO_3
	$Ca_3(PO_4)_2$	$K_4P_2O_7$	$Na_4P_4O_{12}$	$K_5P_3O_{10}$
	$Ca_4O(PO_4)_2$		$Na_5P_3O_{10}$	$3\,NaPO_3 \cdot KPO_3$
				$NaPO_3$

[1] From [67]. Source had multiple typos and other errors. Values for CaO and P_2O_5, which are widely used, were assumed to be correct. Other values were deemed unacceptable.

[2] From [65].

[3] Thermodynamic properties for the solid phase estimated in [47], but values deemed unacceptable.

[4] Phase exists in phase diagrams from [1].

[5] From [84].

$Ca(PO_3)_2$), CaO-K_2O-P_2O_5 (as KPO_3 to $Ca(PO_3)_2$), and K_2O-Na_2O-P_2O_5 (as $NaPO_3$ to KPO_3) were found in *Phase Diagrams for Ceramists*. [1] The phase diagram for the $NaPO_3$-KPO_3 system was examined first, as it was the simplest of the three phase diagrams, containing only one intermediate species and one eutectic point. The Gibbs free energy as a function of temperature for P_2O_5, from Serena et al., along with the formation entropy and enthalpy data and heat capacity as a function of temperature for Na_2O and K_2O, from Yazhenskikh et al. (2006) was used to calculate the free energy for each species in the system. The phase diagram of this system has two temperatures of particular interest, at 547 and 552 °C. The computed free energies of the liquid solution, solid species, and solid solution for these two temperatures can be seen in Figures 3.4a and 3.4b, respectively. The G_{exs} equation used for the liquid solution was

$$\begin{aligned} G_{exs} &= X^*(1-X^*)[(A_0 + A_1T) + B_0(1-2X^*)] \\ A_0 &= 8.3988 * 10^6 \\ A_1 &= -9970.4502 \\ B_0 &= -33016.1954. \end{aligned} \tag{3.13}$$

The phase diagram calculated using this G_{exs} term can be seen in Figure 3.5a. When compared to the actual phase diagram, seen in Figure 3.5b, the 547 to 552 °C range is correct, as are the solidus and liquidus lines for $NaPO_3$ + $3\,NaPO_3 \cdot KPO_3$. However, while the solidus line for $3\,NaPO_3 \cdot KPO_3$ + KPO_3 is correct, the liquidus line is in correct. The melting point for KPO_3 is calculated as being 625 °C, while

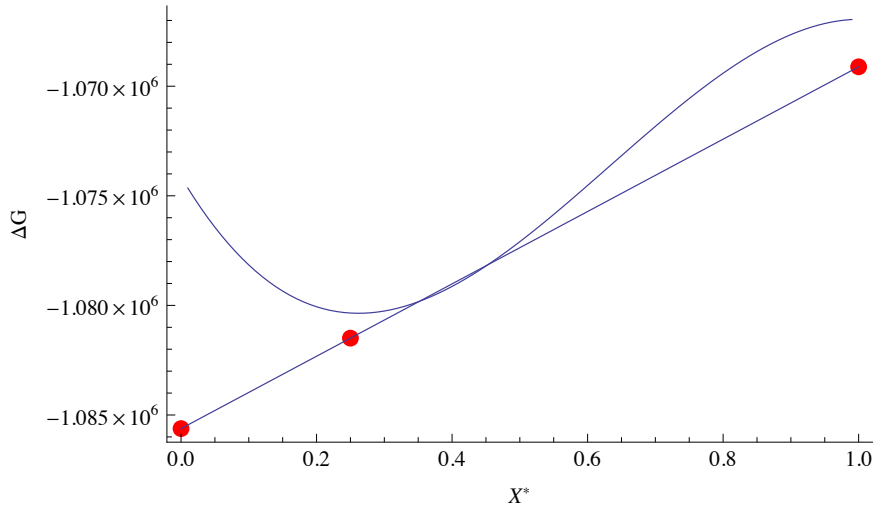

(a)

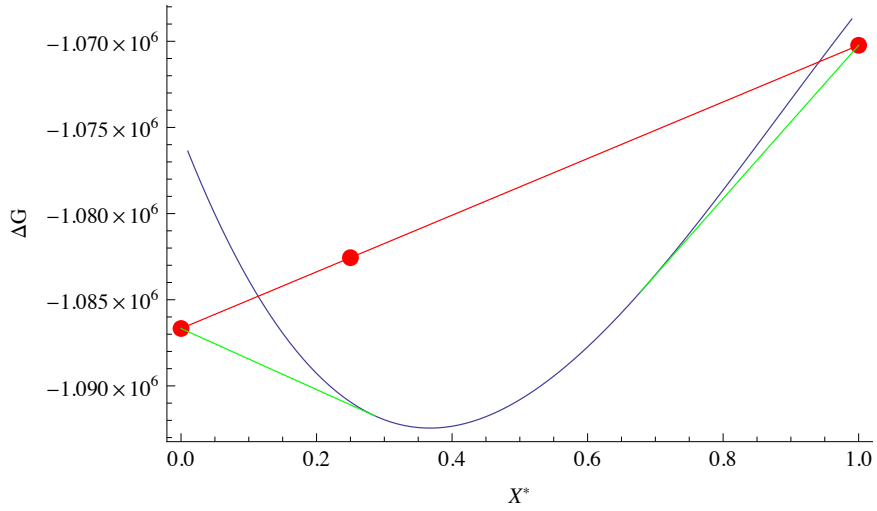

(b)

Figure 3.4: Computed free energy of the liquid solution, solid species, and solid solution in the $NaPO_3$-KPO_3 system at 547 °C (a) and 552 °C (b). (b) also shows tangent lines describing two-phase regions.

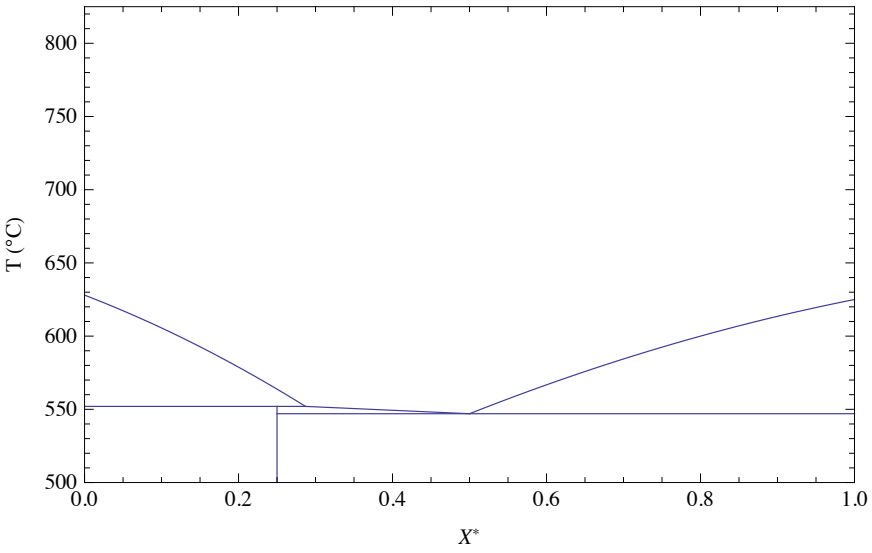

(a)

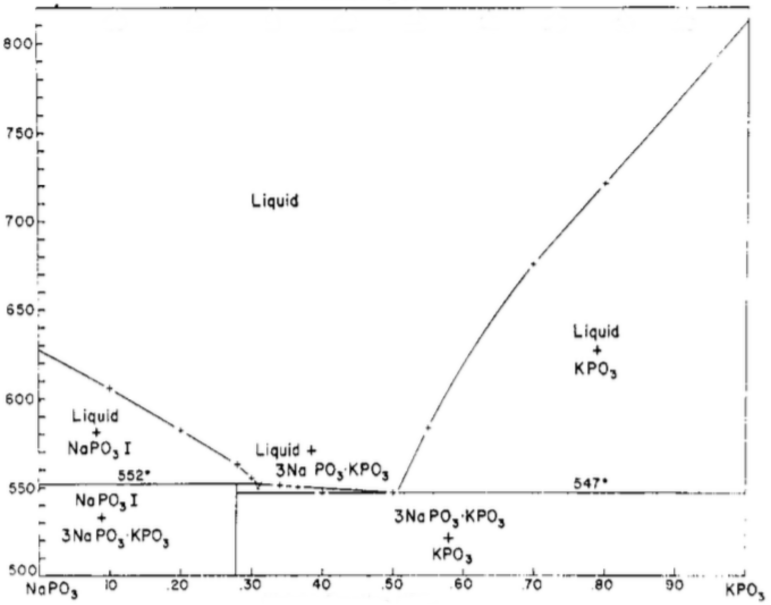

(b)

Figure 3.5: Computed phase diagram of the $NaPO_3$-KPO_3 system (a) and the actual phase diagram (b), reprinted with permission from [56]. Copyright 1954 American Chemical Society.

the correct melting temperature is 807 °C. There is therefore an issue with the thermodynamic data for KPO_3.

Because of the multiple issues with the thermodynamic data for this system, the only calculations that were performed were those to find the species activities in the liquid phase. The system X^* $Ca(PO_3)_2(1-X^*)(\frac{2}{3}NaPO_3\frac{1}{3}KPO_3)$ was chosen for its similarity to glasses produced in this work. Associate species used in the calculation were $3\,NaPO_3 \cdot KPO_3$, $CaNa_4(PO_3)_6$, $CaNa(PO_3)_3$, and $CaK(PO_3)_3$. These species were chosen due to their presence in the phase diagrams for the sub-systems $NaPO_3$-$Ca(PO_3)_2$, KPO_3-$Ca(PO_3)_2$, and $NaPO_3$-KPO_3. Additional associate species might be necessary to determine an accurate phase diagram in the CaO-K_2O-Na_2O-P_2O_5 system, however every species added increases the run time of the calculation. As few as 10 species can be enough to overwhelm the capabilities of a single computer; therefore, additional species must be selected with great care.

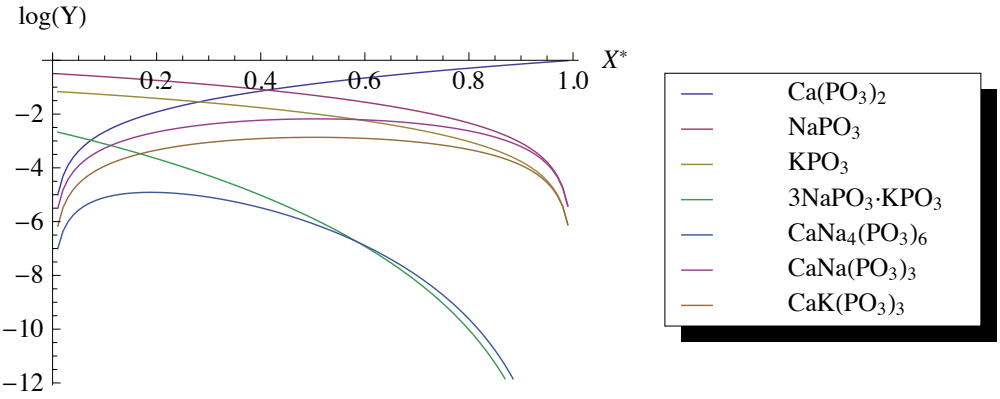

Figure 3.6: Computed mole fractions of the liquid species in the X^* $Ca(PO_3)_2(1-X^*)(\frac{2}{3}NaPO_3\frac{1}{3}KPO_3)$ system.

Chapter 4

Glass Formulation and Testing

4.1 Methods

Anhydrous calcium phosphate ($Ca_2P_2O_7$), potassium dihydrogen phosphate (KH_2PO_4), sodium hydrogen phosphate (Na_2HPO_4), ammonium dihydrogen phosphate ($NH_4H_2PO_4$), iron (III) oxide (Fe_2O_3), and manganese (II) chloride tetrahydrate ($MnCl_2{\cdot}4\,H_2O$) were mixed to form the targeted glass compositions. Seventeen formulations for glasses were melted. The first ten glasses were CaO-K_2O-Na_2O-P_2O_5 mixtures or submixtures (three glasses had no Na and one glass had no K). Glasses 11 through 14 added MnO to one of the existing formulations from the first ten glasses. Glasses 15 though 17 added Fe_2O_3 to existing formulations. Only Glasses 4, 7, 14, 15, 16, and 17 will be discussed, as these six glasses underwent some form of dissolution testing. The formulations of these six glasses can be seen in Table 4.1. The nominal composition for each glass can be seen in Table 4.2.

Glass 7 was based on Glass 4. In Glass 7, the actual weight of $Ca_2P_2O_7$ and $NH_4H_2PO_4$ was halved from that of Glass 4, while the weight of KH_2PO_4 and Na_2HPO_4 was kept the same. Glass 14 was based on Glass 9, which was in turn

Table 4.1: Formulations for glasses that underwent dissolution testing.

Weight %	$Ca_2P_2O_7$	Fe_2O_3	KH_2PO_4	$MnCl_2{\cdot}4\,H_2O$	Na_2HPO_4	$NH_4H_2PO_4$
Glass 4	40.44	-	11.23	-	11.72	36.61
Glass 7	32.90	-	18.27	-	19.06	29.78
Glass 14	32.84	-	13.19	3.07	13.75	37.16
Glass 15	40.30	3.07	11.20	-	8.93	36.50
Glass 16	32.78	3.13	18.21	-	16.21	29.68
Glass 17	32.72	3.15	13.14	3.06	10.91	37.02

based on Glass 7. Glass 14 kept the same KH_2PO_4:Na_2HPO_4 ratio as Glass 7 while increasing $NH_4H_2PO_4$ and $Ca_2P_2O_7$, plus had an addition of MnO in the form of $MnCl_2{\cdot}4\,H_2O$. Glasses 15, 16, and 17 are based on Glasses 4, 7, and 14, respectively. Approximately 3 weight % of Fe_2O_3 was added to each of the original glasses, replacing a portion of the Na_2HPO_4 content.

Once components were weighed and mixed, the glasses were melted in either alumina or porcelain crucibles. The first batch of a glass was melted in a small (5 mL) alumina crucible, while those glasses that were selected for further testing had larger melts made in larger (30 mL) porcelain crucibles. The crucibles were placed inside a room-temperature furnace and slowly raised to 1010 °C, soaking for an hour each at 300, 400, 500, and 800 °C. This was done to minimize spillover due to volatilization. The glass was also allowed to soak at 1010 °C for one hour, then was air quenched by pouring the melt onto a stainless steel pour plate. For some glasses, fibers were

Table 4.2: Nominal composition for glasses which underwent dissolution testing.

		CaO	Fe_2O_3	K_2O	MnO	Na_2O	P_2O_5
Glass 4	Weight %	21.31	-	4.64	-	6.11	67.94
	Mole %	37.76	-	4.90	-	9.79	47.55
Glass 7	Weight %	17.09	-	7.44	-	9.79	65.68
	Mole %	30.34	-	7.87	-	15.73	46.07
Glass 14	Weight %	17.91	-	5.64	1.04	7.42	67.99
	Mole %	32.18	-	6.03	1.48	12.06	48.26
Glass 15	Weight %	21.18	3.65	4.62	-	4.64	65.90
	Mole %	38.20	2.31	4.96	-	7.58	46.95
Glass 16	Weight %	16.98	3.68	7.40	-	8.30	63.64
	Mole %	30.69	2.33	7.96	-	13.58	45.44
Glass 17	Weight %	17.79	3.89	5.60	1.04	5.87	65.82
	Mole %	32.57	2.50	6.11	1.50	9.72	47.61

drawn by hand before quenching. After fibers were drawn, the crucible would be replaced in the furnace and allowed to return to temperature before the remaining melt was quenched.

Selected glasses underwent dissolution testing based on PCT-B, as this test is suitable for non-durable glasses and has limited equipment requirements. However, due to the small amounts of glass produced, the specimen size for testing was no larger than 50 mg. Glass was crushed and sieved to 200 to 325 mesh (45 to 75 μm) and the specimen was placed in a test tube with 15 mL of leachant (DI water, citric acid solution, or hydrochloric acid solution). The test tubes were sealed and placed in a water bath held at 40 °C by a hot plate. At the end of the test period, the test tubes were removed from the water bath, rinsed, and filtered to retain undissolved glass particles. For some tests, the filtered leachate was tested for pH and stored for chemical analysis. The filtered contents of the test tube were allowed to air dry and were weighed to determine the mass lost during the testing period. For some tests, when enough glass remained after testing, the specimens were mounted on glass slides for SEM and/or XRD analysis.

4.2 Results and Discussion

Four dissolution tests were performed on six glass formulations. The first test examined Glasses 4, 7, and 14. These glasses were tested in a 2% citric acid solution (pH = 2.2) at 40 °C. Powdered specimens weighing 38 to 50 mg were used. Intervals for this test were 6 hours, 1 day (24 hours), 2 days (48 hours), and 1 week (168

hours). The three glasses performed very similarly. At the 6 hour mark, all three glasses had lost 10 to 15% of their original mass. At the end of the test, all three glasses had lost 60 to 70% of their original mass. A graph of the results can be seen in Figure 4.1a, while the raw data can be found in Table A.1.

The second test was performed using powdered specimens weighing 22 to 44 mg. A 2% citric acid solution (pH = 2.2) at 40 °C was used, and intervals for this test were 6, 24, 48, and 168 hours. This test examined Glasses 15, 16, and 17. These three glasses are equivalent to Glasses 4, 7, and 14 with the addition of Fe_2O_3. While the predecessor glasses performed in an almost identical manner, these glasses did not. Both Glass 15 and Glass 17 had gained weight at the 6 hour mark, while Glass 16 had neither lost nor gained weight. All three glasses had a lower dissolution rate than their iron-free counterparts, which is as expected. However, even though the three glasses had similar amounts of Fe_2O_3 added, the final weight lost after 1 week was much lower for Glass 15 (12.5%) than for Glasses 16 or 17 (52.6% and 40.9%, respectively). A graph of the results can be seen in 4.1b, while the raw data can be found in Table A.2.

The third test examined the results of using differing leachants with Glass 17. All specimens, which weighed 28 to 32 mg, were tested at 40 °C for 6, 24, 48, and 168 hours. The leachants used were DI water, a hydrochloric acid solution at pH 2, a hydrochloric acid solution at pH 4, a hydrochloric acid solution at pH 5.5, a citric acid solution at pH 4, and a citric acid solution at pH 5.5. The results were compared with the results for Glass 17 from dissolution test 2, to have results from

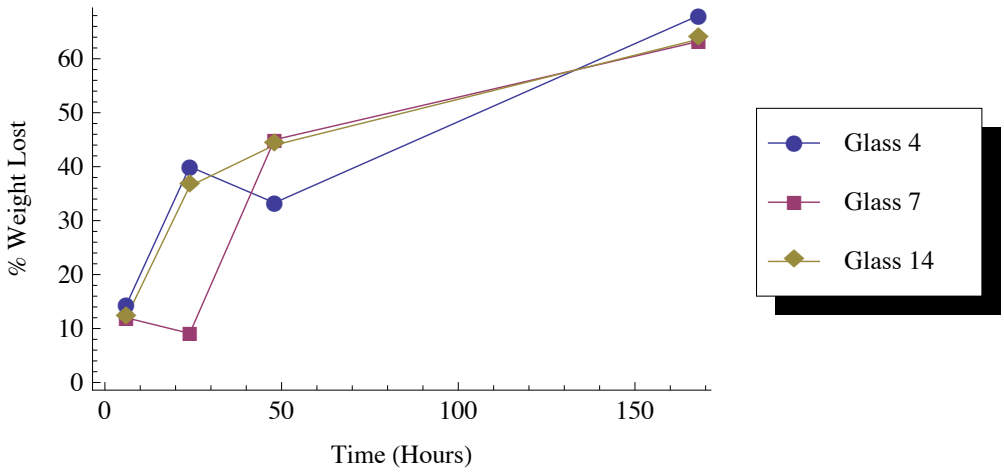

(a)

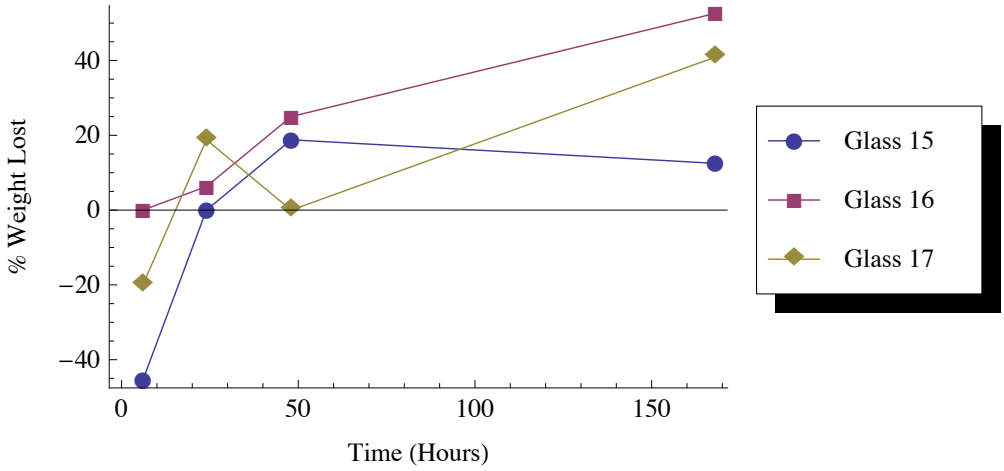

(b)

Figure 4.1: Results from dissolution tests 1 (a) and 2 (b). All glasses tested in a 2% citric acid solution (pH = 2.2) at 40 °C. A negative value indicates weight gain.

a citric acid solution near pH 2 for comparison. The three glass specimens in water and acid solutions at pH 5.5 were found to have gained weight at the end of the testing period. The two specimens at pH 4 either had no change in mass or had lost very little weight. Only those specimens tested at pH 2 showed any significant weight change after one week of testing. The specimen tested in a hydrochloric acid solution at pH 2 had lost more than 85% of its original mass, with the majority of that weight loss occurring in the first 24 hours (73.3% weight lost). A graph of the results can be seen in Figure 4.2, while the raw data can be found in Table A.3.

Based on the results of the first three dissolution tests, the final test was performed using Glass 17 and hydrochloric acid and citric acid solutions at pH 2 and 40 °C. The glass was tested in triplicate in hourly intervals for 1 to 24 hours. A graph of the results can be seen in Figure 4.3a, while the raw data can be found in Tables A.4 and A.5. The pH of the leachate was measured, and a graph of the change in pH

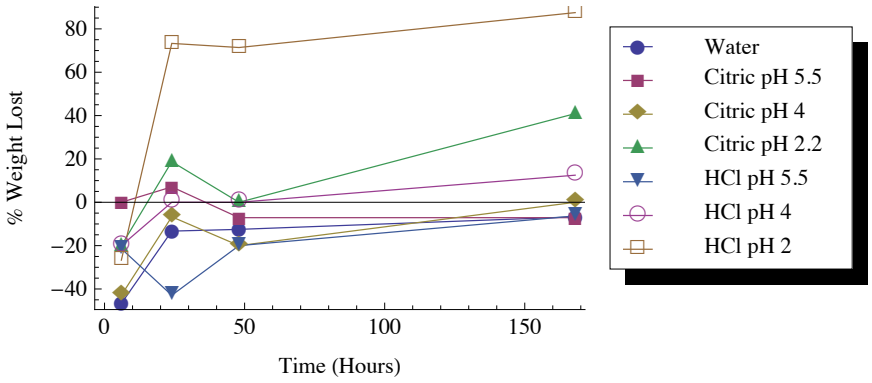

Figure 4.2: Results from dissolution test 3. All tests performed on Glass 17 at 40 °C in DI water, citric acid solutions, or hydrochloric acid solutions at varying pH. A negative value indicates weight gain.

can be found in Figure 4.3b. The raw data can be found in Table A.6. The citric acid acted as a buffer solution, and the pH never rose more than 0.2 points from the initial pH. The hydrochloric acid leachate, however, increased in pH until the 10 hour mark, then leveled out near 0.5 pH points gained.

ICP-OES was performed on leachate from 1, 6, 12, and 24 hour tests. The leachate from all triplicates was combined into one solution for testing, nominally totaling 45 mL. The concentration results for Fe, Mn, Ca, K, and Na can be seen in Figure 4.4 and the raw data can be found in Table A.7. Next, the elemental mass release is normalized, using

$$N_i = \frac{c_i \cdot V}{f_i \cdot m_s}, \tag{4.1}$$

where c_i is the measured concentration of element i, f_i is the nominal mass fraction in the glass of element i, V is the solution volume, and m_s is the mass of the specimen(s). N_i is the fraction of the total available elemental content in the glass that has been released during testing. Graphs showing the normalized elemental mass release can be seen in Figure 4.5. For both the hydrochloric acid and citric acid leachates, the Mn release goes above 100%. This artifact is likely due to the measured Mn content in the leachate being outside the tolerable range for the standard used for calibration of the ICP-OES.

Ma states that "If all glass constituents are released into solution in the same proportion as they are present in the solid, congruent dissolution is observed and [the release rate] is the same for all elements." [53] The release rate is similar for the

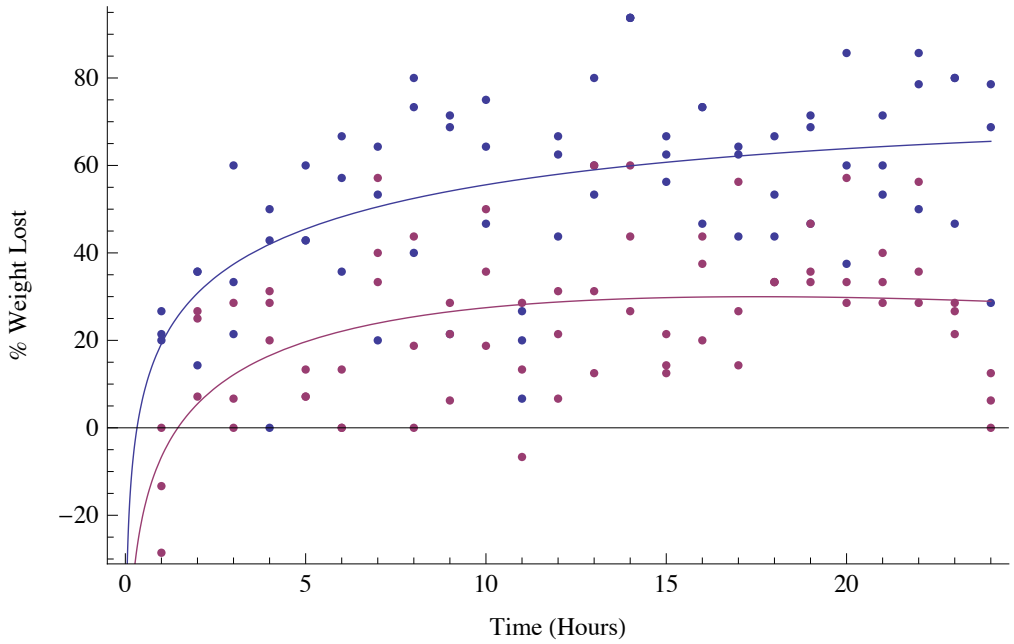

(a)

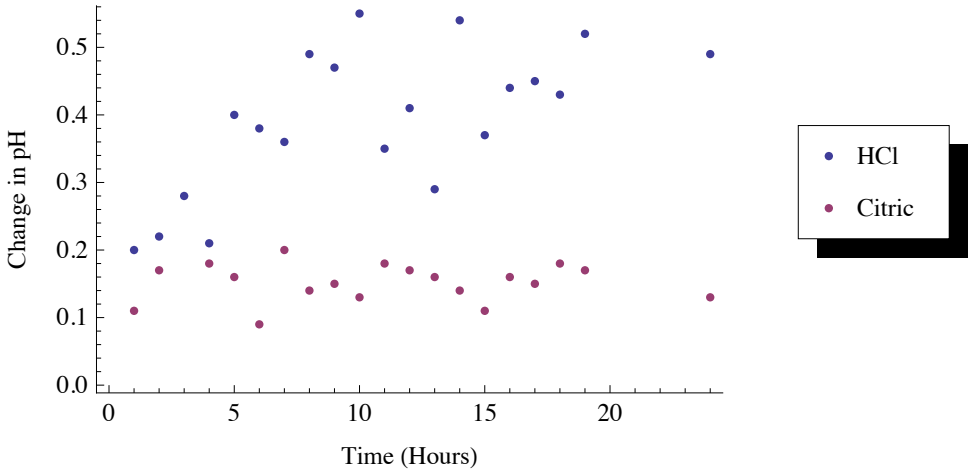

(b)

Figure 4.3: Results from dissolution test 4. All tests performed on Glass 17 at 40 °C in either a hydrochloric acid solution at pH 2 ± 0.04 or a citric acid solution at pH 2 ± 0.08. A negative value indicates weight gain. (a) shows the percent weight loss of the specimens. Lines are drawn as a guide for the eye. (b) shows the change in pH of the solution after testing.

elements measured, with the absolute concentration at 24 hours being approximately 1.5 times that at 1 hour for both hydrochloric acid and citric acid leachate. K, Na, Fe, and Mn are very close to that ratio, while Ca is off a bit (2.7 to 3.3), likely due to the very low concentrations of Ca in solution. However, the proportions of these

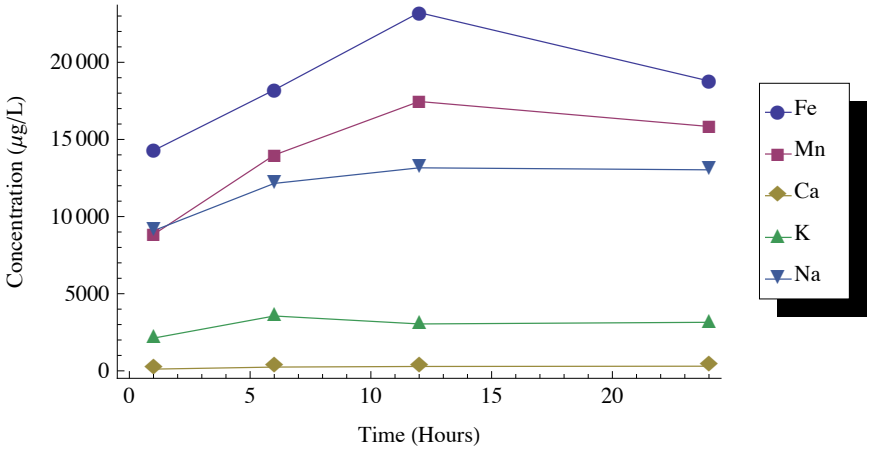

(a)

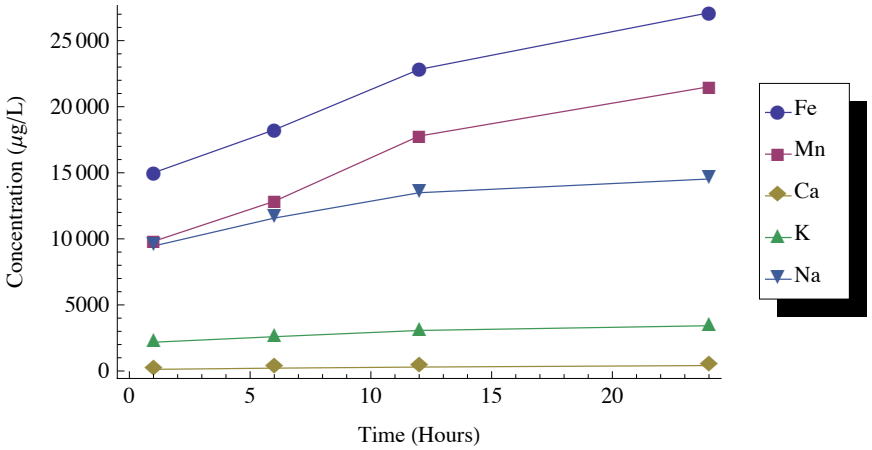

(b)

Figure 4.4: ICP-OES results for hydrochloric acid (a) and citric acid (b) leachates.

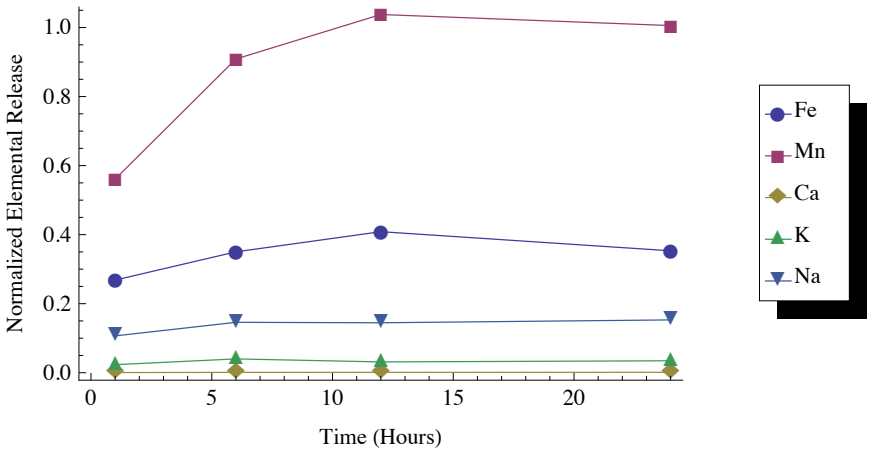

(a)

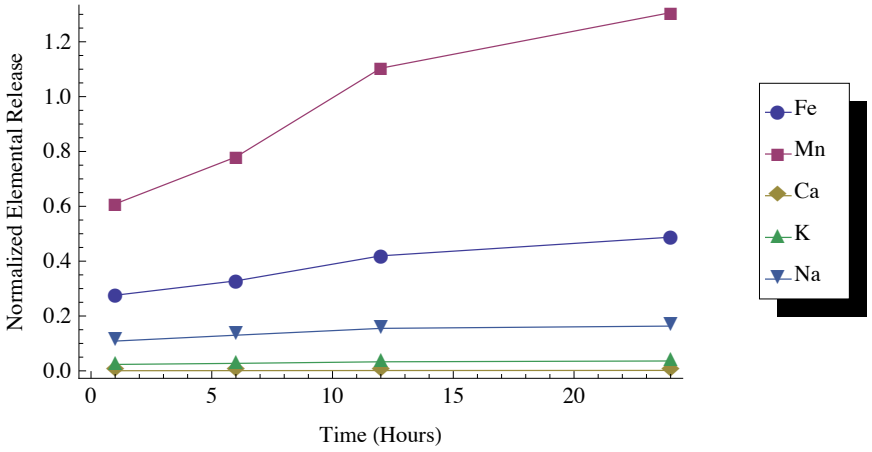

(b)

Figure 4.5: Normalized elemental mass release for hydrochloric acid (a) and citric acid (b) leachates. The normalized elemental mass release is equivalent to the fraction of the total available elemental content in the glass that has been released during testing

elements in the leachate are not the same as that in the glass. Fe and Mn have the highest release, while in the glass they are the smallest components. Additionally, the Ca release is extremely low, when Ca is the second-largest constituent of the glass, following P_2O_5. This indicates that the glass is leaching, not dissolving congruently.

Several specimens of glass were examined by scanning electron microscopy after testing. For comparison, a specimen of untested glass was also examined. A micrograph of the untested glass, seen in Figure 4.6, shows the average particle size, excluding adhering fines, is measured to be 59 by 94 μm, or an average diameter of 76 μm. Conchoidal fracture lines and cracks can be seen on some particles. After just one hour (Figure 4.7), evidence of heterogeneous surface attack can be seen. Etch pits are present on the surface of the glass, and preferential attack of pre-existing cracks has occurred, as evidenced by the widening and blunting of cracks.

After four hours, crazing can be seen on the surface of the particles that have been tested in the citric acid solution (Figure 4.8). Etch pits continue to develop and crack blunting is more pronounced. After eight hours, crazing can also be seen on the hydrochloric acid specimens (Figure 4.9a), while the citric acid specimens (Figure 4.9b) are experiencing spallation of the topmost layer of material. The measured average particle diameter is 64 μm for the hydrochloric acid specimen and 60 μm for the citric acid specimen, a difference of 12 and 16 μm, respectively.

At 16 hours, the hydrochloric acid solution specimen is also experiencing spallation (Figure 4.10a). A very interesting particle can be seen in the micrograph of the

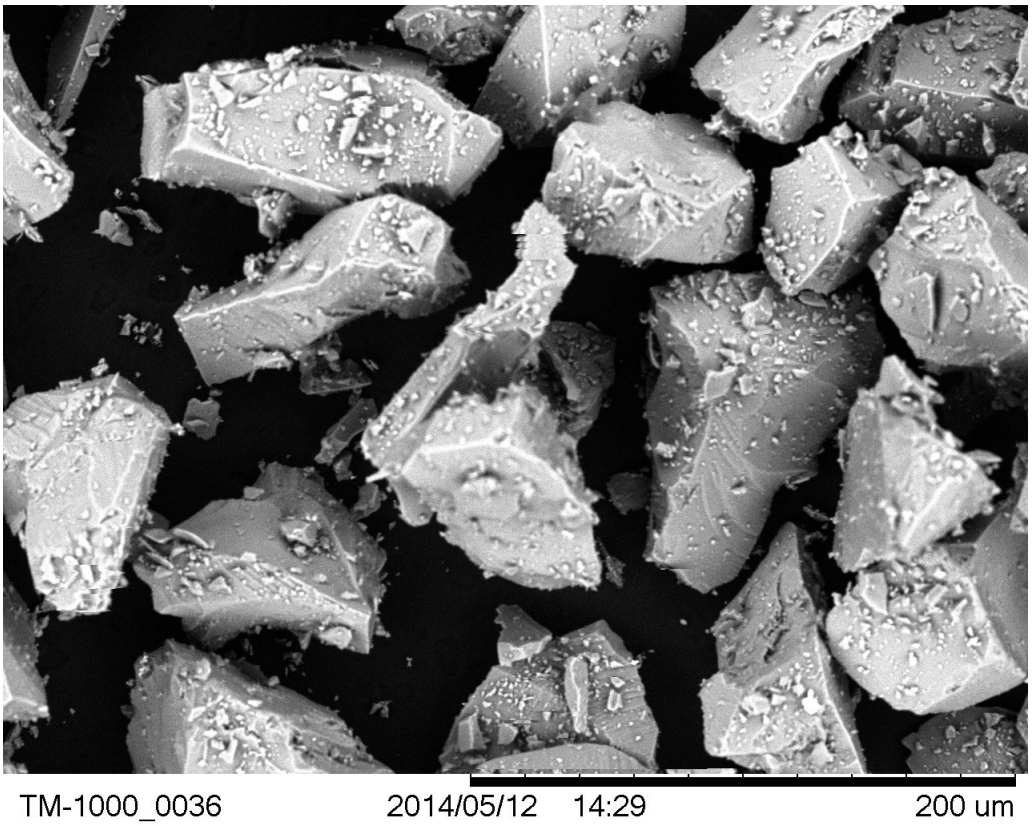

Figure 4.6: SEM micrograph of untested Glass 17. The average particle size, excluding adhering fines, is measured to be 59 by 94 μm.

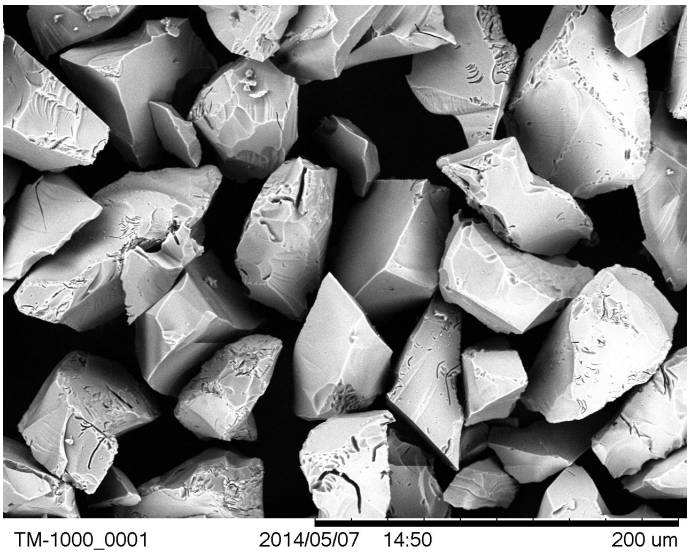

(a)

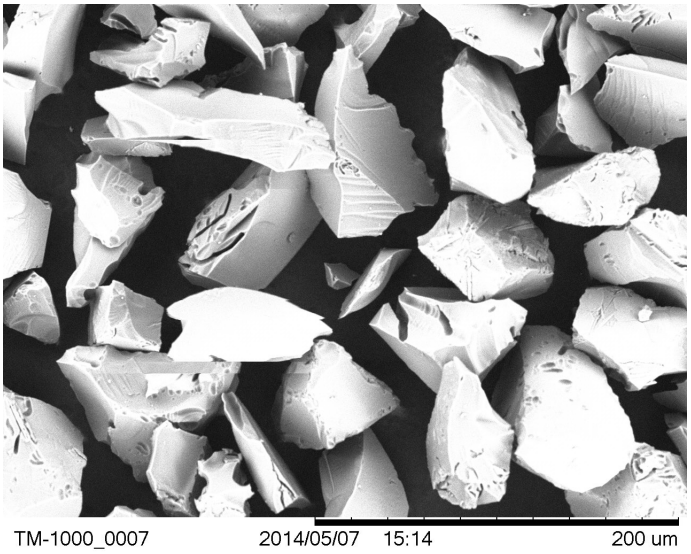

(b)

Figure 4.7: SEM micrographs of Glass 17 after 1 hour in a hydrochloric acid solution at pH 2 (a) and a citric acid solution at pH 2 (b). Both specimens show evidence of heterogeneous surface attack, including etch pits and preferential attack of existing cracks in the glass.

citric acid specimen (Figure 4.10b). This particle has a section of the topmost layer that has spalled off, revealing the remaining glass underneath. The remaining glass also shows signs of crazing and possibly spallation, clearly indicating that a cycle of heterogeneous surface attack is occurring. For glass in the hydrochloric acid solution, evidence of a crazing-spalling cycle can be seen after 22 hours (Figure 4.11).

Bunker et al. (1983) describe this behavior occurring in mixed sodium-potassium-silicate glasses. As the leachant diffuses into the glass, the surface layer is hydrated.

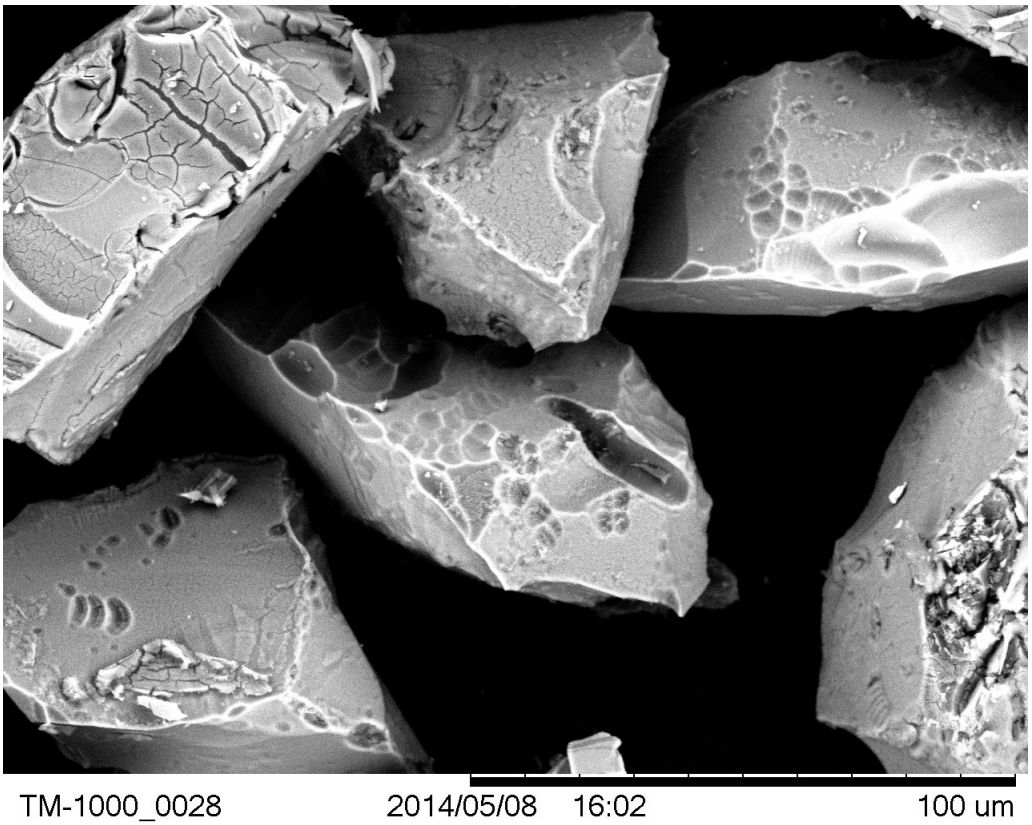

Figure 4.8: SEM micrograph of Glass 17 after 4 hours in a citric acid solution at pH 2. Pitting is more extensive and crazing can be seen on some particles.

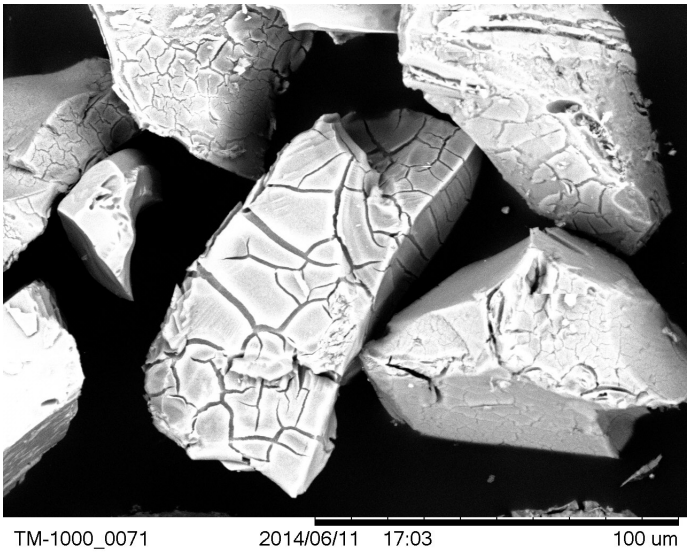

(a)

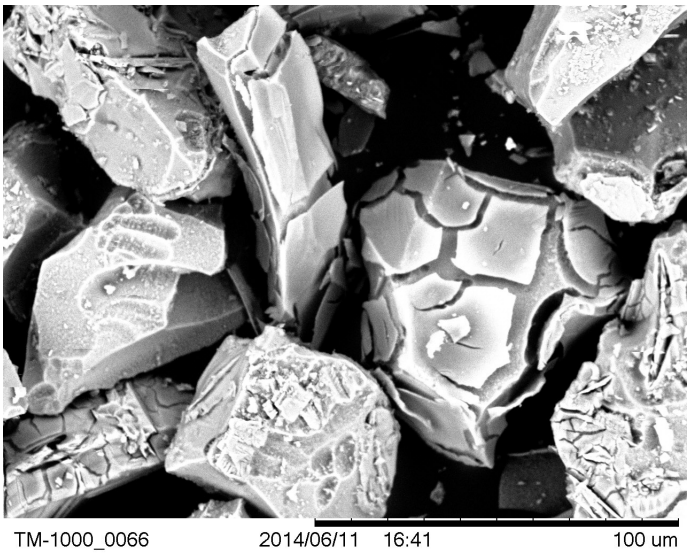

(b)

Figure 4.9: SEM micrographs of Glass 17 after 8 hours in a hydrochloric acid solution at pH 2 (a) and a citric acid solution at pH 2 (b). Crazing can be seen on the HCl specimen, while the citric acid specimen is experiencing spallation of the topmost layer of material. The measured average particle diameter is 64 μm for the HCl specimen and 60 μm for the citric specimen.

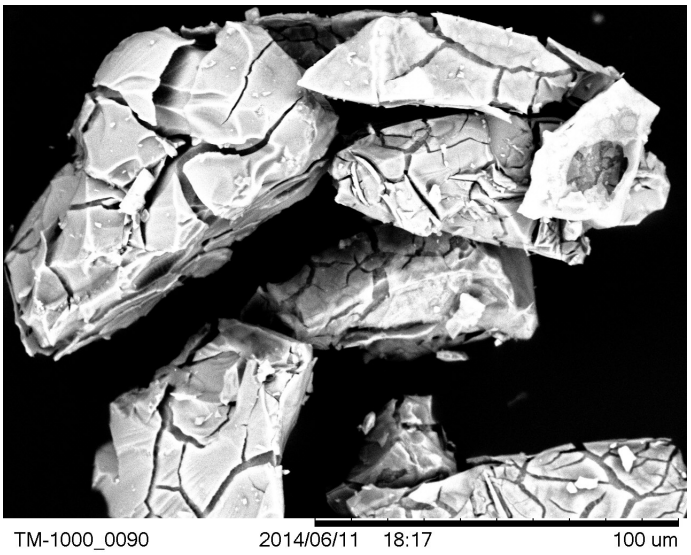

(a)

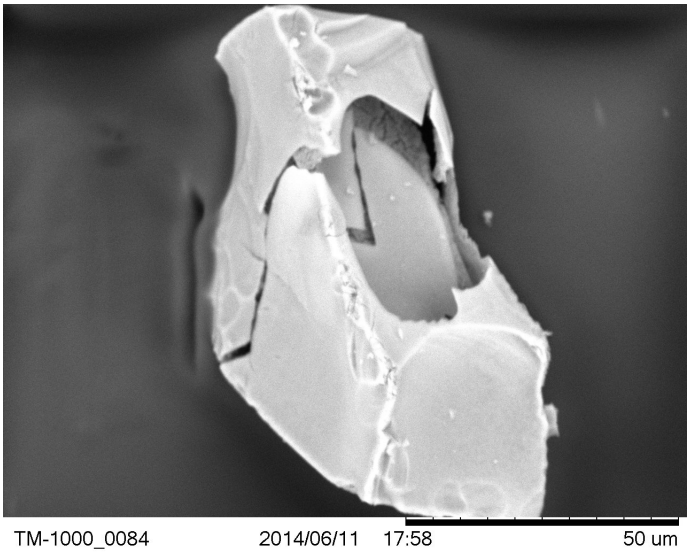

(b)

Figure 4.10: SEM micrographs of Glass 17 after 16 hours in a hydrochloric acid solution at pH 2 (a) and a citric acid solution at pH 2 (b). The hydrochloric acid specimen is spalling. The citric acid specimen shows a cycle of crazing and spallation, as part of the topmost layer has spalled off, revealing crazing on the surface beneath.

Under leaching conditions, this causes this layer to be brittle, and tensile stresses in the material cause the surface to craze. There is a sharp interface between the surface layer and the glass underneath it. While the surface layer remains intact, the interface moves into the glass at a constant rate. When the surface layer spalls off, however, fresh glass is exposed to the leachant, causing a cycle of crazing and spalling. However, in Bunker, Arnold, and Wilder's 1984 paper on phosphate glass dissolution, spalling is only said to occur in basic solutions. Their XRD results show

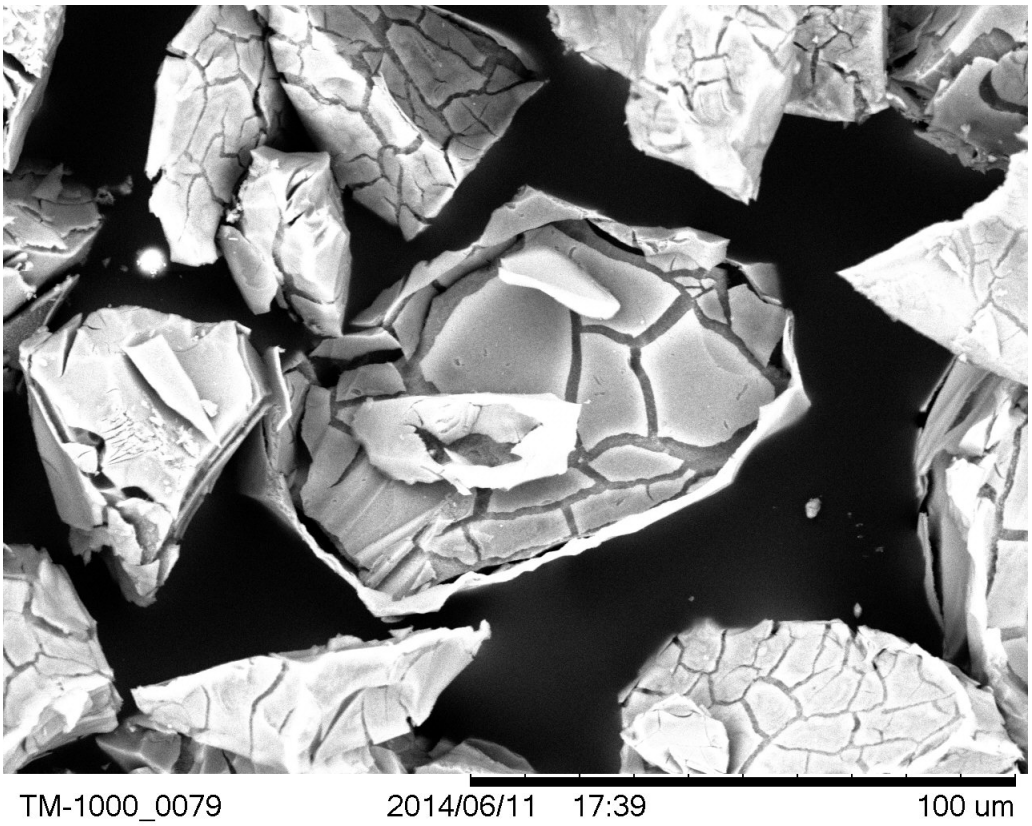

Figure 4.11: SEM micrograph of Glass 17 after 22 hours in a hydrochloric acid solution at pH 2. This specimen is also showing a crazing-spalling cycle, as a layer of material can still be seen along the outside edges of the particle.

that the material that is spalling off the surface is actually crystals of hydroxyapatite.

XRD results for this glass after 24 hours in citric acid solution show only mild crystalline behavior, as shown in Figure 4.12. The crystalline material is not hydroxyapatite, but is instead likely a calcium phosphate or sodium calcium phosphate crystal, as seen in Figure 4.13.

The dissolution data obtained from test number 4 was fit to the shrinking-core models used by Ma (Equations 2.15 and 2.16), using the fraction weight lost as α. Graphs showing the models as fitted can be seen in Figure 4.14. As there is a correlation between crazing occurring and deviation from $t^{1/2}$ leaching kinetics [23], the break point between the diffusion model and the contracting volume model was chosen to be 8 hours for hydrochloric acid and 4 hours for citric acid.

For hydrochloric acid, the first 8 hours of testing were fitted using the diffusion model, while hours 8 to 24 were fitted to the contracting volume model. k_{DM} was found to be 0.0986, while k_{CVM} was equal to 0.00266. The fit for hydrochloric acid was quite good, as seen in Figure 4.15a. For citric acid, however, there is a large scatter in the data, as seen in Figure 4.15b. The first 4 hours of data were fit to the diffusion model, while hours 4 to 24 were fit to the contracting volume model. k_{DM} was found to be 0.124, while k_{CVM} was equal to 0.00231.

The numbers given by the fits in this scenario are logical. A lower k_{DM} indicates that diffusion of the solution into the glass is slower. k_{DM} for citric acid was found to be higher than k_{DM} for hydrochloric. Since crazing (the break point between

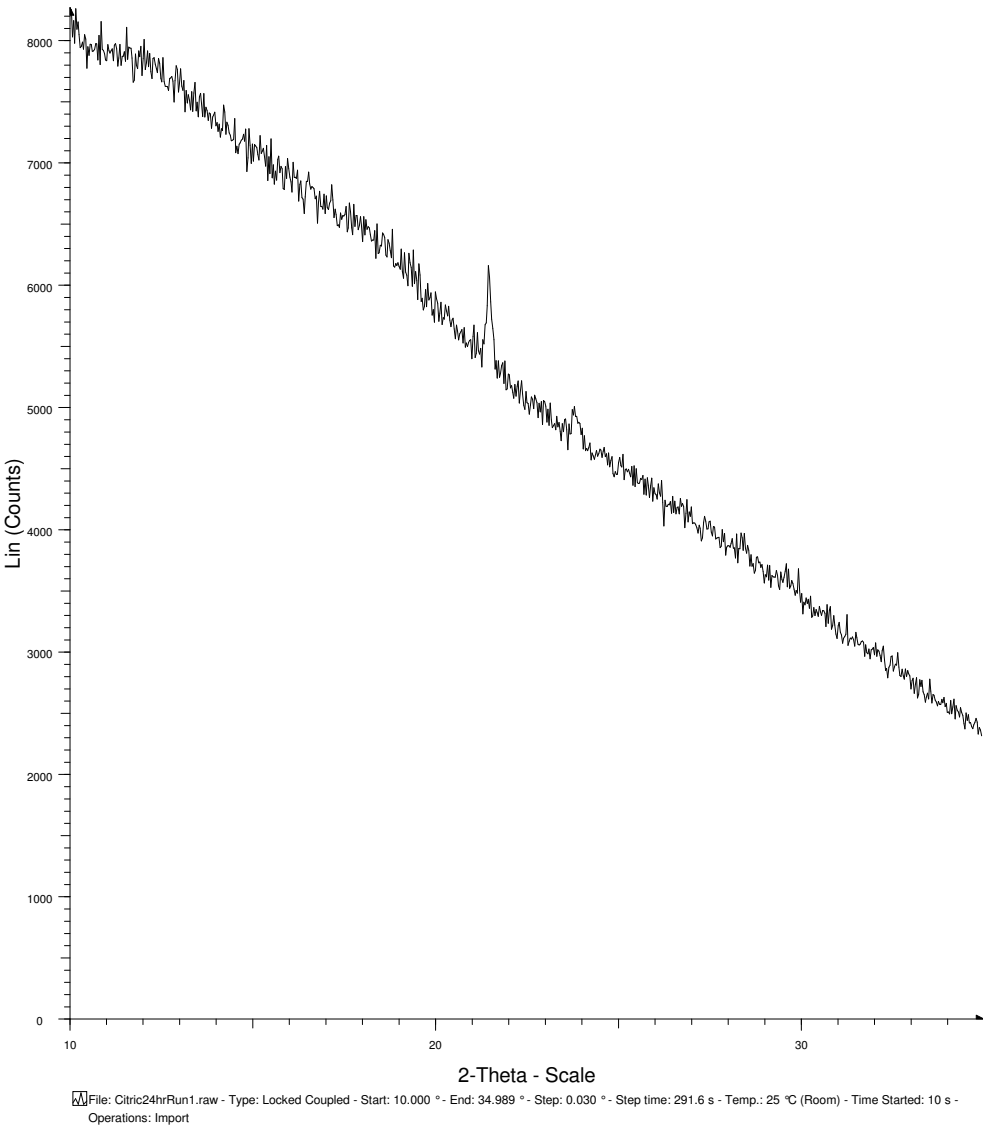

Figure 4.12: Raw data from XRD scans of the glass after 24 hours in citric acid solution. Results show mostly the amorphous hump, with a small amount of crystallinity present.

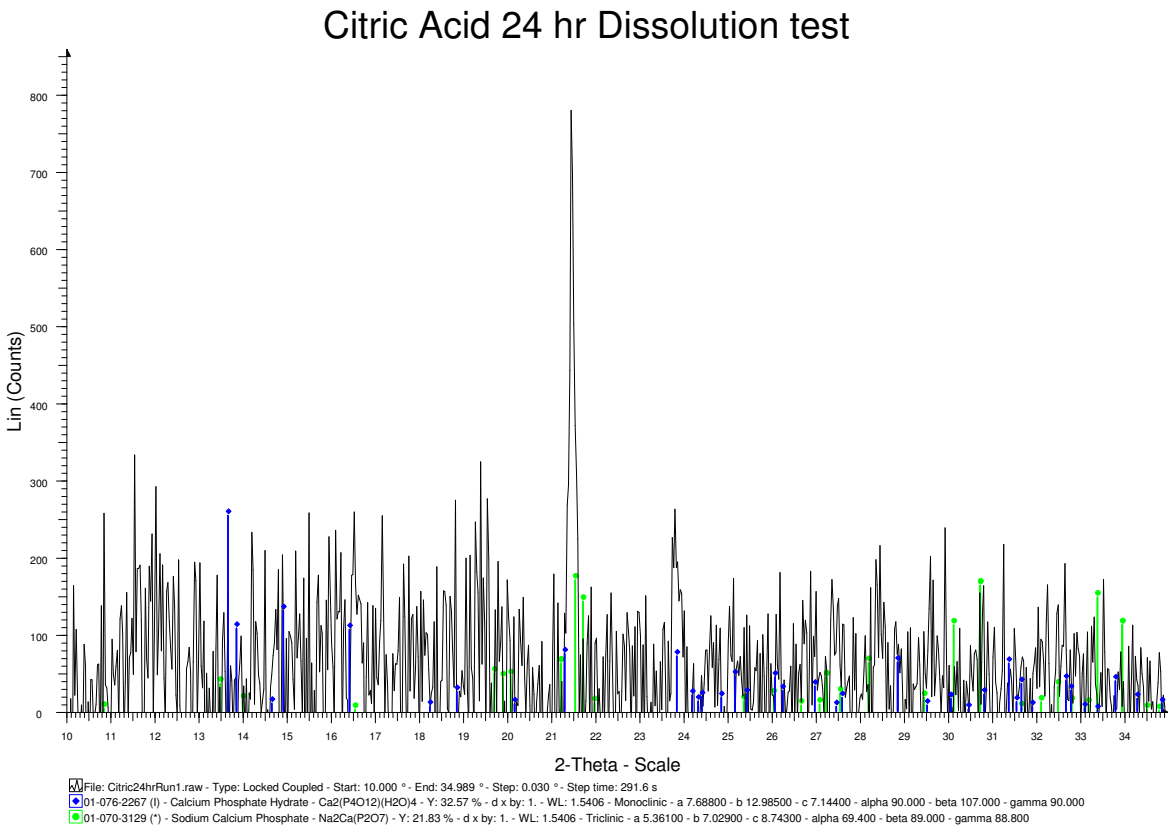

Figure 4.13: XRD scans with amorphous background subtracted out. Possible phases that fit the pattern include calcium phosphate and sodium calcium phosphate crystals, shown in blue and green, respectively.

models) was seen earlier in citric acid solutions than hydrochloric acid solutions (4 and 8 hours, respectively), it is expected that k_{DM} for citric would be higher. k_{CVM} for the two leachants is almost identical (0.00266 for hydrochloric acid versus 0.00231 for citric acid). As the contracting volume model deals with the hydration rates of bonds in the glass, it is logical that the same glass would have similar rates in similar leachants (acid solutions at pH 2).

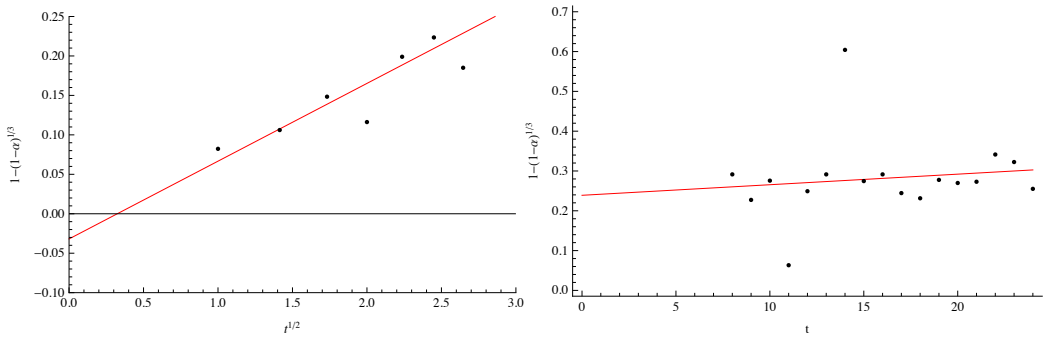

(a) $k_{DM} = 0.0986$ (b) $k_{CVM} = 0.00266$

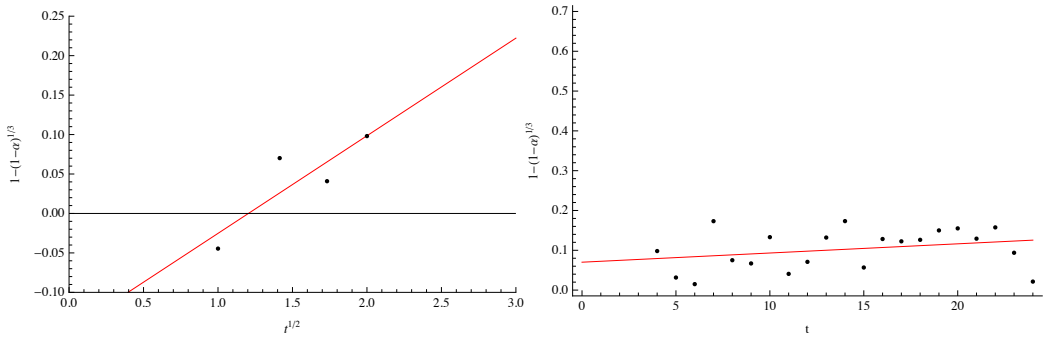

(c) $k_{DM} = 0.124$ (d) $k_{CVM} = 0.00231$

Figure 4.14: Shrinking-core models fit to dissolution test 4 data. The fits for the hydrochloric acid solution can be seen in (a) & (b), while the citric acid solution can be found in (c) & (d).

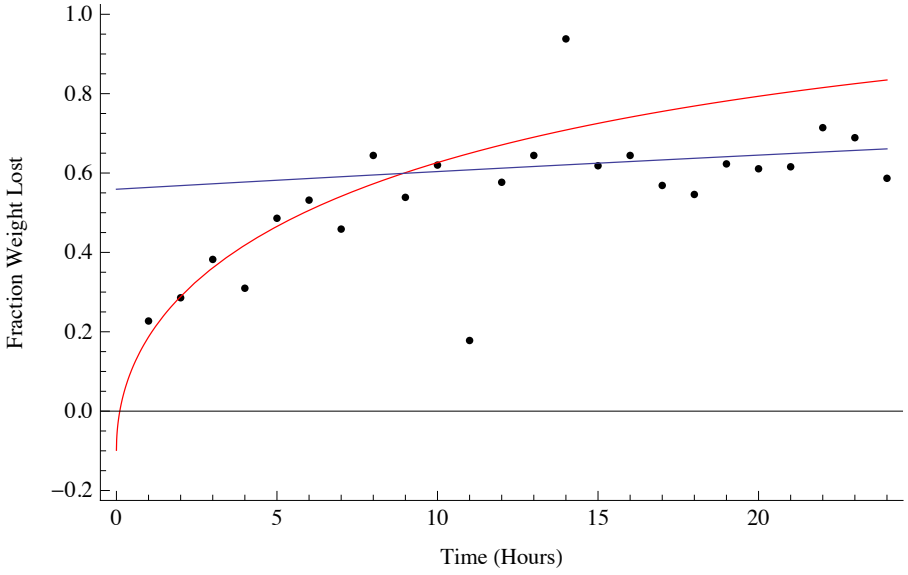

(a)

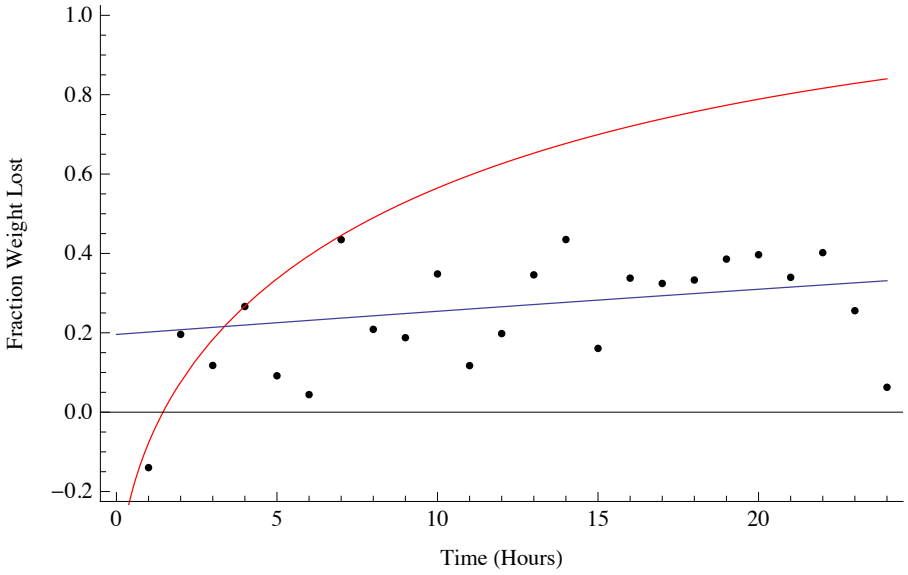

(b)

Figure 4.15: Shrinking-core model fits compared to the average fraction weight lost. The model fits the hydrochloric acid data (a) quite well, while the scatter in the citric acid data (b) makes for a less good-looking fit. In both graphs, the red line is the diffusion model and the blue line is the contracting volume model.

Finally, attempts were made to draw the glass into fibers. Experiments showed that while fibers could be drawn at temperatures as low as 950 °C, the quality of the fibers was best at or above 1000 °C. Fibers up to approximately one meter in length were drawn by hand. No mechanical fiber drawing was attempted.

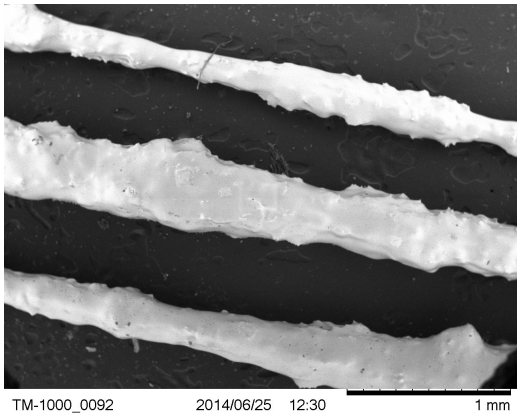

(a)

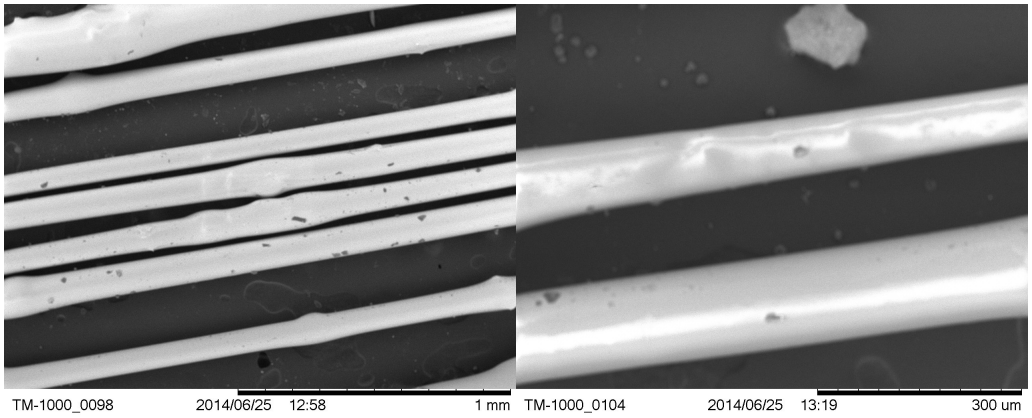

(b) (c)

Figure 4.16: SEM micrograph of glass fibers drawn at 950 °C (a), 1000 °C (b), and 1025 °C (c).

4.3 Conclusion

Contrary to popular belief, this work shows that not all phosphate glasses act like Type V glasses according to Hench and Clark's classification system. ICP-OES analysis of the leachate shows that selective leaching of the glass is occurring. SEM analysis of specimens following dissolution testing does show some evidence of heterogenous surface attack, common to Type V glasses, but a crazing-spalling cycle quickly dominates the reaction. Fitting shrinking-core models to the weight loss data, in conjunction with the time of onset of crazing, provides a very good fit for the hydrochloric acid specimens, but a less good fit for the citric acid specimens, due to the scatter in the data. This glass is a Type IV glass, meaning it develops a non-protective surface layer during dissolution. [35]

Chapter 5

Future Work

A hydro-biodegradable glass has been developed that contains macro- and micro-nutrients necessary for plant growth and can be easily drawn into fibers. However, many technical challenges remain along the path to a completed multi-use, hydro-biodegradable fiberglass composite. The largest hurdle is combining the glass with a degradable polymer, such as PLA. Is a chopped fiber composite a better choice for this material than continuous fiber reinforcement? What filament diameter is best suited for the composite, and what are the conditions needed to draw fibers at that diameter? What sizing needs to be used to protect the fibers before molding the composite, but will allow for complete wetting of the fibers to the polymer? What coating should be used on the finished composite so the material does not degrade too soon? If the coating is damaged, how will it affect the structural integrity of the material? When the material degrades, will all the elements (fiber, matrix, sizing, coating) be non-toxic?

The glass might also need tweaking in order to work as desired as a fertilizer. If the glass is intended to take the place of apatite in a zeoponic system, it is missing the macronutrients Mg and S (and contains the K usually provided by clinoptilolite in zeopics). Other micronutrients, particularly some of the trace metals, would need

to be added as well. Additionally, Fe and Mn leached from the glass at a high rate. Do the levels of those nutrients need to be lowered? Some of these questions could be answered by further testing of the glass, particularly non-accelerated testing. Testing at a more neutral pH and/or at room temperature would give better insight into the dissolution of the glass in more realistic conditions. Of course, like the experiments performed by Gruener et al., the ultimate test of a zeoponic material is growing actual crops with it. Unfortunately, these types of testing can take a very long time to complete and were not able to be included in this work.

Scientific questions concerning the dissolution behavior of this glass remain. Why does this glass behave like a Type IV glass instead of a Type V glass, like most phosphate glasses? What range of compositions exhibits this behavior? Is this simply a function of glasses that contain Na and K, since Bunker et al. showed this behavior occurring in Na-K-silicate glasses? As many nuclear glasses contain these elements in ever-increasing amounts, this seems unlikely. So what other components in the glass affect this behavior? Is there a minimum alkali level needed for this behavior to occur? The dissolution behavior of glass is still not well understood.

Finally, phase diagrams and/or species activity curves covering the whole system should be calculated. Even utilizing the associate species method, which relies on less data than comparable models, it was difficult to find the necessary data to perform the calculations. More work to determine the Gibbs free energy for phosphates should be done. Additionally, any phase diagram results should be experimentally verified.

Chapter 6

Bibliography

[1] *Phase Diagrams for Ceramists, v. 1-8.* American Ceramic Society, 1964-1989.

[2] E.A. Abou Neel, I. Ahmed, J.J. Blaker, A. Bismarck, A.R. Boccaccinia, M.P. Lewis, S.N. Nazhat, and J.C. Knowles. Effect of iron on the surface, degradation and ion release properties of phosphate-based glass fibres. *Acta Biomaterialia*, 1:553–563, 2005.

[3] I. Ahmed, C.A. Collins, M.P. Lewis, I. Olsen, and J.C. Knowles. Processing, characterisation, and biocompatibility of iron-phosphate glass fibres for tissue engineering. *Biomaterials*, 25(16):3223–3232, 2004.

[4] I. Ahmed, M. Lewis, I. Olsen, and J.C. Knowles. Phosphate glasses for tissue engineering: Part 1. Processing and characterisation of a ternary-based P_2O_5-CaO-Na_2O glass system. *Biomaterials*, 25(3):491–499, 2004.

[5] G. Akdogan, H. Johto, and P. Taskinen. Phase equilibria study of K-O-Si system in equilibrium with air. *Journal of the European Ceramic Society*, 34:4053–4058, 2014.

[6] B. Al-Hasni and G. Mountjoy. Structural investigation of iron phosphate glasses using molecular dynamics simulation. *Journal of Non-Crystalline Solids*, 357:2775–2779, 2011.

[7] M.D. Allendorf and K.E. Spear. Thermodynamic analysis of silica refractory corrosion in glass-melting furnaces. *Journal of the Electrochemical Society*, 148(2):B59–B67, 2001.

[8] R. Andrews, A. Koski, J. Murphy, and A.M. Petrovic. Zeoponic materials allow rapid greens grow-in. *Golf Course Management*, 67(2):68–72, 1999.

[9] ANSI/ANS-16.1-2003. *Measurement of the Leachability of Solidified Low-Level Radioactive Wastes by a Short-Term Test Procedure*. American Nuclear Society, 2003.

[10] S. Arnout, M. Guo, D. Durinck, P.T. Jones, J. Elsen, B. Blanpain, and P. Wollants. Phase relations in stainless steel slags. *Proceeding of European Metallurgical Conference (EMC 2007)*, 2007.

[11] ASTM Standard C1285, 2014. *Determining Chemical Durability of Nuclear, Hazardous, and Mixed Waste Glasses and Multiphase Glass Ceramics: The Product Consistency Test (PCT)*. ASTM International, West Conshohocken, PA.

[12] ASTM Standard C1308, 2008. *Accelerated Leach Test for Diffusive Releases from Solidified Waste and a Computer Program to Model Diffusive, Fractional Leach-*

ing from Cylindrical Waste Forms. ASTM International, West Conshohocken, PA.

[13] ASTM Standard C1662, 2010. *Measurement of the Glass Dissolution Rate Using the Single-Pass Flow-Through Test Method*. ASTM International, West Conshohocken, PA.

[14] ASTM Standard C1663, 2009. *Measuring Waste Glass or Glass Ceramic Durability by Vapor Hydration Test*. ASTM International, West Conshohocken, PA.

[15] C.W. Bale, E. Belisle, P. Chartrand, S.A. Decterov, G. Eriksson, K. Hack, I.H. Jung, Y.B. Kang, J. Melancon, A.D. Pelton, C. Robelin, and S. Petersen. FactSage thermochemical software and databases - recent developments. *Calphad*, 33:295–311, 2009.

[16] M.F. Barba, P. Callejas, J.O. Arzabe, and J.M. Villora. Surface dissolution of calcium phosphate glass ceramics in dilute acid conditions. *Journal of the European Ceramic Society*, 23:2893–2896, 2003.

[17] R. Beiersdorfer, D. Ming, and C. Galindo Jr. Solubility and cation exchange properties of zeoponic substrates. *Microporous and Mesoporous Materials*, 61:231–247, 2003.

[18] T. Besmann and K. Spear. Thermochemical modeling of oxide glasses. *Journal of the American Ceramic Society*, 85(12):2887–2894, 2002.

[19] T.M. Besmann, K.E. Spear, and E.C. Beahm. Assessment of nepheline precipitation in nuclear waste glass via thermochemical modeling. *MRS Proceedings*, 608:715, 1999.

[20] P.A. Bingham, R.J. Hand, O.M. Hannant, S.D. Forder, and S.H. Kilcoyne. Effects of modifier additions on the thermal properties, chemical durability, oxidation state and structure of iron phosphate glasses. *Journal of Non-Crystalline Solids*, 355:1526–1538, 2009.

[21] D. Bonnell and J. Hastie. A predictive thermodynamic model for complex high temperature solution phases XI. *High Temperature Science*, 26:313–334, 1990.

[22] R.K. Brow. Review: The structure of simple phosphate glasses. *Journal of Non-Crystalline Solids*, 263 & 264:1–28, 2000.

[23] B.C. Bunker, G.W. Arnold, E.K. Beauchamp, and D.E. Day. Mechanisms for alkali leaching in mixed-Na-K silicate glasses. *Journal of Non-Crystalline Solids*, 58:295–322, 1983.

[24] B.C. Bunker, G.W. Arnold, and J.A. Wilder. Phosphate glass dissolution in aqueous solutions. *Journal of Non-Crystalline Solids*, 64:291–316, 1984.

[25] D. Carta, D. Pickup, J. Knowles, I. Ahmed, M. Smith, and R. Newport. A structural study of sol-gel and melt-quenched phosphate-based glasses. *Journal of Non-Crystalline Solids*, 353:1759–1765, 2007.

[26] L. Chen, D. He, F. Luan, L. Hu, and W. Chen. An efficient erbium doped phosphate laser glass for high average power pumping. *Journal of Alloys and Compounds*, 482(1-2):261–263, 2009.

[27] J. Christie, R. Ainsworth, D. Di Tommaso, and N. de Leeuw. Nanoscale chains control the solubility of phosphate glasses for biomedical applications. *The Journal of Physical Chemistry B*, 117:10652–10657, 2013.

[28] G. Daculsi, O. Laboux, O. Malard, and P. Weiss. Current state of the art of biphasic calcium phosphate bioceramics. *Journal of Materials Science: Materials in Medicine*, 14(3):195–200, 2003.

[29] D.E. Day, Z. Wu, C.S. Ray, and P. Hrma. Chemically durable iron phosphate glass wasteforms. *Journal of Non-Crystalline Solids*, 241(1):1–12, 1998.

[30] F. Delahaye, L. Montagne, G. Palavit, J.C. Touray, and P. Baillif. Acid dissolution of sodium-calcium metaphosphate glasses. *Journal of Non-Crystalline Solids*, 242:25–32, 1998.

[31] G. Eriksson and K. Hack. ChemSage - A computer program for the calculation of complex chemical equilibrium. *Metallurgical and Materials Transactions B*, 21(6):1013–1023, 1990.

[32] D.C. Golden and D. Ming. Nutrient-substituted hydroxyapatites: Synthesis and characterization. *Soil Science Society of America Journal*, 63:657–664, 1999.

[33] J.E. Gruener, D. Ming, C. Galindo Jr., K.E. Henderson, and D.C. Golden. Plant productivity and characterization of zeoponic substrates after three successive

crops of radish (*Raphanus sativus* L.). *Microporous and Mesoporous Materials*, 105:279–284, 2007.

[34] J. Hastie and D. Bonnell. A predictive phase equilibrium model for multicomponent oxide mixtures Part II: Oxides of Na-K-Ca-Mg-Al-Si. *High Temperature Science*, 19:275–306, 1985.

[35] L. Hench and D. Clark. Physical chemistry of glass surfaces. *Journal of Non-Crystalline Solids*, 28:83–105, 1978.

[36] U. Hoppe. A structural model for phosphate glasses. *Journal of Non-Crystalline Solids*, 195:138–147, 1996.

[37] W. Huang, D.E. Day, C.S. Ray, C.W. Kim, and A. Mogus-Milankovic. Vitrification of high chrome oxide nuclear waste in iron phosphate glasses. *Journal of Nuclear Materials*, 327(1):46–57, 2004.

[38] International Standard ISO 719-1985. *Glass - Hydrolytic Resistance of Glass Grains at 98 Degrees C - Method of Test and Classification.* International Organization for Standardization, 1985.

[39] A. Jiricka, J.D. Vienna, P. Hrma, and D.M. Strachan. The effect of experimental conditions and evaluation techniques on the alteration of low activity glasses by vapor hydration. *Journal of Non-Crystalline Solids*, 292:25–43, 2001.

[40] B. Jokic, M. Mitric, V. Radmilovic, S. Drmanic, R. Petrovic, and D. Janackovic. Synthesis and characterization of monetite and hydroxyapatite whiskers

obtained by a hydrothermal method. *Ceramics International*, 37(1):167–173, 2011.

[41] M. Karabulut, G.K. Marasinghe, C.S. Ray, D.E. Day, G.D. Waddill, C.H. Booth, P.G. Allen, J.J. Bucher, D.L. Caulder, and D.K. Shuh. An investigation of the local iron environment in iron phosphate glasses having different Fe(II) concentrations. *Journal of Non-Crystalline Solids*, 306:182–192, 2002.

[42] R.A. Khan, A.J. Parsons, I.A. Jones, G.S. Walker, and C.D. Rudd. Preparation and characterization of phosphate glass fibers and fabrication of poly(caprolactone) matrix resorbable composites. *Journal of Reinforced Plastics and Composites*, 29(12):1838–1850, 2010.

[43] C.W. Kim and D.E. Day. Immobilization of Hanford LAW in iron phosphate glasses. *Journal of Non-Crystalline Solids*, 331(1-3):20–31, 2003.

[44] C.W. Kim, C.S. Ray, D. Zhu, D.E. Day, D. Gombert, A. Aloy, A. Mogus-Milankovic, and M. Karabulut. Chemically durable iron phosphate glasses for vitrifying sodium bearing waste (SBW) using conventional and cold crucible induction melting (CCIM) techniques. *Journal of Nuclear Materials*, 322(2-3):152–164, 2003.

[45] R.J. Kirkpatrick and R.K. Brow. Nuclear magnetic resonance investigation of the structures of phosphate and phosphate-containing glasses: A review. *Solid State Nuclear Magnetic Resonance*, 5:9–21, 1995.

[46] H. Kofuji, T. Yano, M. Myochin, K. Matsuyama, T. Okita, and S. Miyamoto. Chemical durability of iron-phosphate glass as the high level waste from pyrochemical reprocessing. *Procedia Chemistry*, 7:764–771, 2012.

[47] A. La Iglesia. Estimating the thermodynamic properties of phosphate minerals at high and low temperature from the sum of constituent units. *Estudios Geologicos*, 65(2):109–119, 2009.

[48] D. Larink and H. Eckert. Mixed network former effect in ion-conducting alkali borophosphate glasses: Structure/property correlations in the system $[M_2O]_{1/3}[(B_2O_3)_x(P_2O_5)_{1\text{-}x}]_{2/3}$ (M = Li, K, Cs). *The Journal of Physical Chemistry C*, 116:26162–26176, 2012.

[49] J.S. Lee and C.K. Hsu. A study on thermal properties of β-$Ca(PO_3)_2$ whiskers and on devitrification mechanism of calcium phosphate glass system. *Thermochimica Acta*, 339(1):103–109, 1999.

[50] H.C. Li, D.G. Wang, J.H. Hu, and C.Z. Chen. Effect of the partial substitution of K_2O, MgO, B_2O_3 for CaO on crystallization, structure, and properties of Na_2O-CaO-SiO_2-P_2O_5 system glass-ceramics. *Materials Letters*, 106:373–376, 2013.

[51] J. Li, S. Cai, G. Xu, X. Li, W. Zhang, and Z. Zhang. In vitro biocompatibility study of calcium phosphate glass ceramic scaffolds with different trace element doping. *Materials Science and Engineering C*, 32:356–363, 2012.

[52] Z. Liu, C. Qi, S. Dai, Y. Jiang, and L. Hu. Spectra and laser properties of Er^{3+}, Yb^{3+} phosphate glasses. *Optical Materials*, 21(4):789–794, 2003.

[53] L.N. Ma. *Dissolution Behavior of Phosphate Glasses*. PhD thesis, Missouri University of Science and Technology, 2014.

[54] J.S. McCloy, M.J. Schweiger, C.P. Rodriguez, and J.D. Vienna. Nepheline crystallization in nuclear waste glasses: Progress toward acceptance of high-alumina formulations. *International Journal of Applied Glass Science*, 2(3):201–214, 2011.

[55] M.E. Milberg and M.C. Daly. Structure of oriented sodium metaphosphate glass fibers. *Journal of Chemical Physics*, 39(11):2966–2973, 1963.

[56] G.W. Morey. The binary systems $NaPO_3$-KPO_3 and $K_4P_2O_7$-KPO_3. *Journal of the American Chemical Society*, 76(18):4724–4726, 1954.

[57] Y.M. Moustafa. Characterization of iron oxychloride potassium phosphate glasses. *Journal of Physics D: Applied Physics*, 32:2278–2286, 1999.

[58] M. Navarro, S. del Valle, S. Martinez, S. Zeppetelli, L. Ambrosio, J.A. Planell, and M. Pau Ginebra. New macroporous calcium phosphate glass ceramic for guided bone regeneration. *Biomaterials*, 25(18):4233–4241, 2004.

[59] T. Okura, T. Miyachi, and H. Monma. Properties and vibrational spectra of magnesium phosphate glasses for nuclear waste immobilization. *Journal of the European Ceramic Society*, 26:831–836, 2006.

[60] A.J. Parsons, L.D. Burling, C.A. Scotchford, G.S. Walker, and C.D. Rudd. Properties of sodium-based ternary phosphate glasses produced from readily available phosphate salts. *Journal of Non-Crystalline Solids*, 352:5309–5317, 2006.

[61] P. Pascuta, G. Borodi, N. Jumate, I. Vida-Simiti, D. Viorel, and E. Culea. The structural role of manganese ions in some zinc phosphate glasses and glass ceramics. *Journal of Alloys and Compounds*, 504:479–483, 2010.

[62] D.A. Porter and K.E. Easterling. *Phase Transformations in Metals and Alloys*. Nelson Thornes Ltd., second edition, 2001.

[63] B. Qian, X. Liang, C. Wang, and S. Yang. Structure and properties of calcium iron phosphate glasses. *Journal of Nuclear Materials*, 443:140–144, 2013.

[64] C. Roiland, F. Fayon, P. Simon, and D. Massiot. Characterization of the disordered phosphate network in CaO-P_2O_5 glasses by ^{31}P solid-state NMR and Raman spectroscopies. *Journal of Non-Crystalline Solids*, 357:1636–1646, 2011.

[65] M.H. Sandstrom and D. Bostrom. Determination of standard Gibbs free energy of formation for $CaKPO_4$, $CaK_4(PO_4)_2$, $CaK_2P_2O_7$, and $Ca_{10}K(PO_4)_7$ from solid-state e.m.f. measurements using yttria stabilised zirconia as soild electrolyte. *The Journal of Chemical Thermodynamics*, 40:40–46, 2008.

[66] G. Scott and D. Gilead, editors. *Degradable Polymers: Principles and Applications*, chapter 1, 2, 4, and 9. Kluwer Academic Publishers/Chapman and Hall, 1995.

[67] S. Serena, L. Carbajal, M.A. Sainz, and A. Caballero. Thermodynamic assessment of the system CaO-P_2O_5: Application of the ionic two-sublattice model to glass-forming melts. *Journal of the American Ceramic Society*, 94(9):3094–3103, 2011.

[68] B. Shakhmatkin, N. Vedishcheva, and A. Wright. Can thermodynamics relate the properties of melts and glasses to their structure? *Journal of Non-Crystalline Solids*, 293-295:220–226, 2001.

[69] P.Y. Shih. Properties and FTIR spectra of lead phosphate glasses for nuclear waste immobilization. *Materials Chemistry and Physics*, 80:299–304, 2003.

[70] K. Spear, T. Besmann, and E. Beahm. Thermochemical modeling of glass: Application to high-level nuclear waste glass. *MRS Bulletin*, 24(4):37–44, 1999.

[71] K.E. Spear and M.D. Allendorf. Thermodynamic analysis of alumina refractory corrosion by sodium or potassium hydroxide in glass melting furnaces. *Journal of the Electrochemical Society*, 149(12):B551–B559, 2002.

[72] D.M. Strachan, R.P. Turcotte, and B.O. Barnes. MCC-1: A standard leach test for nuclear waste forms. *Nuclear Technology*, 56(2):306–309, 1982.

[73] B. Sutter, L. Hossner, and D. Ming. Dissolution kinetics of iron-, manganese-, and copper-containing synthetic hydroxyapatites. *Soil Science Society of America Journal*, 69:362–370, 2005.

[74] U.S. Environmental Protection Agency. Method 1310B Extraction Procedure (EP) Toxicity Test Method and Structural Integrity Test. In *SW-846 Test*

Methods for Evaluating Solid Waste, Physical/Chemical Methods. 5th edition, 2015.

[75] U.S. Environmental Protection Agency. Method 1311 Toxicity Characteristic Leaching Procedure. In *SW-846 Test Methods for Evaluating Solid Waste, Physical/Chemical Methods*. 5th edition, 2015.

[76] U.S. Environmental Protection Agency. Method 1313 Liquid-Solid Partitioning as a Function of Extract pH Using a Parallel Batch Extraction Procedure. In *SW-846 Test Methods for Evaluating Solid Waste, Physical/Chemical Methods*. 5th edition, 2015.

[77] U.S. Environmental Protection Agency. Method 1314 Liquid-Solid Partitioning as a Function of Liquid-Solid Ratio for Constituents in Solid Materials Using an Up-Flow Percolation Column Procedure. In *SW-846 Test Methods for Evaluating Solid Waste, Physical/Chemical Methods*. 5th edition, 2015.

[78] U.S. Environmental Protection Agency. Method 1315 Mass Transfer Rates of Constituents in Monolithic or Compacted Granular Materials Using a Semi-Dynamic Tank Leaching Procedure. In *SW-846 Test Methods for Evaluating Solid Waste, Physical/Chemical Methods*. 5th edition, 2015.

[79] U.S. Environmental Protection Agency. Method 1316 Liquid-Solid Partitioning as a Function of Liquid-to-Solid Ratio in Solid Materials Using a Parallel Batch Procedure. In *SW-846 Test Methods for Evaluating Solid Waste, Physical/Chemical Methods*. 5th edition, 2015.

[80] U.S. Environmental Protection Agency. Method 1320 Multiple Extraction Procedure. In *SW-846 Test Methods for Evaluating Solid Waste, Physical/Chemical Methods*. 5th edition, 2015.

[81] V. Venkatramu, R. Vijaya, S.F. Leon-Luis, P. Babu, C.K. Jayasankar, V. Lavin, and L.J. Dhareshwar. Optical properties of Yb^{3+}-doped phosphate laser glasses. *Journal of Alloys and Compounds*, 509(16):5084–5089, 2011.

[82] Wolfram Research, Inc. *Mathematica Version 8.0*. Champaign, IL, 2010.

[83] E. Yazhenskikh, K. Hack, and M. Muller. Critical thermodynamic evaluation of oxide systems relevant to fuel ashes and slags. Part 1: Alkali oxide-silica systems. *Calphad*, 30(3):270–276, 2006.

[84] E. Yazhenskikh, K. Hack, and M. Muller. Critical thermodynamic evaluation of oxide systems relevant to fuel ashes and slags part 2: Alkali oxide-alumina systems. *Computer Coupling of Phase Diagrams and Thermochemistry*, 30:397–404, 2006.

[85] E. Yazhenskikh, T. Jantzen, K. Hack, and M. Muller. Critical thermodynamic evaluation of oxide systems relevant to fuel ashes and slags: Potassium oxide-magnesium oxide-silica. *CALPHAD: Computer Coupling of Phase Diagrams and Thermochemisty*, 47:35–49, 2014.

[86] X. Yu, D.E. Day, G.J. Long, and R.K. Brow. Properties and structure of sodium-iron phosphate glasses. *Journal of Non-Crystalline Solids*, 215(1):21–31, 1997.

[87] H. Zhang, Y. Wang, Y. Yan, and S. Li. Precipitation of biocompatible hydroxyapatite whiskers from moderately acid solutions. *Ceramics International*, 29(4):413–418, 2003.

[88] L. Zhang. *Phase Equilibria in Iron Phosphate System*. PhD thesis, Missouri University of Science and Technology, 2010.

[89] L. Zhang, L. Ghussn, M. Schmitt, E. Zanotto, R. Brow, and M. Schlesinger. Thermal stability of glasses from the $Fe_4(P_2O_7)_3$-$Fe(PO_3)_3$ system. *Journal of Non-Crystalline Solids*, 356:2965–2968, 2010.

[90] L. Zhang, C. Schmetterer, and P.J. Mason. Thermodynamic description of the M_2O-SiO_2 (M = K, Na) systems. *Computational Materials Science*, 66:20–27, 2013.

Appendix A

Dissolution Test Raw Data

Table A.1: Raw data from dissolution test 1. All glasses tested in a 2% citric acid solution (pH = 2.2) at 40 °C.

	Duration (h)	Glass Powder Weight (g)	Filter Weight (g)	Combined Weight (g)	Remaining Glass Weight (g)	Percent Weight Lost
Glass 4	6	0.042	0.820	0.856	0.036	14.3
	24	0.050	0.832	0.862	0.030	40.0
	48	0.042	0.834	0.862	0.028	33.3
	168	0.050	0.812	0.828	0.016	68.0
Glass 7	6	0.050	0.856	0.900	0.044	12.0
	24	0.044	0.810	0.850	0.040	9.1
	48	0.040	0.814	0.836	0.022	45.0
	168	0.038	0.824	0.838	0.014	63.2
Glass 14	6	0.050	0.836	0.880	0.044	12.0
	24	0.044	0.836	0.864	0.028	36.4
	48	0.050	0.826	0.854	0.028	44.0
	168	0.044	0.818	0.834	0.016	63.6

Table A.2: Raw data from dissolution test 2. All glasses tested in a 2% citric acid solution (pH = 2.2) at 40 °C. A + in front of the weight lost number indicates the glass gained that much weight.

	Duration (h)	Glass Powder Weight (g)	Filter Weight (g)	Combined Weight (g)	Remaining Glass Weight (g)	Percent Weight Lost
Glass 15	6	0.022	0.814	0.846	0.032	+45.5
	24	0.028	0.788	0.816	0.028	0
	48	0.032	0.810	0.836	0.026	18.8
	168	0.032	0.828	0.856	0.028	12.5
Glass 16	6	0.030	0.824	0.854	0.030	0
	24	0.032	0.804	0.834	0.030	6.3
	48	0.032	0.828	0.852	0.024	25.0
	168	0.038	0.802	0.820	0.018	52.6
Glass 17	6	0.030	0.812	0.848	0.036	+20.0
	24	0.032	0.810	0.836	0.026	18.8
	48	0.038	0.828	0.866	0.038	0
	168	0.044	0.798	0.824	0.026	40.9

Table A.3: Raw data from dissolution test 3. All tests performed on Glass 17 at 40 °C in DI water, citric acid solutions, or hydrochloric acid solutions at varying pH. A + in front of the weight lost number indicates the glass gained that much weight.

	Duration (h)	Glass Powder Weight (g)	Filter Weight (g)	Combined Weight (g)	Remaining Glass Weight (g)	Percent Weight Lost
Water	6	0.030	0.808	0.852	0.044	+46.7
	24	0.030	0.836	0.870	0.034	+13.3
	48	0.032	0.838	0.872	0.036	+12.5
	168	0.030	0.818	0.850	0.032	+6.7
Citric pH 5.5	6	0.028	0.830	0.858	0.028	0
	24	0.028	0.832	0.858	0.026	7.1
	48	0.028	0.798	0.828	0.030	+7.1
	168	0.028	0.842	0.872	0.030	+7.1
Citric pH 4	6	0.028	0.836	0.876	0.040	+42.9
	24	0.030	0.852	0.884	0.032	+6.7
	48	0.030	0.846	0.882	0.036	+20.0
	168	0.030	0.812	0.842	0.030	0
HCl pH 5.5	6	0.028	0.848	0.882	0.034	+21.4
	24	0.028	0.808	0.848	0.040	+42.9
	48	0.030	0.832	0.868	0.036	+20
	168	0.032	0.834	0.868	0.034	+6.3
HCl pH 4	6	0.030	0.832	0.868	0.036	+20.0
	24	0.028	0.800	0.828	0.028	0
	48	0.032	0.824	0.856	0.032	0
	168	0.032	0.836	0.864	0.028	12.5
HCl pH 2	6	0.030	0.820	0.858	0.038	+26.7
	24	0.030	0.836	0.844	0.008	73.3
	48	0.028	0.852	0.860	0.008	71.4
	168	0.032	0.818	0.822	0.014	87.5

Table A.4: Raw data for hydrochloric acid solutions from dissolution test 4. All tests performed on Glass 17 at 40 °C in a hydrochloric acid solution at pH 2 ± 0.04.

Duration (h)	Glass Powder Weight (g)	Filter Weight (g)	Combined Weight (g)	Remaining Glass Weight (g)	Percent Weight Lost
1	0.030	0.902	0.926	0.024	20.0
	0.030	0.874	0.896	0.022	26.7
	0.028	0.888	0.910	0.022	21.43
2	0.028	0.856	0.874	0.018	35.7
	0.028	0.924	0.942	0.018	35.7
	0.028	0.848	0.872	0.024	14.3
3	0.028	0.868	0.890	0.022	21.4
	0.030	0.918	0.938	0.020	33.3
	0.030	0.868	0.880	0.012	60.0
4	0.028	0.868	0.884	0.016	42.9
	0.028	0.892	0.906	0.014	50.0
	0.028	0.862	0.890	0.028	0
5	0.028	0.860	0.876	0.016	42.9
	0.030	0.914	0.926	0.012	60.0
	0.028	0.840	0.856	0.016	42.9
6	0.028	0.894	0.906	0.012	57.1
	0.028	0.856	0.874	0.018	35.7
	0.030	0.866	0.876	0.010	66.7
7	0.028	0.902	0.912	0.010	64.3
	0.030	0.896	0.920	0.024	20.0
	0.030	0.898	0.912	0.014	53.3
8	0.030	0.902	0.920	0.018	40.0
	0.030	0.926	0.934	0.008	73.3
	0.030	0.900	0.906	0.006	80.0
9	0.032	0.880	0.890	0.010	68.8
	0.028	0.918	0.926	0.008	71.4
	0.028	0.882	0.904	0.022	21.4
10	0.030	0.890	0.906	0.016	46.7
	0.032	0.900	0.908	0.008	75.0
	0.028	0.892	0.902	0.010	64.3

Duration (h)	Glass Powder Weight (g)	Filter Weight (g)	Combined Weight (g)	Remaining Glass Weight (g)	Percent Weight Lost
11	0.030	0.892	0.914	0.022	26.7
	0.030	0.868	0.892	0.024	20.0
	0.030	0.904	0.932	0.028	6.7
12	0.032	0.894	0.912	0.018	43.8
	0.030	0.918	0.928	0.010	66.7
	0.032	0.874	0.886	0.012	62.5
13	0.030	0.908	0.920	0.012	60.0
	0.030	0.908	0.914	0.006	80.0
	0.030	0.882	0.896	0.014	53.3
14	0.032	0.900	0.902	0.002	93.8
	0.032	0.906	0.908	0.002	93.8
	0.032	0.874	0.876	0.002	93.8
15	0.032	0.900	0.914	0.014	56.3
	0.032	0.870	0.882	0.012	62.5
	0.030	0.868	0.878	0.010	66.7
16	0.030	0.900	0.908	0.008	73.3
	0.030	0.912	0.920	0.008	73.3
	0.032	0.900	0.916	0.016	46.7
17	0.032	0.882	0.900	0.018	43.8
	0.032	0.888	0.900	0.012	62.5
	0.028	0.882	0.892	0.010	64.3
18	0.030	0.894	0.904	0.010	66.7
	0.030	0.926	0.940	0.014	53.3
	0.032	0.886	0.904	0.018	43.8
19	0.030	0.904	0.920	0.016	46.7
	0.028	0.902	0.910	0.008	71.4
	0.032	0.894	0.904	0.010	68.8
20	0.028	0.908	0.912	0.004	85.7
	0.030	0.860	0.872	0.012	60.0
	0.032	0.892	0.912	0.020	37.5
21	0.030	0.924	0.938	0.014	53.3
	0.030	0.878	0.890	0.012	60.0
	0.028	0.898	0.906	0.008	71.4

Duration (h)	Glass Powder Weight (g)	Filter Weight (g)	Combined Weight (g)	Remaining Glass Weight (g)	Percent Weight Lost
22	0.032	0.904	0.920	0.016	50.0
	0.028	0.876	0.880	0.004	85.7
	0.028	0.908	0.914	0.006	78.6
23	0.030	0.910	0.916	0.006	80.0
	0.030	0.864	0.870	0.006	80.0
	0.030	0.904	0.920	0.016	46.7
24	0.028	0.900	0.906	0.006	78.6
	0.032	0.872	0.882	0.010	68.8
	0.028	0.856	0.876	0.020	28.6

Table A.5: Raw data for citric acid solutions from dissolution test 4. All tests performed on Glass 17 at 40 °C in a citric acid solution at pH 2 ± 0.08. A + in front of the weight lost number indicates the glass gained that much weight.

Duration (h)	Glass Powder Weight (g)	Filter Weight (g)	Combined Weight (g)	Remaining Glass Weight (g)	Percent Weight Lost
1	0.028	0.902	0.938	0.036	+28.6
	0.030	0.870	0.908	0.034	+13.3
	0.032	0.874	0.906	0.032	0
2	0.032	0.908	0.932	0.024	25.0
	0.028	0.848	0.874	0.026	7.1
	0.030	0.898	0.920	0.022	26.7
3	0.028	0.918	0.938	0.020	28.6
	0.032	0.882	0.914	0.032	0
	0.030	0.904	0.932	0.028	6.7
4	0.032	0.882	0.904	0.022	31.3
	0.028	0.864	0.884	0.020	28.6
	0.030	0.906	0.930	0.024	20.0
5	0.028	0.892	0.918	0.026	7.1
	0.028	0.908	0.934	0.026	7.1
	0.030	0.894	0.920	0.026	13.3
6	0.030	0.880	0.910	0.030	0
	0.032	0.864	0.896	0.032	0
	0.030	0.878	0.904	0.026	13.3
7	0.028	0.896	0.908	0.012	57.1
	0.030	0.884	0.904	0.20	33.3
	0.030	0.922	0.940	0.018	40.0
8	0.032	0.918	0.936	0.018	43.8
	0.032	0.918	0.944	0.026	18.8
	0.030	0.896	0.926	0.030	0
9	0.032	0.914	0.944	0.030	6.3
	0.028	0.890	0.912	0.022	21.4
	0.028	0.892	0.912	0.020	28.6
10	0.028	0.912	0.926	0.014	50.0
	0.028	0.898	0.916	0.018	35.7
	0.032	0.896	0.922	0.026	18.8

Duration (h)	Glass Powder Weight (g)	Filter Weight (g)	Combined Weight (g)	Remaining Glass Weight (g)	Percent Weight Lost
11	0.030	0.836	0.868	0.032	+6.7
	0.030	0.810	0.836	0.026	13.3
	0.028	0.906	0.926	0.020	28.6
12	0.028	0.908	0.930	0.022	21.4
	0.030	0.892	0.920	0.028	6.7
	0.032	0.886	0.908	0.022	31.3
13	0.032	0.880	0.908	0.028	12.5
	0.032	0.890	0.912	0.022	31.3
	0.030	0.876	0.888	0.012	60.0
14	0.032	0.890	0.908	0.018	43.8
	0.030	0.900	0.922	0.022	26.7
	0.030	0.876	0.888	0.012	60.0
15	0.028	0.884	0.906	0.022	21.4
	0.032	0.872	0.900	0.028	12.5
	0.028	0.872	0.896	0.024	14.3
16	0.030	0.888	0.912	0.024	20.0
	0.032	0.872	0.892	0.020	37.5
	0.032	0.910	0.928	0.018	43.8
17	0.032	0.932	0.946	0.014	56.3
	0.030	0.886	0.908	0.022	26.7
	0.028	0.906	0.930	0.024	14.3
18	0.030	0.910	0.930	0.020	33.3
	0.030	0.906	0.926	0.020	33.3
	0.030	0.906	0.926	0.020	33.3
19	0.030	0.904	0.924	0.020	33.3
	0.030	0.892	0.908	0.016	46.7
	0.028	0.868	0.886	0.018	35.7
20	0.030	0.964	0.984	0.020	33.3
	0.028	0.912	0.932	0.020	28.6
	0.028	0.854	0.866	0.012	57.1
21	0.030	0.868	0.888	0.020	33.3
	0.030	0.932	0.950	0.018	40.0
	0.028	0.864	0.884	0.020	28.6

Duration (h)	Glass Powder Weight (g)	Filter Weight (g)	Combined Weight (g)	Remaining Glass Weight (g)	Percent Weight Lost
22	0.032	0.868	0.882	0.014	56.3
	0.028	0.906	0.926	0.020	28.6
	0.028	0.884	0.902	0.018	35.7
23	0.028	0.872	0.894	0.022	21.4
	0.030	0.908	0.930	0.022	26.7
	0.028	0.880	0.900	0.020	28.6
24	0.028	0.884	0.912	0.028	0
	0.032	0.868	0.896	0.028	12.5
	0.032	0.852	0.882	0.030	6.3

Table A.6: Raw data for pH changes during dissolution test 4. Measurements were not made for 20, 21, 22, and 23 hours.

Duration (h)	HCl Start pH	HCl End pH	Citric Start pH	Citric End pH
1	2.01	2.21	2.05	2.16
2	2.03	2.25	2.08	2.25
3	2.03	2.31	2.08	-
4	2.03	2.24	2.08	2.26
5	2.03	2.43	2.08	2.24
6	2.01	2.39	2.05	2.14
7	2.00	2.36	2.03	2.23
8	2.00	2.49	2.03	2.17
9	2.00	2.47	2.03	2.18
10	2.00	2.55	2.03	2.16
11	1.96	2.31	2.06	2.24
12	1.96	2.37	2.06	2.23
13	1.96	2.25	2.06	2.22
14	1.96	2.50	2.06	2.20
15	2.01	2.38	2.05	2.16
16	2.03	2.47	2.05	2.21
17	2.03	2.48	2.05	2.20
18	2.03	2.46	2.05	2.23
19	2.03	2.55	2.05	2.22
24	2.01	2.50	2.05	2.18

Table A.7: Raw data from ICP-OES.

	Duration (h)	Fe (μg/L)	Mn (μg/L)	Ca (μg/L)	K (μg/L)	Na (μg/L)
HCl	1	14280	8837	112.2	2121	9084
	6	18210	13990	244.5	3556	12150
	12	23220	17460	284	3040	13160
	24	18790	15840	301.1	3147	13030
Citric	1	15000	9807	123.5	2177	9457
	6	18250	12840	213.8	2595	11570
	12	22820	17780	296.9	3067	13490
	24	27110	21510	410.7	3424	14530

Appendix B

Permission to Include Material from Cambridge University Press

License Number	3842730611390
License date	Apr 05, 2016
Licensed Content Publisher	Cambridge University Press
Licensed Content Publication	MRS Bulletin
Licensed Content Title	Thermochemical Modeling of Glass: Application to High-Level Nuclear Waste Glass
Licensed Content Author	Karl E. Spear, Theodore M. Besmann and Edward C. Beahm
Licensed Content Date	Nov 29, 2013
Licensed Content Volume	24
Licensed Content Issue	04
Start page	37
End page	44
Type of Use	Dissertation/Thesis
Requestor type	Author
Portion	Text extract
Number of pages requested	1
Author of this Cambridge University Press article	No
Author / editor of the new work	Yes
Order reference number	None
Territory for reuse	World
Title of your thesis / dissertation	Fiberglass Goes Green: Developing Phosphate Glass for Use in Biodegradable Composites
Expected completion date	May 2016
Estimated size(pages)	150
Requestor Location	Christina Arendt [redacted] None None [redacted] United States Attn: Christina Arendt
Billing Type	Invoice
Billing address	Christina Arendt [redacted] None None [redacted] United States Attn: Christina Arendt
Total	**0.00 USD**

Appendix C

Permission to Include Material from Elsevier

License Number	3842711160815
License date	Apr 05, 2016
Licensed Content Publisher	Elsevier
Licensed Content Publication	Solid State Nuclear Magnetic Resonance
Licensed Content Title	Nuclear magnetic resonance investigation of the structures of phosphate and phosphate-containing glasses: a review
Licensed Content Author	R.James Kirkpatrick,Richard K. Brow
Licensed Content Date	October 1995
Licensed content volume number	5
Licensed content issue number	1
Number of pages	13
Type of Use	reuse in a thesis/dissertation
Portion	figures/tables/illustrations
Number of figures/tables/illustrations	1
Format	electronic
Are you the author of this Elsevier article?	No
Will you be translating?	No
Original figure numbers	Figure 2
Title of your thesis/dissertation	Fiberglass Goes Green: Developing Phosphate Glass for Use in Biodegradable Composites
Expected completion date	May 2016
Estimated size (number of pages)	150
Elsevier VAT number	GB 494 6272 12
Price	0.00 USD
VAT/Local Sales Tax	0.00 USD / 0.00 GBP
Total	**0.00 USD**

License Number	3842720259728
License date	Apr 05, 2016
Licensed Content Publisher	Elsevier
Licensed Content Publication	Journal of Non-Crystalline Solids
Licensed Content Title	Phosphate glass dissolution in aqueous solutions
Licensed Content Author	B.C. Bunker,G.W. Arnold,J.A. Wilder
Licensed Content Date	May 1984
Licensed content volume number	64
Licensed content issue number	3
Number of pages	26
Type of Use	reuse in a thesis/dissertation
Portion	figures/tables/illustrations
Number of figures/tables/illustrations	1
Format	both print and electronic
Are you the author of this Elsevier article?	No
Will you be translating?	No
Original figure numbers	Figure 12
Title of your thesis/dissertation	Fiberglass Goes Green: Developing Phosphate Glass for Use in Biodegradable Composites
Expected completion date	May 2016
Estimated size (number of pages)	150
Elsevier VAT number	GB 494 6272 12
Price	0.00 USD
VAT/Local Sales Tax	0.00 USD / 0.00 GBP
Total	**0.00 USD**

License Number	3842720383152
License date	Apr 05, 2016
Licensed Content Publisher	Elsevier
Licensed Content Publication	Journal of Non-Crystalline Solids
Licensed Content Title	The effect of experimental conditions and evaluation techniques on the alteration of low activity glasses by vapor hydration
Licensed Content Author	A Jiřička,J.D Vienna,P Hrma,D.M Strachan
Licensed Content Date	November 2001
Licensed content volume number	292
Licensed content issue number	1-3
Number of pages	19
Type of Use	reuse in a thesis/dissertation
Portion	figures/tables/illustrations
Number of figures/tables/illustrations	1
Format	both print and electronic
Are you the author of this Elsevier article?	No
Will you be translating?	No
Original figure numbers	Figure 2
Title of your thesis/dissertation	Fiberglass Goes Green: Developing Phosphate Glass for Use in Biodegradable Composites
Expected completion date	May 2016
Estimated size (number of pages)	150
Elsevier VAT number	GB 494 6272 12
Price	0.00 USD
VAT/Local Sales Tax	0.00 USD / 0.00 GBP
Total	**0.00 USD**

License Number	3842721161491
License date	Apr 05, 2016
Licensed Content Publisher	Elsevier
Licensed Content Publication	Microporous and Mesoporous Materials
Licensed Content Title	Plant productivity and characterization of zeoponic substrates after three successive crops of radish (Raphanus sativus L.)
Licensed Content Author	J.E. Gruener,D.W. Ming,C. Galindo,K.E. Henderson,D.C. Golden
Licensed Content Date	1 October 2007
Licensed content volume number	105
Licensed content issue number	3
Number of pages	6
Type of Use	reuse in a thesis/dissertation
Portion	figures/tables/illustrations
Number of figures/tables/illustrations	1
Format	both print and electronic
Are you the author of this Elsevier article?	No
Will you be translating?	No
Original figure numbers	Figure 1
Title of your thesis/dissertation	Fiberglass Goes Green: Developing Phosphate Glass for Use in Biodegradable Composites
Expected completion date	May 2016
Estimated size (number of pages)	150
Elsevier VAT number	GB 494 6272 12
Price	0.00 USD
VAT/Local Sales Tax	0.00 USD / 0.00 GBP
Total	**0.00 USD**

License Number	3842721289456
License date	Apr 05, 2016
Licensed Content Publisher	Elsevier
Licensed Content Publication	Journal of Non-Crystalline Solids
Licensed Content Title	Review: the structure of simple phosphate glasses
Licensed Content Author	Richard K Brow
Licensed Content Date	1 March 2000
Licensed content volume number	263
Licensed content issue number	n/a
Number of pages	28
Type of Use	reuse in a thesis/dissertation
Portion	figures/tables/illustrations
Number of figures/tables/illustrations	1
Format	both print and electronic
Are you the author of this Elsevier article?	No
Will you be translating?	No
Original figure numbers	Figure 1
Title of your thesis/dissertation	Fiberglass Goes Green: Developing Phosphate Glass for Use in Biodegradable Composites
Expected completion date	May 2016
Estimated size (number of pages)	150
Elsevier VAT number	GB 494 6272 12
Price	0.00 USD
VAT/Local Sales Tax	0.00 USD / 0.00 GBP
Total	**0.00 USD**

Appendix D

Permission to Include Material from John Wiley and Sons

License Number	3842711511686
License date	Apr 05, 2016
Licensed Content Publisher	John Wiley and Sons
Licensed Content Publication	Journal of the American Ceramic Society
Licensed Content Title	Thermochemical Modeling of Oxide Glasses
Licensed Content Author	Theodore M. Besmann,Karl E. Spear
Licensed Content Date	Dec 20, 2004
Licensed Content Pages	8
Type of Use	Dissertation/Thesis
Requestor type	University/Academic
Format	Print and electronic
Portion	Figure/table
Number of figures/tables	1
Original Wiley figure/table number(s)	Figure 1
Will you be translating?	No
Title of your thesis / dissertation	Fiberglass Goes Green: Developing Phosphate Glass for Use in Biodegradable Composites
Expected completion date	May 2016
Expected size (number of pages)	150
Requestor Location	Christina Arendt [redacted] None None [redacted] United States Attn: Christina Arendt
Billing Type	Invoice
Billing address	Christina Arendt [redacted] None None [redacted] United States Attn: Christina Arendt
Total	**0.00 USD**

Curriculum Vita

Christina Arendt was born in Greenville, SC to Dr. and Mrs. Nick McLane. After graduating from Christ Church Episcopal School in 2004, she attended Virginia Tech for six years, during which time she earned a B.S. and an M.S. in Aerospace Engineering. An internship at NASA's Marshall Space Flight Center in 2007 introduced her to composites, leading her to join the Materials Science and Engineering program at the University of Texas at El Paso in the fall of 2010. While working on her dissertation, she was a Ph.D. intern at the Pacific Northwest National Laboratory in Richland, WA.

Permanent Address: mclanec@vt.edu